# LIUTEX-BASED VORTEX IDENTIFICATION METHODS AND THEIR APPLICATION IN DNS STUDY OF FLAT PLATE BOUNDARY LAYER TRANSITION

by

PUSHPA SHRESTHA

Presented to the Faculty of the Graduate School of

The University of Texas at Arlington in Partial Fulfillment

of the Requirements

for the Degree of

DOCTOR OF PHILOSOPHY

THE UNIVERSITY OF TEXAS AT ARLINGTON

August 2021

LIUTEX-BASED VORTEX IDENTIFICATION METHODS AND THEIR APPLICATION IN DNS STUDY OF THE BOUNDARY LAYER TRANSITION

The following members of the Committee approve the doctoral dissertation of

PUSHPA SHRESTHA

Dr. Chaoqun Liu

_____

(Supervising professor)

Dr. Hristo Kojouharov

_____

Dr. Guojun Liao

_____

Dr. Yue Liu, (David)

_____

Copyright © by Pushpa Shrestha 2021

All right reserved.

# DEDICATION

I would like to dedicate this dissertation to my late mother Maya Devi Shrestha, who left this world when I was just a year. I love you maa and I hope that I have made you proud today. I wish you were here with me to share this moment. I will miss you forever. May the god be always with you. Rest in peace mamma.

ACKNOWLEDGEMENT

I would like to express my deep gratitude to my advisor professor Dr. Chaoqun Liu for his relentless guidance, support, and encouragement. I am thankful for his trust in giving me the research project and continuously encouraging and helping me out to get the results that I am including in this thesis. He has helped me a lot to grow and mature as a person as well as an academic researcher. I have also received some valuable suggestions and tips from him on becoming an effective teacher. I appreciate him for his help for guiding and recommending for several conferences, fellowship, and summer schools. I would also like to thank him for requesting CHAOS 2020 conference organizer to waive my registration fees. Without him, it would not have been possible to attend many conferences and seminars and write high quality journal and conference papers.

I am one of the members of Dr. Liu's research team, Center for Numerical Simulation and Modeling (CNSM) at University of Texas at Arlington. I would like to thank all my fellow friends and researchers at CNSM- Yifie Yu, Charles Nottage, Oscar Avarez, Dalal Almutairi, Vishwa Patel, Xuan My Trieu, and Aayush Bhattarai. I enjoyed every project and task that professor assigned me with the CNSM team. I am grateful for all their support and quality time they spent with me in problem solving and research discussions.

I would like to remember and thank my senior Dr. Sita Chakrit and post-doctoral students at CNSM, Dr. Yisheng Gao, Dr. Xiangrui Dong and Dr. James Liu for helping me in programming and modeling vortex structure. I have spent hours and hours of quality time studying and discussing several problems of fluid dynamics with Yifie Yu, which I will always remember.

I am very thankful to my graduate advisor, Dr. Hristo Kojouharov, who is also the first person I met in the department when I first came to the United States. Since then, he has been directing and helping me in every aspect of academic life that international students go through at the university. I thank him for keeping me up to date with the graduate timetable and helping in other academic and administrative issues I encountered during these four fruitful years. I would like to thank administrative officer Lona Donnelly for helping me regarding my administrative and other paper work related to teaching assistantship in the department. Michael Schmidtkunz is another important person of my Ph.D. journey who helped me a lot in computer

and technology management. I received a lot of help from him in my teaching class, calculus lab, conferences etc., in using classroom teaching technology. Thank you for everything!

I would like to thank my father, Khir Bahadur Shrestha, and my brothers Man Bahadur Shrestha and Yagya Shrestha for their support. My second brother Yagya was my classmate from pre-school to high school level. He is just not my brother but also a true friend to whom I can always trust and discuss the problems I am facing. I thank him for being a wonderful childhood companion.

A special thanks goes to my lovely wife, Ashmita Pradhan Shrestha, who is always been the bedrock of my success. She has been with me in so many ups and downs during these difficult times. She has been the source of my inspiration and I am grateful for her unconditional love and support. I feel so privileged and lucky that I have a caring, loving, and supportive wife like her.

I am grateful to my father-in law Amogh Pradhan and mother -in law Shova Pradhan for their love and support. I am grateful to always have their blessings with me.

Finally, I am thankful to all the teachers at Shree Seti Devi Higher Secondary School, Bhumlu-1, Saping, Kavre, Nepal and professors at Tribhuvan University, Nepal who have taught me at various levels. I want to say that I am what I am today because of all those teachers who taught at different levels. Once again, Thank you teachers !

ABSTRACT

LIUTEX BASED VORTEX IDENTIFICATION METHODS AND THEIR APPLICATION IN DNS STUDY OF THE BOUNDARY LAYER TRANSITION

PUSHPA SHRESTHA, Ph.D.

The University of Texas at Arlington, 2021

Supervising Professor: Dr. Chaoqun Liu

Vortices are intuitively known as the rotational motion of fluid particles, however a unambiguous and universally accepted methods of vortex definition and identification is not available till the date in the literature. First-generation of vortex identification methods, also known as vorticity-based vortex criterion, was first proposed by Helmholtz. But these methods have their own problems. These methods have shear contamination problem, and these methods did not accurately show the direction of fluid rotation. So, to overcome these problems, eigenvalues based second-generation vortex identification methods like Q, $\Delta$, $\lambda_2$, , $\lambda_{ci}$, and $\Omega$ have been proposed. Most of these second-generation methods are scalar quantities based on the Cauchy-Stokes decomposition of the velocity gradient tensor. But Cauchy-Stokes's decomposition itself is not Galilean invariant and its physical meaning is not clear.

In 2017/2018, the Center for Numerical Simulation and Modeling (CNSM) at the University of Texas at Arlington proposed a Liutex vector based on eigenvector of velocity gradient tensor to define vortex structure mathematically. Liutex method can give the local direction of fluid rotation and rotational strength. Since then, Liutex based vortex identification methods like Liutex core lines, Liutex tubes, Liutex-Omega method ( $\Omega_L$ ), and Modified Liutex-Omega method ( $\widetilde{\Omega}_L$ ), etc., have been proposed in fluid dynamics.

In this dissertation, the Direct Numerical Simulation (DNS) data is applied to all three generations of vortex identification methods and a comparative study has been done and proposed a best method to define and visualize vortex boundary. If we are focusing on vortex direction and uniqueness of the vortex structure, then Liutex core lines method is the appropriate method. However, if we are looking for smooth and clear iso-surface plotting of vortex structure, then we recommend Modified Liutex-Omega method.

A new coordinate system known as Principal Coordinates based on Liutex definition is proposed. A new unique velocity gradient tensor known as Principal Tensor has been proposed which is Galilean invariant. Then Principal Tensor is decomposed into rotation, stretching and shear part. Unlike traditional Cauchy-Stoke's decomposition, Principal Tensor decomposition is unique and Galilean invariant. Also, in this dissertation, first and second-generations vortex identification methods have been redefined and each redefined vortex definition can give the degree of contamination by shear and stretching or compressing effect. These new definitions also provide the dimension of each criterion which can help us decide which criterion is close to fluid rotation and choose the better one.

In final chapter of this dissertation, proper orthogonal decomposition (POD) is used with Liutex vector as an input instead of velocity vector to extract the coherent structure of late boundary layer flow transition but with significantly lower dimension. A singular value decomposition (SVD) algorithm is used as the POD method. It is observed that given fluid motion can be modeled by few early modes as they contain the large portion of total kinetic energy and later modes can be neglected as their kinetic energy converges to zero.

# TABLE OF CONTENTS

LIST OF ILLUSTRATIONS

LIST OF SYMBOLS

$M_\infty$ = Mach number

$Re$= Reynolds number

$x_{in}$ = distance between leading edge of flat plate and upstream boundary of computational domain

$\delta_{in}$ = inflow displacement thickness

$Lx$ = length of computational domain along x direction

$Ly$ = length of computational domain along y direction

$Lz_{in}$= height at inflow boundary

$T_w$ = wall temperature

$T_\infty$ = free stream temperature

Q = Q criterion

$\Delta$ = Delta criterion

$\lambda_2$ = Lambda-2 criterion

$\lambda_{ci}$ = Lambda-ci criterion

**R** = Liutex vector

R= Liutex magnitude

**r** = Liutex direction

$\Omega$ = Omega criterion

$\Omega_L$= Liutex-Omega criterion

$\widetilde{\Omega}_L$= Modified Liutex-Omega criterion

$\| \ \|_F$ = Frobenius norm

$\nabla v$= Gradient velocity tensor

$\nabla$V= Principal Tensor

$A^T$= Transpose of a matrix *A*

# CHAPTER 1

# INTRODUCTION

Vortices are naturally known as the rotational movement of liquid particles, and it tends to be seen everywhere in nature; from moving water to smoke to the storm. Turbulence is produced with various vortices of various sizes and qualities, known as coherent structures, in the fluid flow field. All in all, a vortex is known as the rotational movement of a fluid molecule in the vortex field. The idea of the vortex is yet a secret that presently cannot seem to be characterized mathematically unambiguously, despite the plentiful endeavors put in by researchers and specialists on this theme for quite a long time. Turbulence has several mysterious features like compressibility, instability, irregularity in motion, and difficulty in measuring it. These exceptional attributes of turbulence make it hard to define and determine. So, there is even not a solitary all around acknowledged mathematical meaning of turbulence that can give discreet and quantitative meaning. However, turbulence plays a prominent role in real life, like in the design, development, and maintenance of airplanes, predicting the weather, and studying the motion of blood in veins to avoid blockage etc.

Over the past three decades, several vortex identification methods such as Q, $\Delta$, $\lambda_2$, and $\lambda_{ci}$ have been proposed and applied in Direct Numerical Simulation (DNS) data to model and visualize the vortex structure in the transitional boundary layer. In 2009, Wu and Moin [1] recorded a DNS data for a flow transitions in a flat plate boundary layer with zero-pressure gradient. After the introduction of DNS data, different vortex identification schemes have been established and used amply with DNS data to survey the flow transition zones and the coherent structure in the boundary layer [2,3].

Helmholtz proposed vorticity-based methods like vortex lines, vortex tube, vortex filaments etc. in 1958 in Helmholtz's three theorem [4] and it was believed that these vorticity-based methods would provide a mathematical definition of the fluid rotational motion until 1990. In another words, at that time vorticity was considered as vortex. So, the concept of the vorticity concentration and other vorticity-based methods given by Helmholtz [4] and, H.; Saffma, P. [5] were widely accepted by many researchers in the literature. Zhou and Antonia [6] developed the spatially phase correlated vorticity to characterize large-scale and organized structures in the cylinder wake; but some serious dilemmas appeared in turbulent viscous flows. Also, it is proved by Epps, B., 2017 [7] that vorticity cannot distinguish a vortex region from a strong shear layer.

Yu et. all [8] conducted a correlation analysis among vorticity, Q method and Liutex, and found that vorticity is in fact poorly corelated with actual vortex, especially near the wall in the boundary layer. Moreover, Shrestha et. [55] all concluded that vorticity vector is severely contaminated by shear. The shear force is dominant in the boundary layer of turbulent viscous flows, but vorticity counts shear force as vortex, which is not. This contamination was the main reason behind weak correlation mentioned in [8]. Also, we noted that the direction of vorticity and vortex do not align with each other.

According to Lugt [9]and Robinson [10], an insightful existence of a vortex can be verified by closed or spiraling streamlines or path lines in fluid flow. Nevertheless, the streamlines or path lines are not Galilean invariant and thus cannot be an appropriate criterion for vortex identification.

There was a sheer need of new vortex identification method as vorticity and streamlines methods were deemed not good enough to model the vortex structure. In 1987, a critical theory was proposed by Perry and Chong [11] to describe eddying motions and flow patterns. Few years later in 1990, Chong and Perry [12] modified it to judge the presence of the local rotational motion. In fact, this method proposes a method for identifying vortices which refers to the presence of circular or spiral streamlines, which is also known as Δ- criterion. Although the Δ- criterion has been used successfully in many turbulence researches to mode and depict vortical structure, it has its own limitation. According to Jeong and Hussain [13], it does not always necessarily perform well. Moreover, it is extremely dependent on the selection of right threshold, and a proper threshold must be chosen to visualize the iso-surface plotting efficaciously.

The popular Q- criterion proposed by Hunt et al. [14] gives the region with positive second invariant of velocity gradient tensor. This method represents a local balance between the rotation and deformation rates of a fluid element. In fact, it gives the difference these two. Hence this method basically uses the same definition of a vortex as that invented by Chong et al. in 1990 [12], which is, a vortex is a connected region where the antisymmetric component of velocity gradient tensor predominates over the symmetric one. This criterion can capture and show the vortical structure effectively. However, this method is also threshold sensitive which could add a degree of ambiguity in vortex visualization. Moreover, Jeong and Hussain [13] pointed out that definition based on Q-method is not helpful in certain situations, especially when the streamline pattern becomes locally closed or spiral, without the presence of a truly vertical structure. Also,

Shrestha et. All [55] concluded that Q-method is severely contaminated by shearing and stretching or compressing effects.

Jeong and Hussain [13] introduced the $\lambda_2$ -criterion which is very famous in the literature. $\lambda_2$ is the second eigenvalue, when placed in increasing or decreasing order, of the symmetric tensor given by the sum of squares of symmetric and anti-symmetric components of velocity gradient tensor which is discussed briefly later in chapter 3. Although this method was developed to alleviate the possible drawbacks of Q and Δ criteria, this method is also threshold sensitive. Additionally, this method works only for a steady inviscid planar flow.

The $\lambda_{ci}$ criterion proposed by Zhou et al. [15] by improving Δ- criterion uses the imaginary part of the complex eigenvalues of the velocity gradient tensor to model and visualize the vortex structure. It is based on the idea that the local time-frozen streamlines display a rotational flow pattern when $\nabla\vec{v}$ has a pair of complex conjugate eigenvalues. This method also has the limitation as it also introduces the concept of arbitrary threshold.

According to Liu et al. (2019) [16] , vorticity-based methods are classified as the first generation (1G) of vortex identification methods, eigen-values based methods such as Q, Δ, $\lambda_2$ , and $\lambda_{ci}$ are regarded as the second generation (2G) of vortex identification methods, and the Liutex method, Liutex-Omega method (Liu et al., 2018) , Liutex-Core –Line method and other Liutex-based methods are regarded as third generation (3G) of vortex identification methods. Third generation of vortex identification method is considered best among the prevalent methods as it can answer the following questions that other methods cannot.

1) What is the absolute strength of vortex?
2) What is the relative strength of vortex?
3) What is the rotation axis of vortex?
4) What is the vortex core center?
5) What is the size of vortex core?
6) Where is the vortex boundary?

According to Liu [16], scalar based second-generation of vortex identification criteria like Δ, Q, $\lambda_2$ and $\lambda_{ci}$ have their shortcomings. One of them is that they can only depicted via iso-surface and are threshold sensitive which is case-related, empirical, and hard to adjust. In addition, $Q$ and $\lambda_2$ are restrictive for vortex identification for incompressible flows due to their

incompressibility assumption. Also, as per Shrestha [55], these methods were contaminated by shear and stretching at different levels. To alleviate this problem, Dr. Liu introduced the vortex identification schemes like Omega, Liutex, Liutex-omega, Liutex core lines etc. schemes. He proposed the new Ω-method (omega-method) in 2016 [17] as a new identification method to capture vortex structures which is moderately tolerant to threshold change. The Ω-method is nothing but a proportion of vorticity in the fluid rotation that also has deformation mixed in it and when that proportion is more than 50 percent, the Ω-method can capture the vortical structure. In this research, we have used $\Omega = 0.52$. Unlike other schemes, the Ω-method has a clear physical meaning.

Despite being able to get some popularity in the literature, the robustness of these method was always questionable since they were all scalar quantities. Fluid rotation certainly has a direction. So, vortex identification schemes were supposed to represent that, but these methods were just scalar quantities. This was one of the biggest hindrances in turbulence research. Additionally, for most these scalar-based vortex identification criteria, the sensitivity to the threshold selection provides a large number of difficulties in making a judgment to define the boundary of vortical structures. These issues prompted the development of the new concept of Liutex/Rortex [18,19]. Unlike the first- and second-generation vortex identification criteria, the Liutex method is a novel eigenvector-based method which is local, accurate, unique, and systematically defined. Furthermore, the systematical definition of Liutex is given in scalar, vector, and tensor forms. Liutex is defined as a vector and its local direction is given by eigen vector of velocity gradient tensor. The scalar form of Liutex represents the rotational strength of the fluid rotation, whereas the vector form gives the direction of the local fluid rotation. The idea of Liutex scheme proposed by Liu was able to give a local direction as well as strength of the fluid rotation. Gao and Liu also gave the scalar, vector, and tensor form of the Liutex method and compare with other eigenvalue-based methods [19]. According to Liu, If the velocity gradient tensor of a three-dimensional flow field has a pair of complex conjugate eigenvalues and a real eigenvalue, the instantaneous streamline pattern presents a local swirling motion around the axis of the local fluid rotation, which is the real eigenvector of velocity gradient tensor and known as direction of Liutex. Yu et al [20] proposed the concept of Principal Coordinates and gave the new unique tensor decomposition in the Principal Coordinates based on Liutex method.

After the advent of Liutex method, many other Liutex based methods such as Liutex-omega [21], Modified Liutex-omega [22], Liutex core lines [23] etc. were developed. Liutex-omega method was proposed as a combination of Liutex and Omega methods, which gives the best iso-surface structure of vortex as Liutex-Omega method is free from shear. This is the reason Liutex-omega method was able to give smooth and accurate structure. In this thesis, we use Liutex-Omega method for this reason. Despite being able to capture both weak and strong vortices simultaneously, it displayed a bulging phenomenon on iso-surface while displaying the vortex boundary. So, to get rid of this inadequacy, Modified Liutex-omega [22] method was proposed. Modified Liutex-omega method is a robust on capturing vortex boundary, it was still moderately affected by threshold change. So, Dr. Liu proposed a new method called Liutex core lines [23] which is unique and is free from iso-surface. So, it exempts us from the nuisance of choosing the proper threshold. Also, Liutex tensor decomposition is presented in the reference [24]. The Liutex vector is also Galilean invariant [25,26].

In this dissertation, we introduce the concept of unique Principal coordinate and tensor decomposition in Principal coordinate, also known as principal tensor decomposition. we demonstrate the shear and stretching contamination of several 2G vortex identification methods from both mathematical formula and numerical experiments. After calculating the velocity gradient tensor at a point inside the vortex boundary, the velocity gradient tensor is decomposed, which is unique and is done in the Principal Coordinate. In other words, the velocity gradient tensor is uniquely decomposed into rigid rotation part, stretching part, and shearing part in the Principal Coordinate.

In chapter 6 of this dissertation, the proper orthogonal decomposition (POD) is used with the modified Omega-Liutex method to capture the vortices of POD modes in the late boundary layer to model and visualize the coherent structure of vortices efficiently in the boundary layer and attain more structures in both weak and strong vortices at the same time. Since the late flow transition is more complex and random than early flow transition, POD decomposition is a very useful and convenient tool to extract the whole structure into coherent structures according to the features such as energy content and mode shape. In another words, complex vortex structures can be reconstructed with same energy content but with significantly lower dimension.

The POD is one of the most broadly applied modal decompositions and dimensionality reduction method to analyze vortex structure in fluid flows. There are two versions of POD technique. Initially the POD was proposed by Lumley [27] in 1967 to explore the turbulent flow. In 1987 Sirovich [28] introduced the other version of POD known as snapshot POD. Both versions of POD are equivalent to singular value decomposition (SVD) method. So. SVD method is used in this dissertation for POD analysis of late flow transition. In recent years, there have been many applications about POD in many fields of fluid dynamics. POD can be used to analyze and model turbulent flow because this method makes it possible to analyze and combine space–time data at the same time (averaged time). In POD method, the orthogonal modes ranked according to their kinetic energy content. Due to limited computing memory, POD modes with high energy content are used to optimize the computation. First mode contains the largest kinetic energy of the flow and it decreases gradually as we go on to next mode. Many researchers have used POD method to study the flow structure. In research [29-32], POD was used to analyze the flow structures in various cases and scenarios. Dong et. all applied POD analysis on vortical structures in MVG wake by Liutex core line identification [33]. POD method has also been applied to flow transition in the boundary layer. Gunes used proper orthogonal decomposition method to reconstruct a transitional boundary layer with and without control [34]. Yand et. all studied the POD Analyses on vortex structure in the late transition [35]. The study done by Chakrit et. all [36] also applies POD method for analysis of losing symmetry in late flow transition but unlike us, she proposes that antisymmetric flow starts from the middle part of boundary layer. Recently, Cavalieri, A., Schlatter P., Vinuesa, R., Henningson, D. and Abreu, L. conducted the comparative study between spectral proper orthogonal decomposition (SPOD) and resolvent analysis of near-wall coherent structures in turbulent pipe flows where they concluded that the SPOD modes are simply the response modes from resolvent analysis, with SPOD eigenvalues equal to the square of resolvent gains [37].

# CHAPTER 2
# NUMERICAL CASE SETUP

For all the research and results in this dissertation, the Direct Numerical Simulation (DNS) data of fluid flow in the flat plate boundary layer transition was received from Texas Advanced Computing Center (TACC) and is used to model and simulate the fluid flow. The FORTRAN code DNSUTA_HS developed by Center for Numerical Simulation and Modeling (CNSM) at UTA in the leadership of professor Dr. Chaoqun Liu in 2009 and was also validated and approved by NASA Langley. The results were compared to experiments and other DNS results [1, 2] found consistent and accurate.

The motion of a fluid can be described by the conservation of mass, momentum, and of energy for an arbitrary control volume. So, first we discuss about the governing equations.

## 2.1 Governing Equations

### 2.1.1 Conservation of Mass (Continuity Equation)

Let $S$ be a closed surface with volume $V$ which has $a$ fixed position with respect to x, y and z coordinates. Suppose the density of the fluid be $\rho$ at a position (x, y, z) and at time $t$, then,

The mass of the fluid enclosed by the surface at any instant $= \int \rho \, dV$,

and,

the net rate at which the mass flows outwards across the surface $= \int \rho \, \boldsymbol{u}.\boldsymbol{n} \, dS$,

where $\boldsymbol{u}$ is the velocity of mass flowing outwards across the surface, unit normal vector $\boldsymbol{n}$ is directed outward of the surface $S$, and $dV$ and $dS$ are respectively infinitesimal volume and area of the closed surface.

Note: volume = area × distance = $dS \times \boldsymbol{u} \times t$

According to the conservation of mass of the fluid, net rate of fluid mass flowing in is equal to the net rate of fluid mass flowing outwards across the surface, i.e.

$$\frac{\partial}{\partial t} \int \rho \, dV = - \int \rho \, \boldsymbol{u}.\boldsymbol{n} \, dS.$$

$$\int \frac{\partial \rho}{\partial t}\, dV + \int \rho\, \boldsymbol{u}.\boldsymbol{n}\, dS = 0. \tag{2.1}$$

Then, since the volume *V* is fixed in space, the differentiation under the integral sign, and the transformation of the surface integral (by the Gaussian divergence theorem) gives

$$\int \frac{\partial \rho}{\partial t}\, dV + \int \nabla.(\rho \boldsymbol{u})\, dV = 0.$$

or

$$\int [\frac{\partial \rho}{\partial t} + \nabla.(\rho \boldsymbol{u})] dV = 0. \tag{2.2}$$

This relation is true for all *V* that lies entirely in the fluid, and therefore, it is continuous in *x*, *y* and *z*. So, it must be identically zero everywhere in the fluid. Hence, we have the continuity equation,

$$\frac{\partial \rho}{\partial t} + \nabla.(\rho \boldsymbol{u}) = 0. \tag{2.3}$$

Note: Divergence theorem states that flux across the surface *S* is equal to total divergence of $\boldsymbol{u}$ over the region that covers volume *V*. i.e.,

$$\iint \rho \boldsymbol{u}.\boldsymbol{n}\, ds \;=\; \iiint \nabla.\boldsymbol{u}\, dV$$

2.1.2 Conservation of Momentum (Equation of Motion)

The conservation of momentum in a control volume V requires that the changes of momentum in this volume must be equal to net rate of momentum gained/lost through the surface that encloses this volume and what is created/consumed by sources and sinks inside the control volume. As in continuity equation, consider a volume of fluid *V* enclosed by a surface *S*, fixed with respect to the coordinate axes. For this body of fluid, the momentum is given by the equation,

$$\int \rho \boldsymbol{u}\, dV,$$

and rate of change of momentum is given by,

$$\frac{\partial}{\partial t} \int \rho \boldsymbol{u}\, dV = \int \frac{\partial (\rho \boldsymbol{u})}{\partial t}\, dV. \tag{2.4}$$

Now, the net rate of what is gained or lost through the surface *S* is given by,

$$\int \rho \boldsymbol{u}(\boldsymbol{u} \cdot \boldsymbol{n})\, dS = \int \nabla \cdot (\rho \boldsymbol{u} \otimes \boldsymbol{u})\, dV,$$

which is gotten from the divergence theorem i.e. the flux of a vector field through a closed surface is equal to the divergence of the field in the volume enclosed and $\otimes$ represents the outer product, that is,

$\rho \boldsymbol{u} \otimes \boldsymbol{u} = \rho \boldsymbol{u}\boldsymbol{u}^T$ which is a tensor.

If we let $\boldsymbol{b}$ be the sources and sinks inside the control volume V, then the conservation of momentum inside the volume *V* is given by,

$$\int \frac{\partial(\rho \boldsymbol{u})}{\partial t}\, dV = -\int \nabla \cdot (\rho \boldsymbol{u} \otimes \boldsymbol{u}) dV + \int \rho \boldsymbol{b}\, dV,$$

Which can be written as

$$\int \left[\frac{\partial(\rho \boldsymbol{u})}{\partial t} + \nabla \cdot (\rho \boldsymbol{u} \otimes \boldsymbol{u}) - \rho \boldsymbol{b}\right] dV = 0.$$

Since the volume *V* is arbitrary inside the fluid, we must have,

$$\frac{\partial(\rho \boldsymbol{u})}{\partial t} + \nabla \cdot (\rho \boldsymbol{u} \otimes \boldsymbol{u}) - \rho \boldsymbol{b} = 0,$$

or

$$\frac{\partial(\rho \boldsymbol{u})}{\partial t} + \nabla \cdot (\rho \boldsymbol{u} \otimes \boldsymbol{u}) = \rho \boldsymbol{b}. \tag{2.5}$$

where forces $\boldsymbol{b}$ may be separated into two types: the stress form forces and body forces.

Then, we have,

$$\rho \boldsymbol{b} = \rho \boldsymbol{f} + (\nabla \cdot \sigma), \tag{2.6}$$

where $\boldsymbol{f}$ represents the body forces and $\sigma$ is the stress force tensor. The stress force is forces acting within a body as a response to external applied forces and body forces. It can be divided into normal and shear components.

If we assume a Newtonian fluid, there is a linear relation between the stress ($\sigma$) and the rate of strain of the fluid, then by Stokes (1845),

$$\sigma = -(p - \mu_v \nabla \cdot \boldsymbol{u})\boldsymbol{I} + \mu\left[\nabla \boldsymbol{u} + (\nabla \boldsymbol{u})^T - \frac{2}{3}(\nabla \cdot \boldsymbol{u})\boldsymbol{I}\right], \tag{2.7}$$

where $p$ is the pressure, $\mu_v$ is the bulk viscosity related to the viscosity $\mu$ by

$$\mu_v = \lambda + \frac{2}{3}\mu, \tag{2.8}$$

and according to Stokes' hypothesis, $\mu$ is taken to make $\mu_v = 0$.

Therefore,

$$\sigma = -p\boldsymbol{I} + \lambda(\nabla \cdot \boldsymbol{u})\boldsymbol{I} + \mu[\nabla \boldsymbol{u} + (\nabla \boldsymbol{u})^T] = -\left[p + \frac{2}{3}\mu(\nabla \cdot \boldsymbol{u})\right]\boldsymbol{I} + \mu[\nabla \boldsymbol{u} + (\nabla \boldsymbol{u})^T]. \tag{2.9}$$

Hence, the conservation of momentum equations can be written as

$$\frac{\partial(\rho \boldsymbol{u})}{\partial t} + \nabla \cdot (\rho \boldsymbol{u} \otimes \boldsymbol{u}) = \rho \boldsymbol{f} - \nabla p - \frac{2}{3}\nabla[\mu(\nabla \cdot \boldsymbol{u})] + \nabla[\mu(\nabla \boldsymbol{u} + (\nabla \boldsymbol{u})^T)]. \tag{2.10}$$

### 2.1.3 Conservation of Energy

From the first law of Thermodynamics, the conservation of energy for a fluid of volume $V$ contained within a surface $S$ can be found by calculating the work done on the mass of fluid by volume, surface forces, and the heat gained through transfer across the boundary and other sources inside the volume. The total energy $E$ provides the conserved quantity, and is defined as the sum of its internal energy and kinetic energy per unit mass, i.e.

$$E = e + \frac{1}{2}\boldsymbol{u} \cdot \boldsymbol{u}, \tag{2.11}$$

where $e$ is the internal energy per unit mass of the fluid.

The rate of change of the total energy inside the volume $V$ contained within a surface $S$ is given by,

$$\frac{\partial}{\partial t}\int \rho E \, dV = \int \frac{\partial(\rho E)}{\partial t} \, dV,$$

while the net rate of energy gained or lost through the surface is given by

$$\int (\rho E)\boldsymbol{u} \cdot \boldsymbol{n} \, dS = \int \nabla \cdot (\rho E)\boldsymbol{u} \, dV.$$

Also, heat is transferred to the fluid in the volume by molecular conduction through the surface *S*,

So, we have,

$$\int (k\nabla T) \cdot \boldsymbol{n} \, dS = \int \nabla \cdot (k\nabla T) \, dV,$$

where *T* is the absolute temperature and *k* is the thermal conductivity coefficient of the fluid.

The work done on the fluid by forces can be divided into volume and surface sources.

The volume sources include the volume forces $\boldsymbol{f}$, and heat sources $q_H$ other than conduction, such as radiation or heat released by chemical reactions. This gives the work done for the volume *V*,

$$\int (\rho \boldsymbol{f} \cdot \boldsymbol{u} + q_H) \, dV.$$

The work done on the fluid by the surface sources, i.e., internal shear stresses ($\sigma$) acting on the surface of the volume considering that there are no external surface heat sources, is given by,

$$\int (\sigma \cdot \boldsymbol{u}) \cdot \boldsymbol{n} \, dS = \int \nabla \cdot (\sigma \cdot \boldsymbol{u}) \, dV.$$

By grouping all terms, we get the energy conservation equation,

$$\int \frac{\partial(\rho E)}{\partial t} \, dV + \int \nabla \cdot (\rho E)\boldsymbol{u} \, dV = \int \nabla \cdot (k\nabla T) \, dV + \int (\rho \boldsymbol{f} \cdot \boldsymbol{u} + q_H) \, dV + \int \nabla \cdot (\sigma \cdot \boldsymbol{u}) \, dV,$$

or

$$\frac{\partial(\rho E)}{\partial t} + \nabla \cdot (\rho E)\boldsymbol{u} - \nabla \cdot (k\nabla T) - \nabla \cdot (\sigma \cdot \boldsymbol{u}) = \rho \boldsymbol{f} \cdot \boldsymbol{u} + q_H, \tag{2.12}$$

with

$$\sigma = -\left[p + \frac{2}{3}\mu(\nabla \cdot \boldsymbol{u})\right]\boldsymbol{I} + \mu[\nabla \boldsymbol{u} + (\nabla \boldsymbol{u})^T]. \tag{2.13}$$

2.2. Numerical Setup

The numerical domain has the grid number $1920\times 128\times 241$, representing the number of grids in streamwise (x), spanwise (y), and wall normal (z) directions. In normal direction, these grids are stretched while in streamwise and spanwise directions, they are uniform. The length of the first grid interval in the normal direction at the entrance is found to be 0.43 in wall units (Z+ = 0.43). The flow parameters are listed in Table 1. Here, $M_\infty$ is Mach number, $Re$ is Reynolds number and, $T_w$ $and$ $T_\infty$ are wall and free stream temperature, respectively. Likewise, $x_{in}$ represents the distance between leading edge and inlet of the flat plate and, $Lx, Ly$, $Lz_{in}$ is the inflow displacement thickness.

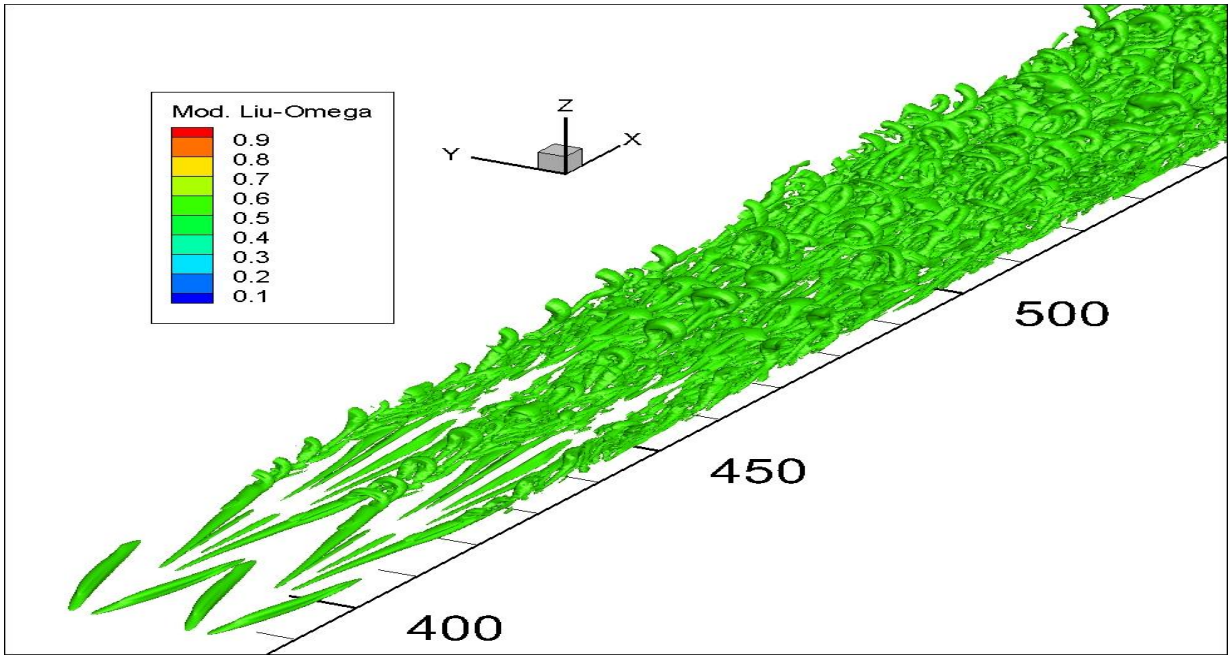


Figure 2.1. Vortex structure in transitional boundary with $\widetilde{\Omega}_L = 0.52$.

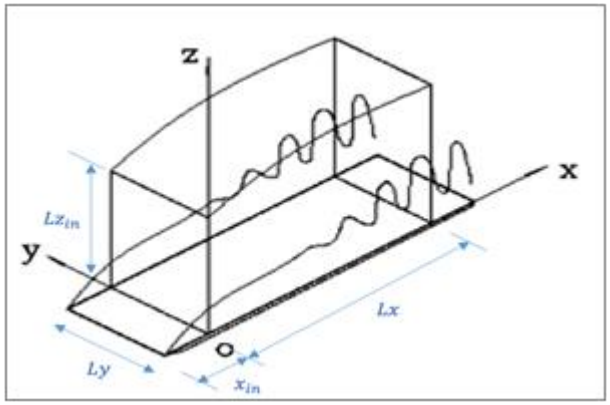


Figure 2.2. Computation domain

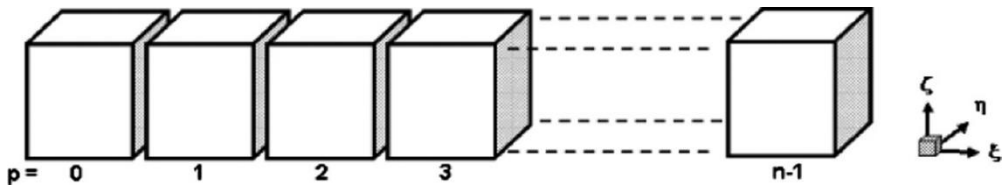


Figure 2.3. Domain decomposition along the streamwise direction in the computational space.

| $M_\infty$ | $Re$ | $x_{in}$ | $Lx$ | $Ly$ | $Lz_{in}$ | $T_w$ | $T_\infty$ |
|---|---|---|---|---|---|---|---|
| 0.5 | 1000 | $300.79\delta_{in}$ | $798.03\delta_{in}$ | $22\delta_{in}$ | $40\delta_{in}$ | 273.15K | 273.15K |

Table 2.1. DNS parameters

The parameters in Table 1 are defined as

$M_\infty$ = Mach number

$Re$ = Reynolds number

$x_{in}$ = distance between leading edge of flat plate and upstream boundary of computational domain

$\delta_{in}$ = inflow displacement thickness

$Lx$ = length of computational domain along x direction

$Ly$ = length of computational domain along y direction

$Lz_{in}$= height at inflow boundary

$T_w$ = wall temperature

$T_\infty$ = free stream temperature

For more detail about case setup and validation of code, one can see the references [2,3]. Similar case setup can be found in the references [38-40]. But for POD analysis of late flow transition, a particular region in late flow transition is selected which is discussed in chapter 6 in details.

# CHAPTER 3

# VORTEX IDENTIFICATION METHODS

Over the past three decades, many vortex identification methods have been proposed and developed in the literature to model and simulate the vortex structures. They all have their pros and cons. So, we are yet to find an unambiguous and globally accepted vortex identification methods. According to Liu [16], vortex identification methods are categorized in to three generations. Vorticity vector-based methods are known as first-generation methods while eigenvalue-based methods are known as second generation methods. Liutex [18,19] and other Liutex based methods such as Liutex tube, Omega-Liutex methods [21], Modified Omega-Liutex method [22], Liutex core lines [23], etc., are known as third-generation methods of vortex identification. In this chapter, first we briefly review them and then discuss about their strengths and limitations in details.

## 3.1 First Generation Vortex Identification Methods.

All the vorticity-based methods such as vorticity lines, vorticity tubes, vorticity filaments are known as first generation methods of vortex identification. These vorticity-based methods were popular in fluid dynamics till early 1990 and then different eigenvalue-based methods were proposed which are still in use.

Definition 3.1:

Vorticity vector is the curl of vector field. i.e., if v is the velocity of a fluid particle, then,

$$\text{Vorticity} = \text{Curl}\,\mathbf{v} = \nabla \times \mathbf{v} = \begin{vmatrix} \mathbf{i} & \mathbf{j} & \mathbf{k} \\ \frac{\partial}{\partial x} & \frac{\partial}{\partial y} & \frac{\partial}{\partial z} \\ u & v & w \end{vmatrix}$$

$$\text{Vorticity} = \mathbf{i}\left(\frac{\partial w}{\partial y} - \frac{\partial v}{\partial z}\right) - \mathbf{j}\left(\frac{\partial w}{\partial x} - \frac{\partial u}{\partial z}\right) + \mathbf{k}\left(\frac{\partial v}{\partial x} - \frac{\partial u}{\partial y}\right)$$

Vorticity based methods like vortex lines, vortex tube, vortex filaments etc. were introduced by Helmholtz in 1958 in Helmholtz's three theorem [4].

### 3.1.1 Vorticity-based methods

Definition 3.2.

A vortex line is a line whose tangent is everywhere parallel to the local vorticity vector. A vortex line is related to vorticity vector as the same way streamlines relate to velocity vector.

Definition 3.3.

The vortex lines drawn through each point of a closed curve in the velocity field form the surface which is called a vortex tube.

Definition 3.4.

A vortex filament is a vortex tube whose cross-section is of infinitesimal dimensions. In another word, vortices consist of small vorticity tubes which are called vortex filaments.

Since Helmholtz introduced the concept of vorticity tube/filament in 1858 [4], many researchers have assumed that vortices consist of vortex filaments, and the magnitude of vorticity gives the vortex strength. In fluid mechanics, Helmholtz's three theorems explain the three-dimensional motion of fluid particles in the surrounding area of vortex filaments. These theorems apply to inviscid flows, which means flows where the impact of viscous forces are so small that it can be overlooked.

Helmholtz's first theorem:
The strength of a vortex filament is constant along its length.
Helmholtz's second theorem:
A vortex filament cannot end in a fluid; it must extend to the boundaries of the fluid or form a closed path.
Helmholtz's third theorem:
In the absence of rotational external forces, a fluid that is initially irrotational remains irrotational.

As mentioned before, Helmholtz's theorems apply to inviscid flows only. But, in viscous flows, the strength of the vortices always decays slowly due to the dissipative effect of viscous forces.

3.2 Second Generation Vortex Identification Methods.

3.2.1 Δ Method

According to Chong et al., 1990 [12] The Δ method defines a vortex to be the region where the velocity gradient tensor $\nabla\vec{v}$ has a pair of complex conjugate eigenvalues and a real eigenvalue. If $\lambda_1, \lambda_2 \; and \; \lambda_3$ are three eigenvalues of the 3× 3 matrix of $\nabla\vec{v}$, then the characteristic equation can be written as:

$$\lambda^3 + I_1\lambda^2 + I_2\lambda + I_3 = 0 \tag{3.1}$$

where, $I_1$, $I_2$, and $I_3$ are the first, second and third invariants of the characteristic equation (3.1) and given by

$$I_1 = -(\lambda_1 + \lambda_2 + \lambda_3) = -tr(\nabla\vec{v}) \tag{3.2}$$

$$I_2 = \lambda_1\lambda_2 + \lambda_2\lambda_3 + \lambda_3\lambda_1 = -\frac{1}{2}[\mathrm{tr}(\nabla\vec{v}^2) - \mathrm{tr}(\nabla\vec{v})^2] \tag{3.3}$$

$$I_3 = -\lambda_1\lambda_2\lambda_3 = -\det(\nabla\vec{v}) \tag{3.4}$$

The discriminant of the characteristic equation (3.1) of the velocity gradient tensor is given by

$$\Delta = \left(\frac{\tilde{Q}}{3}\right)^3 + \left(\frac{\tilde{R}}{2}\right)^2 \tag{3.5}$$

where, $\tilde{Q} = I_2 - \frac{1}{3}{I_1}^2$ and, $\tilde{R} = I_3 + \frac{2}{27}\,{I_1}^3 - \frac{1}{3}I_1I_2$.

For incompressible flow, the first invariant of the characteristic equation (3.1) $I_1 = 0$. So, in this case, the discriminant of the characteristic equation (3.5) becomes $\Delta = \left(\frac{I_2}{3}\right)^3 + \left(\frac{I_3}{2}\right)^2$. If $\Delta \leq 0$, all three eigenvalues of $\nabla\vec{v}$ are real, in this case there is no fluid rotation. If $\Delta > 0$, there exists one real and two conjugate complex eigenvalues which means that the point is inside a vortex region. $\Delta$ method is a scalar method by using the iso-surface to show the vortex structure. The iso-surface is very sensitive to the selection of threshold, which is man-made and arbitrary in general.

### 3.2.2 $Q$ Criterion

The $Q$ method is one of the most popular methods to model and visualize the vortex structure, which was proposed by Hunt et al. (1988) [14]. Although $Q$ is the second invariant in the eigenvalue equation (3.1) given above, the value of $Q$ can also be calculated as half of the difference of squares of the Frobenius norm of vorticity tensor and strain-rate tensor. i.e.,

$$Q = \frac{1}{2}(\|B\|_F^2 - \|A\|_F^2) \tag{3.6}$$

where $A$ and $B$ are the symmetric and anti-symmetric part of the velocity gradient tensor, respectively.

$$A = \frac{1}{2}(\nabla\vec{v} + \nabla\vec{v}^T) = \begin{bmatrix} \frac{\partial u}{\partial x} & \frac{1}{2}\left(\frac{\partial u}{\partial y} + \frac{\partial v}{\partial x}\right) & \frac{1}{2}\left(\frac{\partial u}{\partial z} + \frac{\partial w}{\partial x}\right) \\ \frac{1}{2}\left(\frac{\partial v}{\partial x} + \frac{\partial u}{\partial y}\right) & \frac{\partial v}{\partial y} & \frac{1}{2}\left(\frac{\partial v}{\partial z} + \frac{\partial w}{\partial y}\right) \\ \frac{1}{2}\left(\frac{\partial w}{\partial x} + \frac{\partial u}{\partial z}\right) & \frac{1}{2}\left(\frac{\partial w}{\partial y} + \frac{\partial v}{\partial z}\right) & \frac{\partial w}{\partial z} \end{bmatrix} \tag{3.7}$$

$$B = \frac{1}{2}(\nabla\vec{v} - \nabla\vec{v}^T) = \begin{bmatrix} 0 & \frac{1}{2}\left(\frac{\partial u}{\partial y} - \frac{\partial v}{\partial x}\right) & \frac{1}{2}\left(\frac{\partial u}{\partial z} - \frac{\partial w}{\partial x}\right) \\ \frac{1}{2}\left(\frac{\partial v}{\partial x} - \frac{\partial u}{\partial y}\right) & 0 & \frac{1}{2}\left(\frac{\partial v}{\partial z} - \frac{\partial w}{\partial y}\right) \\ \frac{1}{2}\left(\frac{\partial w}{\partial x} - \frac{\partial u}{\partial z}\right) & \frac{1}{2}\left(\frac{\partial w}{\partial y} - \frac{\partial v}{\partial z}\right) & 0 \end{bmatrix} \tag{3.8}$$

The $Q$ method considers that a vortex occurs in the region where the second invariant of the characteristic equation (3.1) is positive, i.e., $Q > 0$. $Q$ method can easily determine the boundary of the vortex structure through iso-surface. Despite being convenient to use, Q method has its drawback as well. First, $Q$ is a scalar, and a proper threshold is required to visualize the vortex region. Also, there does exist an inconsistency between the $\Delta$ method and $Q$ method as $\left(\frac{\tilde{R}}{2}\right)^2$ is always positive and even if $Q < 0$, it is still possible that $\Delta$ could be positive, which indicates the point is still inside a vortex region.

### 3.2.3 $\lambda_{ci}$ Criterion

The $\lambda_{ci}$ criterion proposed by Zhou et al., 1999; [15] uses the imaginary part of the complex eigenvalues of the velocity gradient tensor to find the boundary of the vortex structure. This criterion is based on the idea that the local time-frozen streamlines display a rotational flow

pattern when $\nabla\vec{v}$ has a pair of complex conjugate eigenvalues. In this case, the tensor transformation of $\nabla\vec{v}$ is given by

$$\nabla\vec{v} = [\vec{v}_r\ \vec{v}_{cr}\ \vec{v}_{ci}]\begin{bmatrix}\lambda_r & 0 & 0\\ 0 & \lambda_{cr} & \lambda_{ci}\\ 0 & -\lambda_{ci} & \lambda_{cr}\end{bmatrix}[\vec{v}_r\ \vec{v}_{cr}\ \vec{v}_{ci}]^{-1} \tag{3.9}$$

where $\lambda_r$ is the real eigenvalue with corresponding eigenvector $\vec{v}_r$ and the complex conjugate pair of complex eigenvalues are $\lambda_{cr} \pm i\lambda_{ci}$ with corresponding eigenvectors $\vec{v}_{cr} \pm i\ \vec{v}_{ci}$. In this case, in the local curvilinear system $(c_1, c_2, c_3)$ spanned by the eigenvector $(\vec{v}_r, \vec{v}_{cr}, \vec{v}_{ci})$, the instantaneous streamlines exhibit spiral motion. The equations of such streamlines can be written as:

$$c_1(t) = c_1(0)e^{\lambda_r t} \tag{3.10}$$

$$c_2(t) = [c_2(0)\cos(\lambda_{ci}t) + c_3(0)sin(\lambda_{ci}t)]e^{\lambda_{cr}t} \tag{3.11}$$

$$c_3(t) = [c_3(0)\cos(\lambda_{ci}t) - c_2(0)sin(\lambda_{ci}t)]e^{\lambda_{cr}t} \tag{3.12}$$

The strength of this swirling motion was improperly quantified by $\lambda_{ci}$ as the $\lambda_{ci}$ cannot be exactly the pure rotation strength. $\lambda_{ci}$ is also characterized as a scalar-valued criterion. Note that Eq. (3.9) represents a similar transformation (not orthogonal transformation) that cannot keep vorticity unchanged. In another words, due to unorthogonal nature, this method is hugely dependent on coordinate selection.

### 3.2.4 $\lambda_2$ Criterion

The $\lambda_2$ criterion states the facts that pressure is minimum on the axis of rotation when the centrifugal force is balanced by the pressure force (the so-called cyclostrophic balance). It is valid only in a steady inviscid planar flow (Jeong, J., and Hussain, F., 1995). However, this assumption fails to identify vortices under strong unsteady and viscous effects accurately. By neglecting these unsteady and viscous effects, the symmetric part S of the gradient of the incompressible Navier–Stoke's equation can be expressed as:

$$S = A^2 + B^2 = -\frac{\nabla(\nabla p)}{\rho} \tag{3.13}$$

where *p* is the pressure and the equation (3.13) is a representation of the pressure Hessian matrix

$((\nabla(\nabla p))_{ij} = \frac{\partial^2 p}{\partial x_i \partial y_i}$. To capture the region of local pressure minimum in a plane perpendicular to vortex core line, Jeong & Hussain defined the vortex core as a connected region with two positive eigenvalues of the pressure Hessian matrix, i.e., a connected region with two negative eigenvalues of the symmetric tensor S. If $\lambda_{S1}, \lambda_{S2}$ & $\lambda_{S3}$ are three real eigenvalues of the symmetric tensor S and when setting them in order in such a way that $\lambda_{S1} \geq \lambda_{S2} \geq \lambda_{S3}$, there must be $\lambda_{S2} < 0$ as two eigenvalues are negative( second derivative negative at maximum points ,i.e. pressure is minimum and $A^2 + B^2$ is maximum), which confirms that there exists vortex. In general, $\lambda_{S2}$ cannot be expressed in terms of eigenvalues of velocity gradient tensor; however, in some special cases when eigenvectors are orthonormal, $\lambda_{S2}$ can be exclusively determined by eigenvalues of velocity gradient tensor. Vortex structure can be visualized as iso-surface by selecting a proper threshold of $\lambda_{S2}$. The relation between the eigenvalues of the symmetric tensor $A^2 + B^2$ and second invariant $Q$ is given by:

$$Q = -\frac{1}{2} tr(A^2 + B^2) = -\frac{1}{2}(\lambda_{S1} + \lambda_{S2} + \lambda_{S3}) \tag{3.14}$$

It can be shown that while the $Q$ criterion measures the excess of vorticity rate over the strain rate magnitude in all directions, the $\lambda_2$ criterion looks for this excess only on a specific plane. Another similar article, "on the relationship between vortex identifications methods" by Chakraborty & Balachandar (2005) [41] is also reviews the vortex identification methods.

3.2.5. $\Omega$ – method

Omega method proposed by Dr. Chaoqun Liu et. al in 2016 [21] measures the relative strength of vortices and it is defined as the ratio of Frobenius norm of vorticity tensor squared over the sum of Frobenius norm of vorticity tensor squared and Frobenius norm of deformation tensor squared.

$$\Omega = \frac{\|B\|_F^2}{\|A\|_F^2 + \|B\|_F^2} = \frac{b}{a+b+\varepsilon} \tag{3.15}$$

where $A = \frac{1}{2}(\nabla\vec{v} + \nabla\vec{v}^t)$, $B = \frac{1}{2}(\nabla\vec{v} - \nabla\vec{v}^t)$, $a = Trace(A^t A)$, $b = Trace(B^t B)$, and $\varepsilon$ is a small positive number used to avoid division by zero.

According to [16], the $\Omega-$ method was compared with the other identification methods like $Q$ and $\lambda_2$ and it is confirmed that Ω-method has some advantages mentioned below:

1) the $\Omega-$ method can capture vortex very well and is very easy to use.
2) the physical meaning of Ω is clear.
3) $Q$ and $\lambda_2$ iso-surface visualization needs appropriate thresholds to capture the vortex structure properly. But Ω method does not need much adjustment and the iso-surfaces of Ω=0.52 can always capture the vortices properly in all the cases at different time steps.
4) $Q$ and $\lambda_2$ methods can only capture either strong or weak vortex. When threshold is set high, only the strong vortex is captured while weak vortices are lost. Similarly, when threshold is set low, only weak vortices are captured but strong vortices are smeared. But Ω method with threshold of Ω=0.52 can capture both weak and strong vortices simultaneously.

Since $\Omega-$ method was introduced in 2016 for the first time in the literature, it has been used by several researchers as it is very effective to capture both weak and strong vortices [42,43]. However, the value of $\varepsilon$ is case-related and requires an appropriate adjustment. Then, Dong et al. [44] gave an explicit formula to determine the value of $\varepsilon$ as

$$\varepsilon = 0.001(b-a)_{max} = 0.002Q_{max} \tag{3.16}$$

The term $(b-a)_{max}$ is easy to obtain as a fixed number at each time step in a certain case. In [44], it is shown that $\varepsilon$ is a proper number for many cases. After $\varepsilon$ is determined, the adjustment of $\varepsilon$ in any case in vortex visualization is not necessary. Therefore, we can capture and visualize the vortex structure by Omega method with $\varepsilon$ given by above formula.

## 3.3 Third Generation Vortex Identification Methods.

### 3.3.1 Liutex Method

Definition 3.5.

Liutex is a vector defined as

$$\boldsymbol{R} = R\boldsymbol{r} \tag{3.17}$$

Where R is the magnitude of Liutex, and $\boldsymbol{r}$ is the direction of Liutex.

According to Liu and Gao [18,19], the criterion to determine the existence of local fluid rotation on the *XY*-plane is $\alpha^2 - \beta^2 < 0$, where $\alpha$ and $\beta$ are the 2D principal rate of strain and vorticity on the plane perpendicular to the local rotation axis and can be expressed as

$$\alpha = \frac{1}{2}\sqrt{\left(\frac{\partial v}{\partial y} - \frac{\partial u}{\partial x}\right)^2 + \left(\frac{\partial v}{\partial x} + \frac{\partial u}{\partial y}\right)^2} \tag{3.18}$$

$$\beta = \frac{1}{2}\left(\frac{\partial v}{\partial x} - \frac{\partial u}{\partial y}\right) \tag{3.19}$$

Then, the magnitude of Liutex is defined as twice the minimal absolute value of the off-diagonal component of the 2×2 upper left submatrix and can be given as

$$R = \begin{cases} 2(|\beta| - \alpha), & \beta^2 > \alpha^2 \\ 0, & o.w. \end{cases} \tag{3.20}$$

According to Wang et. al [45], $r$ is the real eigenvector of the velocity gradient tensor, and the explicit formula of R is

$$R = \vec{\boldsymbol{\omega}} \cdot \vec{\boldsymbol{r}} - \sqrt{(\vec{\boldsymbol{\omega}} \cdot \vec{\boldsymbol{r}})^2 - 4\lambda_{ci}^2} \tag{3.21}$$

Mathematically, Liutex is rigid rotation of fluids and its application in turbulence research can be seen here [46-48].

### 3.3.2 Liutex-Omega Method ($\Omega_L$)

Even though Omega method was a significant improvement among the rest of the second-generation method, it was still contaminated by shear as this method also follows traditional Cauchy-Stokes's decomposition of velocity gradient tensor. So, Dong and Liu [21] defined Omega method in Liutex sense. i.e., Liutex omega method offers the definition of vortex structure as local rigid rotation of fluid particles, and this method is not contaminated by shear. So, this method can distinguish the rotational vortex structures from shear layer, discontinuity structures, and other non-physical structures. Liutex-Omega method was proposed for the normalization of Liutex method, combining with the concept of Omega method. According to Liu and Gao [18,19], the criterion to determine the existence of local fluid rotation on the *XY*-plane is $\alpha^2 - \beta^2 < 0$, where $\alpha$ and $\beta$ are the 2D principal rate of strain and vorticity on the plane perpendicular to the local rotation axis and can be expressed as

$$\alpha = \frac{1}{2}\sqrt{\left(\frac{\partial v}{\partial y} - \frac{\partial u}{\partial x}\right)^2 + \left(\frac{\partial v}{\partial x} + \frac{\partial u}{\partial y}\right)^2} \tag{3.22}$$

$$\beta = \frac{1}{2}\left(\frac{\partial v}{\partial x} - \frac{\partial u}{\partial y}\right) \tag{3.23}$$

Then, $\Omega_L$ is defined as the ratio of $\beta$ squared over the sum of $\beta$ squared and $\alpha$ squared and can be written as:

$$\Omega_L = \frac{\beta^2}{\beta^2+\alpha^2+\varepsilon} \tag{3.24}$$

where $\varepsilon$ is a small parameter introduced in the denominator of $\Omega_L$ to remove the noises caused by the computer rounding error case by case. In another word, $\varepsilon$ is a small positive number added in the denominator so that division by zero can be avoided. $\varepsilon$ can be defined as a function of the maximum of the term $\beta^2 - \alpha^2$, proposed as follows:

$$\varepsilon = b * (\beta^2 - \alpha^2)_{max} \tag{3.25}$$

where $b$ is a small positive number around 0.001-0.002.

$\varepsilon$ is case related since noises in different cases have different dimensions. But $b$ is a constant and the term $(\beta^2 - \alpha^2)_{max}$ is a fixed number for each time step and can be easily obtained. So, the manual adjustment of $\varepsilon$ for each case can be avoided.

### 3.3.3 Modified Liutex-Omega Method ($\widetilde{\Omega}_L$)

Despite Liutex-Omega method being able to capture local rigid rotation of fluid flow, it still showed some bulge on iso-surface plotting. So, the new vortex identification method named modified Liutex-Omega ($\widetilde{\Omega}_L$) has been proposed in 2019 by Liu and Liu [22] as an effective method to capture vortices without any bulge. It was developed to improve the Omega method [17] and the published Liutex-Omega method [21] and to replace the previous exiting methods such as $Q$-criterion, $\lambda_2$-criterion, $\lambda_{ci}$-criterion, etc.

Since the introduction of the Omega method in 2016 [17], many studies have shown that it is more powerful to capture vortices than the existing vortex identification methods. The original Liutex-Omega method is also powerful to visualize vortices but there are some bulging

phenomena on the iso-surfaces. As a result, the modified Liutex-Omega method was introduced to resolve some deficiencies in the original Liutex-Omega method.

The modified Liutex-Omega, $\widetilde{\Omega}_L$, is defined by

$$\tilde{\Omega}_L = \frac{\beta^2}{\beta^2+\alpha^2+{\lambda_{cr}}^2+\frac{1}{2}{\lambda_r}^2+\varepsilon} \tag{3.26}$$

$$\beta = \frac{1}{2}\boldsymbol{\omega}.\boldsymbol{r} \tag{3.27}$$

$$\alpha = \frac{1}{2}\sqrt{(\boldsymbol{\omega}.\boldsymbol{r})^2 - 4{\lambda_{ci}}^2} \tag{3.28}$$

where $\omega$ is a local vorticity vector and $\lambda_r, \lambda_{cr}$ and $\lambda_{ci}$ are a real eigenvalue, a real part of the complex eigenvalue, and an imaginary part of the complex eigenvalue of $\nabla V$, respectively. Here, $\varepsilon$ is a small positive number used to avoid division by zero or an extremely small number and $\varepsilon = b(\beta^2 - \alpha^2)_{max}$ , where $b$ is a small positive number around $0.001\sim0.002$. In this paper, $b$ is set by $b = 0.001$ and $\widetilde{\Omega}_L = 0.52$ is applied as an empirical value according to [44].

### 3.3.4 Liutex Core lines Method

All the second-generation vortex identification methods are scalar. So, we use iso-surface to model and visualize the vortex structure. But iso-surface requires the proper threshold adjustment. Also, the threshold is arbitrary and man-made, and it is very difficult to know the best value of threshold to represent vortices prior to the suited selection. So, threshold selection is tedious and very time consuming. This conundrum sometimes may lead to the incorrect interpretation of the structures and formations of vortices. Note that Figure 3.1 (a), (b) and (c) were drawn by the same DNS data but different thresholds have given different vortex structures. In the similar manner , all currently popular second-generation vortex identification methods may possibly give different vortex structures using the same DNS data.

Because of all these limitations of all second-generation vortex identification methods, there was an enormous need to develop a unique vortex identification method. So, the unique vortex core line method based on Liutex has been mathematically proposed and it has been used in turbulence research successfully [49,50].it can be used to represent the vortex structure Uniquely. Moreover, the vortex core lines alleviate the burden of choosing a proper threshold.

According to [47], some important definitions are introduced as follows.

$$\boldsymbol{R} = \boldsymbol{\omega}.\boldsymbol{r} - \sqrt{(\boldsymbol{\omega}.\boldsymbol{r})^2 - 4\lambda_{ci}^2}, \tag{3.29}$$

where $\boldsymbol{\omega}$ is a local vorticity vector and $\lambda_{ci}$ is an imaginary part of the complex eigenvalue of $\nabla V$.

Definition 2: The vortex core line or the vortex rotation axis is defined as a special Liutex line passing through the points, that satisfies the condition:

$$\nabla R \times \boldsymbol{r} = 0, R > 0 \tag{3.30}$$

where $\boldsymbol{r}$ represents the direction of the Liutex vector.

3.4 Application of Vortex Identification Method to DNS data to find vortex boundary.

The DNS data is for a compressible, zero-pressure-gradient flat-plate boundary layer as in [1, 2]. The case set up for this research is presented in section 2 above. We have applied Liutex based methods and other traditional vortex identification schemes to DNS data and compared them. The iso-surface presented below are for early transition of boundary layer data.

A. Δ Criterion

Iso-surface of various Δ values are presented in the figure 3.1 below. Fig 3.1 a) shows the iso-surface with $\Delta = 0$ which seems thick and smeared. Also, spanwise vortex in the beginning of the flat plate appears clearly. But when we increase the threshold to 0.005, ∧ and hairpin vortices become sharp and spanwise vortices disappear. When we further increase the threshold to 0.03, ∧ as well as hairpin vortices disappear, and the vortex structure looks broken like a collection of debris. This is largely because of the threshold selection which creates the confusion in determining the proper vortex boundary accurately if we do not have prior knowledge about the structure of fluid flow in the boundary layer. This method does not give us the proper guideline to construct the flow structure as flow structures keep changing with the change in threshold.

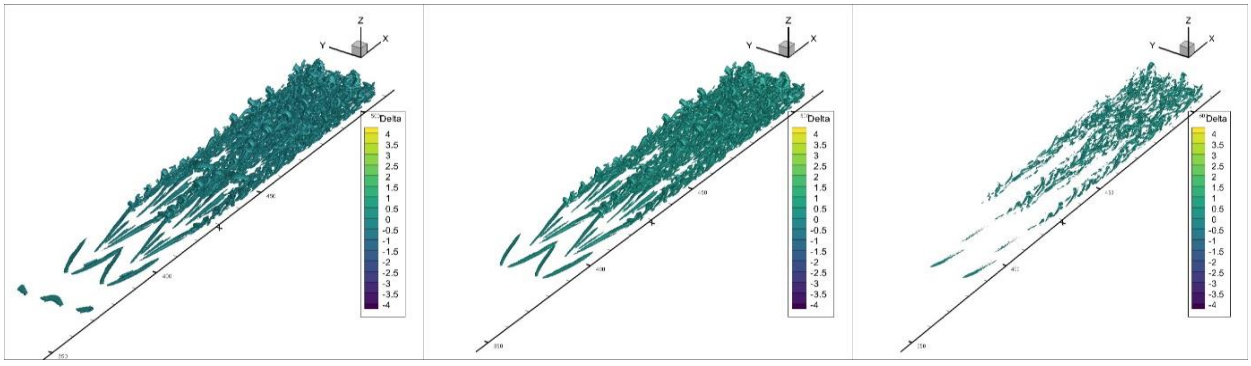

a) $\Delta$=0 b) $\Delta$=0.005 c) $\Delta$=0.03

Fig 3.1. a) – c) Iso-surface plotting of $\Delta$ at various thresholds.

B. $Q$ Criterion

Iso-surface of $Q$ at various thresholds are presented in the figure 3.2 below. Fig 3.2 a) shows the iso-surface with Q=0.001, where spanwise vortices, lambda vortices and hairpin vortices are overcoated and unclear due to inclusion of weak vortices by a small threshold. As in $\Delta$ method, as we keep increasing threshold uniformly, the flow structure becomes thinner and sharp, and ultimately it starts to disappear, making it very hard to select the proper threshold.

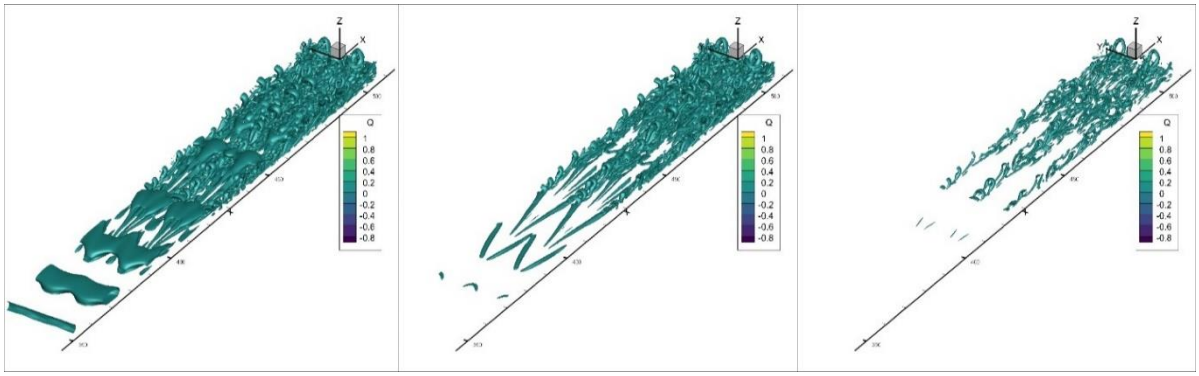

a)Q=0.001 b)Q=0.003 c)Q=0.03

Fig. 3.2 a) - c) Iso-surface plotting of Q at various thresholds.

C. $\lambda_{ci}$ Criterion

As in ∧ and Q methods, streamwise vortex can be seen in Fig 3.3 a) with small threshold. When threshold is increased a thin and sharp lambda vortex can be seen as in Fig 3.3 b). But hairpin vortex in this method is not as clear as ∧ and Q method. As we further decrease the threshold, the head of hairpin vortex starts disappearing which shows that head of the hairpin vortex has weaker vortex strength compared to legs.

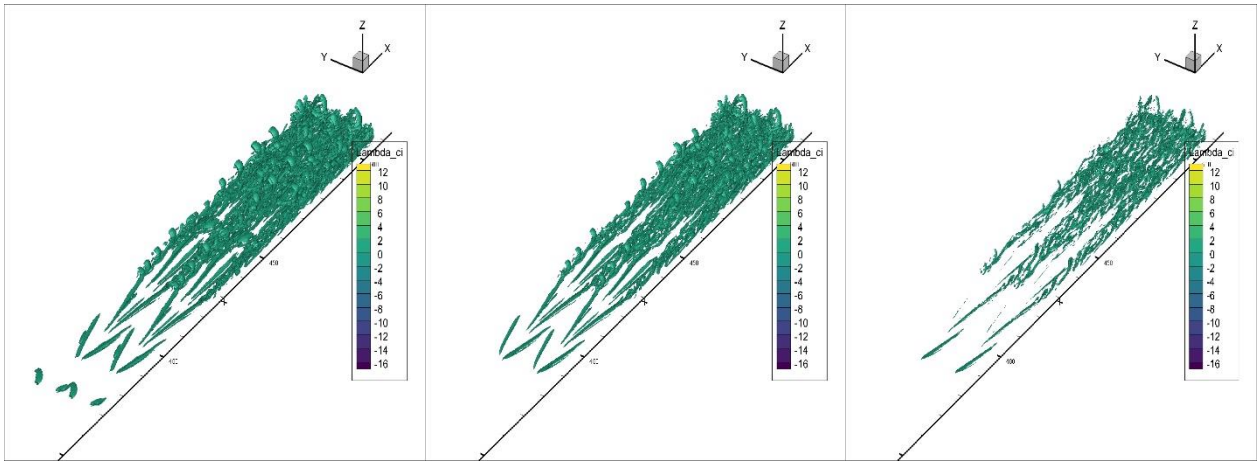

a) $\lambda_{ci} = 0.00005$ b) $\lambda_{ci} = 0.05$ c) $\lambda_{ci} = 0.5$

Fig. 3.3 a) – c) Iso-surface plotting of $\lambda_{ci}$ at various thresholds.

D. $\lambda_2$ Criterion

Fig 3.4 a) shows the iso-surface plot of $\lambda_2 = -0 \cdot 0001$ which is thick and smeared. As in previous method, the more we decrease the threshold (in negative values) or increase the value of $|\lambda_2|$, the more the vortex structure starts to break down as only strong vortices are captured.

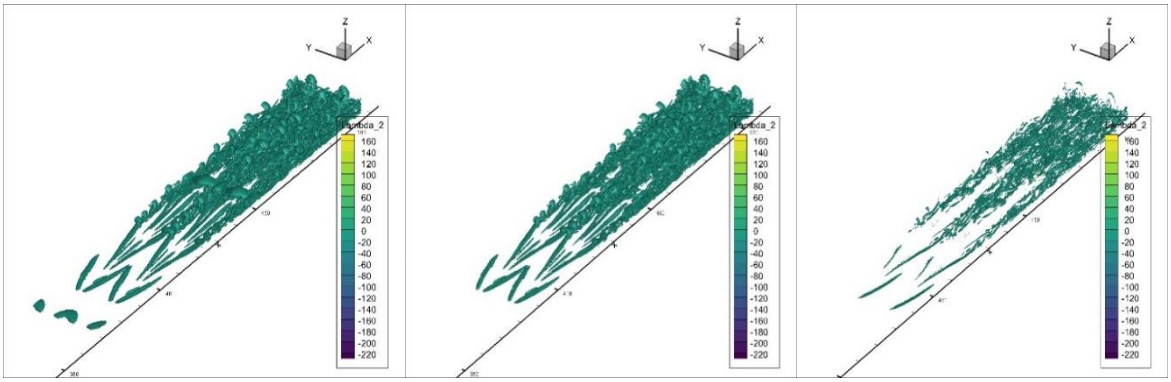

a) $\lambda_2 = -0 \cdot 0001$ b) $\lambda_2 = -0 \cdot 1$ c) $\lambda_2 = -0 \cdot 7$

Fig. 3.4 a) – c) Iso-surface plotting of $\lambda_2$ at various thresholds

E. Omega criterion

Since Omega method gives the relative strength of vorticity in fluid flow coupled with deformation, we set threshold a little bigger than 50 percent. Fig. 3.5 a) - c) represents the iso-surface of flow structure of transitional boundary layer at various thresholds. But there is not much change in the vortex structure, providing the ample evident that this method is only mildly affected by threshold change. This method can capture both weak and strong vortex structure simultaneously as it represents the relative strength of vorticity and is expressed between 0 and 1.

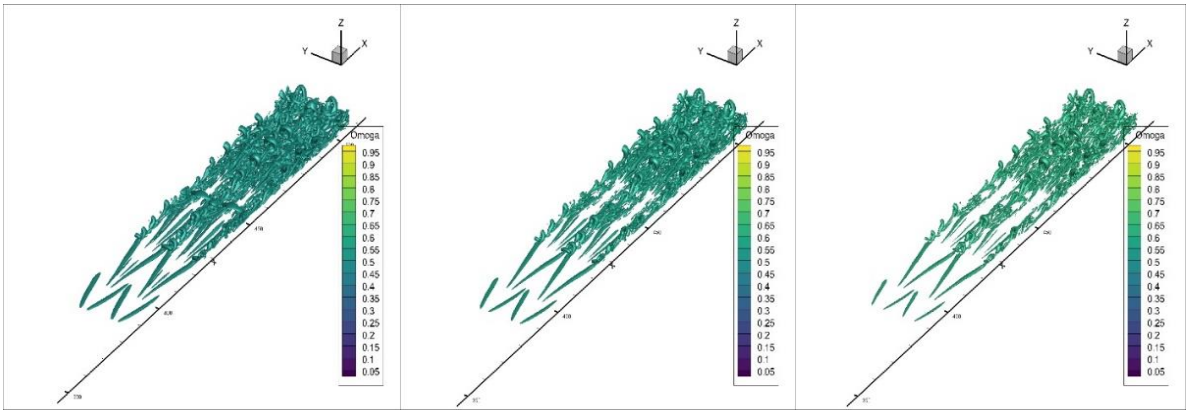

a) $\Omega = 0.52$ B) $\Omega = 0.57$ C) $\Omega = 0.62$

Fig.3.5 a) - c) Iso-surface plotting of $\Omega$ at various thresholds.

F. Modified Liutex-Omega method

This method was proposed by Liu and Liu [22] to improve the Liutex-Omega method, which is a combination of Liutex and Omega method. Although Liutex-Omega method robustly able to capture both weak and strong vortex structures, the iso-surface plotting was not smooth and had bulging phenomena. So, Modified Liutex-Omega method was proposed to resolve these problems. Like Omega method and Liutex-Omega, this method also calculates the relative strength of vorticity in the rotated frame XYZ where Z-axis is parallel to the real eigen vector $r$ of velocity gradient tensor. This method is also a relative method, so both weak and strong vortex can be captured simultaneously. Furthermore, this method is minimally affected by threshold changes. So, this is the most effective method if we want to get rid of threshold selection dilemma. The iso-surface plotting of this is clear and smooth. This method is recommended to find the vortex boundary by iso-surface because this method is based on local rigid rotation (Liutex) and is free from stretching and shearing effects. The figure 3.6 shows that we can accurately capture the vortex structure by Modified Liutex method and it can be also seen that threshold changes barely affect the vortex boundary.

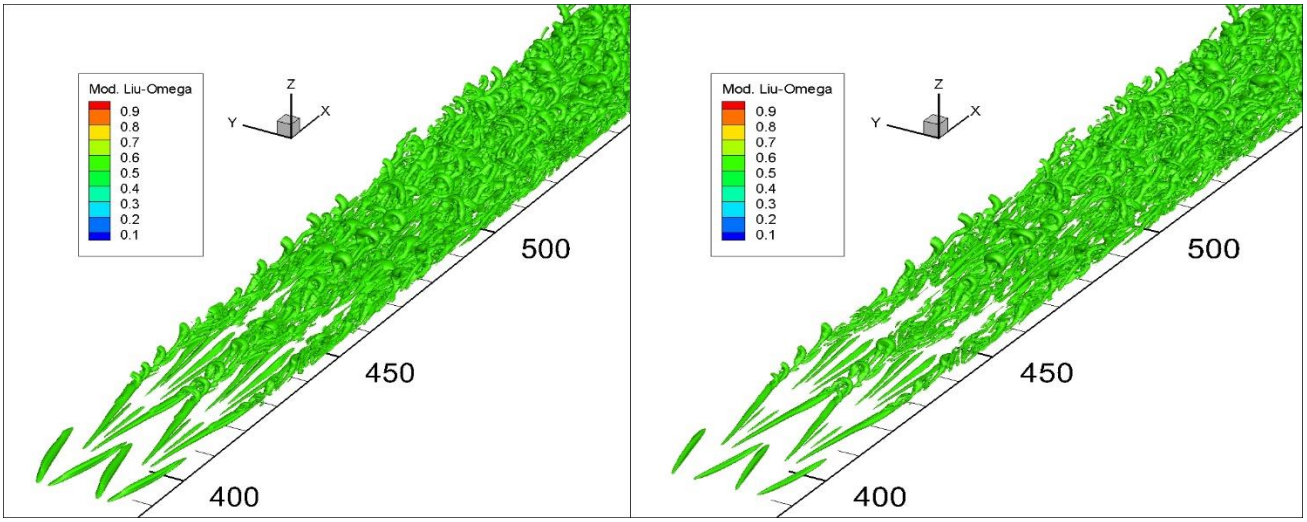


a) $\widetilde{\Omega}_L$=0.52 b) $\widetilde{\Omega}_L$=0.60

Fig. 3.6. a) – b) Vortex structure of boundary layer transition with Modified Liutex-Omega method.

G. Liutex core lines method

Fig 3.7. a)- c) represents the flow structure of early transition of boundary layer by Liutex core lines. Liutex core lines [23] are local maximum of Liutex magnitude in the plane perpendicular to the axis of rotation. Since this is a line, not the iso-surface, so all the annoyances

that come with selection of threshold for iso-surface plotting is not the case anymore. Therefore, not only we are exempted from nuisance of choosing a proper threshold, Liutex core lines method is also unique that can display the vortex structure with ease. Moreover, this method can clearly depict the strength of vortex cores at vortex positions like lambda vortex, hairpin vortex, etc. In the following figure, different colors represent different strength of vortex core lines.

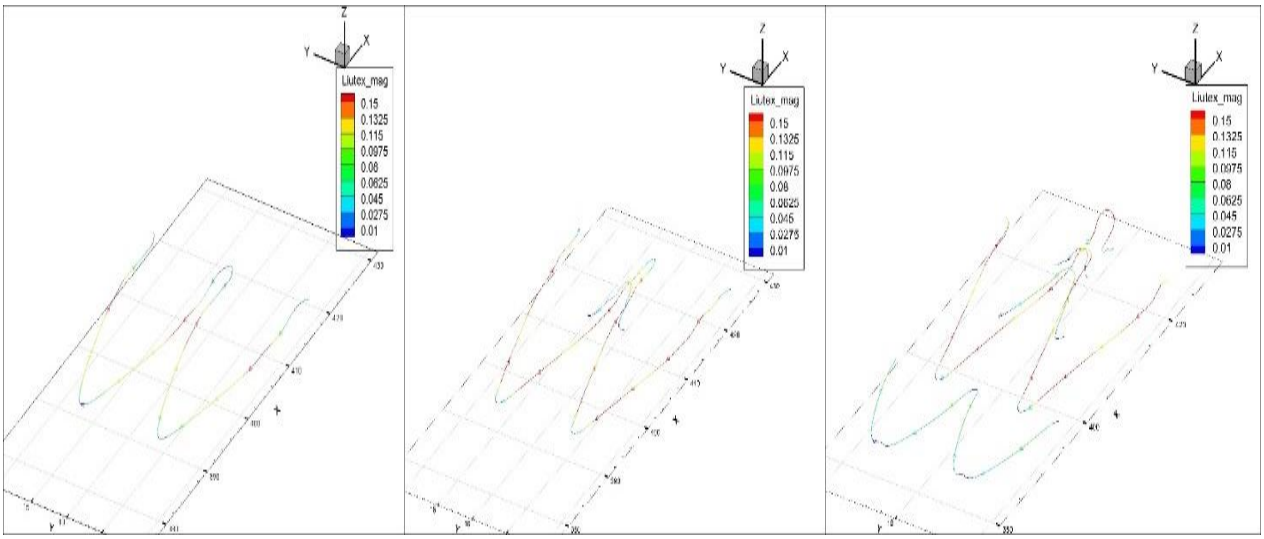


a) b) c)

Fig. 3.7 a) - c) Evolution of Liutex core lines in early transition boundary layer.

# CHAPTER 4

# PRINCIPAL COORDINATES AND PRINCIPAL TENSOR DECOMPOSITION

Fluid kinematics is a complex topic. It depends on density, viscosity, compressibility, velocity of fluid, and roughness of the surface on which the fluid is following. These factors of the fluid motion cause fluid particles to deform and ultimately results in forming a vortex. The vortex is severely affected by translation, rotation, stretching, and shear deformation of fluid particles. So, one of the ideas to reduce the complexity of fluid motion is to decompose the velocity gradient tensor of fluid. In this chapter, first we review and discuss the drawbacks of the Cauchy-Stokes Tensor decomposition and then we propose a new unique velocity gradient tensor decomposition method based on Liutex definition, known as Principal Tensor decomposition.

## 4.1. Helmholtz/Cauchy-Stokes's velocity gradient tensor decomposition

Helmholtz velocity decomposition, also known as Cauchy-Stokes's decomposition, has been used by many researchers in the literature since Helmholtz first proposed his theory in 1858 [4]. Most of the journal papers and textbooks in fluid dynamics consider Cauchy-Stokes decomposition as the fundamental theory of fluid kinematics. In general, Cauchy-Stokes's decomposition decomposes the velocity gradient tensor into two parts with a symmetric part and anti-symmetric part.

$$A = \frac{1}{2}(\nabla\vec{v} + \nabla\vec{v}^T) = \begin{bmatrix} \frac{\partial u}{\partial x} & \frac{1}{2}\left(\frac{\partial u}{\partial y} + \frac{\partial v}{\partial x}\right) & \frac{1}{2}\left(\frac{\partial u}{\partial z} + \frac{\partial w}{\partial x}\right) \\ \frac{1}{2}\left(\frac{\partial v}{\partial x} + \frac{\partial u}{\partial y}\right) & \frac{\partial v}{\partial y} & \frac{1}{2}\left(\frac{\partial v}{\partial z} + \frac{\partial w}{\partial y}\right) \\ \frac{1}{2}\left(\frac{\partial w}{\partial x} + \frac{\partial u}{\partial z}\right) & \frac{1}{2}\left(\frac{\partial w}{\partial y} + \frac{\partial v}{\partial z}\right) & \frac{\partial w}{\partial z} \end{bmatrix} \tag{4.1}$$

$$B = \frac{1}{2}(\nabla\vec{v} - \nabla\vec{v}^T) = \begin{bmatrix} 0 & \frac{1}{2}\left(\frac{\partial u}{\partial y} - \frac{\partial v}{\partial x}\right) & \frac{1}{2}\left(\frac{\partial u}{\partial z} - \frac{\partial w}{\partial x}\right) \\ \frac{1}{2}\left(\frac{\partial v}{\partial x} - \frac{\partial u}{\partial y}\right) & 0 & \frac{1}{2}\left(\frac{\partial v}{\partial z} - \frac{\partial w}{\partial y}\right) \\ \frac{1}{2}\left(\frac{\partial w}{\partial x} - \frac{\partial u}{\partial z}\right) & \frac{1}{2}\left(\frac{\partial w}{\partial y} - \frac{\partial v}{\partial z}\right) & 0 \end{bmatrix} \tag{4.2}$$

where A and B are the symmetric and anti-symmetric part of the velocity gradient tensor, respectively.

The anti-symmetric part $B$ represents vorticity, $\nabla \times \vec{v}$ which is what people used to consider as rotation of fluids believing that vorticity is angular speed for rigid body rotation in solid mechanics. In generally, Cauchy-Stokes's decomposition is correct in mathematics, however, there is doubt over its physical meanings. Scientists and researchers have kept doubting whether vorticity can represent rotation of fluids within the past several decades. Robinson [38] pointed out that the asociarte region can have strong vorticity but its actual vortices are quite weak. Also, Wang et al. [39] found that the vorticity magnitude is much smaller inside the vortex region than the neighboring area outside the vortex from a DNS study on vortex and vorticity in late boundary layer transition. Along with problem related to vorticity, Cauchy-Stokes's decomposition is also not a Gallilean invariant. Galilean invariance is a property first described by Galilean [51] in 1632 in studying the dialogue concerning the two chief world systems, indicating that any physical quantity that is Gallilean invariant does not change under different coordinates.

The change in coordinates due to coordinates rotation or coordinates flipping or some other coordinate deformation will affect the Cauchy-Stokes's decomposition. So, Dr. Liu and his team produced the idea of Principal coordinate and Principal Principal Tensor Decomposition. This decomposition is unique and is Gallilean invariant.

### 4.2. Problems with Cauchy-Stokes's decomposition

Cauchy-Stokes's (CS) decomposition has some loopholes which can be explained in the following two sub-headings.

#### 4.2.1 Physical meaning of CS decomposition is questionable.

The 2-D Couette flow is a laminar flow of a viscous fluid in the space between two surfaces, one of which is fixed and the other is moving tangentially.

The 2-D Couette flow is given by following equations,

$$\begin{cases} u = 2ay \\ v = 0 \end{cases}$$

Here $a$ is a positive constant, $u$ and $v$ are respectively the $x-$component and $y-$component of the velocity.

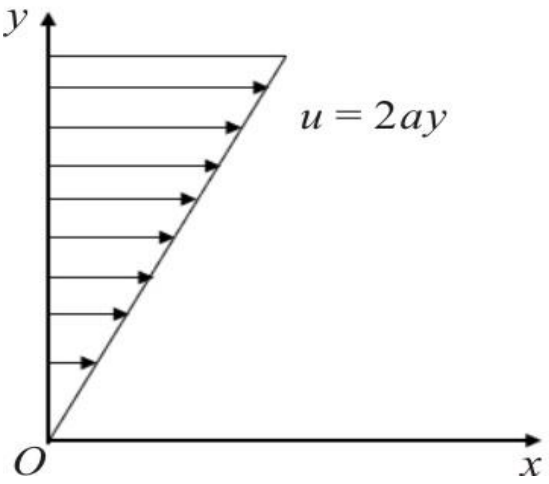


Fig. 4.1. 2-D Couette flow

The velocity gradient tensor related to 2-D Couette flow is given by,

$$\nabla V = \begin{bmatrix} \frac{\partial u}{\partial x} & \frac{\partial u}{\partial y} \\ \frac{\partial v}{\partial x} & \frac{\partial v}{\partial y} \end{bmatrix} = \begin{bmatrix} 0 & 2a \\ 0 & 0 \end{bmatrix} \tag{4.3}$$

The traditional Cauchy-Stokes decomposition is given by,

$$\nabla V = \frac{1}{2}(\nabla V + \nabla V^T) + \frac{1}{2}(\nabla V - \nabla V^T)$$

$$\nabla V = \begin{bmatrix} 0 & 2a \\ 0 & 0 \end{bmatrix} = \begin{bmatrix} 0 & a \\ a & 0 \end{bmatrix} + \begin{bmatrix} 0 & a \\ -a & 0 \end{bmatrix}$$

$$\nabla V = A + B \tag{4.4}$$

Mathematically, this decomposition is correct. However, its physical meaning is questionable and is not acceptable as it violates the definition of original 2-D Couette flow. 2-D Couette flow is a laminar flow that contains no rotation, but Cauchy-Stokes's decomposition gives a rotational part that does not exist in the original fluid flow.

4.2.2 Elements in CS decomposition is not Galilean invariant.

Any small change in coordinate system causes a big problem in Cauchy-Stokes's decomposition. If the decomposition is different under different coordinates, then we will have a huge dilemma in choosing the correct decomposition. So, this problem cannot be ignored, and

this led us to introduce a Principal Tensor Decomposition, which we will discuss in the next section.

Let us observe a 3-D example.

$$\nabla v_0 = \begin{bmatrix} 0 & 2a & 0 \\ 0 & 0 & 0 \\ 0 & 0 & 0 \end{bmatrix}$$

From Cauchy-Stokes's decomposition, we will get,

$$\nabla v_0 = \begin{bmatrix} 0 & 2a & 0 \\ 0 & 0 & 0 \\ 0 & 0 & 0 \end{bmatrix} = \frac{1}{2}\left(\nabla v_0 + \nabla {v_0}^T\right) + \frac{1}{2}\left(\nabla v_0 - \nabla {v_0}^T\right)$$

$$\nabla v_0 = \begin{bmatrix} 0 & a & 0 \\ a & 0 & 0 \\ 0 & 0 & 0 \end{bmatrix} + \begin{bmatrix} 0 & a & 0 \\ -a & 0 & 0 \\ 0 & 0 & 0 \end{bmatrix}$$

$$\nabla v_0 = A_0 + B_0$$

(4.5)

Where $A_0$ and $B_0$ are symmetric and antisymmetric parts.

Again, rotating the coordinate under rotation matrix $P_1 = \begin{bmatrix} \frac{\sqrt{3}}{2} & \frac{1}{2} & 0 \\ \frac{1}{2} & \frac{\sqrt{3}}{2} & 0 \\ 0 & 0 & 1 \end{bmatrix}$, we get,

$$\nabla v_1 = P_1 \nabla v_0 P_1^T$$

$$\nabla v_1 = \begin{bmatrix} \frac{\sqrt{3}}{2} & \frac{1}{2} & 0 \\ \frac{1}{2} & \frac{\sqrt{3}}{2} & 0 \\ 0 & 0 & 1 \end{bmatrix} \begin{bmatrix} 0 & 2a & 0 \\ 0 & 0 & 0 \\ 0 & 0 & 0 \end{bmatrix} \begin{bmatrix} \frac{\sqrt{3}}{2} & \frac{1}{2} & 0 \\ \frac{1}{2} & \frac{\sqrt{3}}{2} & 0 \\ 0 & 0 & 1 \end{bmatrix}$$

$$\nabla v_1 = \begin{bmatrix} 0 & a\sqrt{3} & 0 \\ 0 & a & 0 \\ 0 & 0 & 1 \end{bmatrix} \begin{bmatrix} \frac{\sqrt{3}}{2} & \frac{1}{2} & 0 \\ \frac{1}{2} & \frac{\sqrt{3}}{2} & 0 \\ 0 & 0 & 1 \end{bmatrix}$$

$$\nabla v_1 = \begin{bmatrix} \frac{a\sqrt{3}}{2} & \frac{3a}{2} & 0 \\ \frac{a}{2} & \frac{a\sqrt{3}}{2} & 0 \\ 0 & 0 & 1 \end{bmatrix}$$

Again, rotating the coordinate under rotation matrix $P_2 = \begin{bmatrix} \frac{\sqrt{3}}{2} & 0 & \frac{1}{2} \\ 0 & 1 & 0 \\ -\frac{1}{2} & 0 & \frac{\sqrt{3}}{2} \end{bmatrix}$, we get

$$\nabla v_2 = P_2 \nabla v_1 P_2^T$$

$$\nabla v_2 = \begin{bmatrix} \frac{\sqrt{3}}{2} & 0 & \frac{1}{2} \\ 0 & 1 & 0 \\ -\frac{1}{2} & 0 & \frac{\sqrt{3}}{2} \end{bmatrix} \begin{bmatrix} \frac{a\sqrt{3}}{2} & \frac{3a}{2} & 0 \\ \frac{a}{2} & \frac{a\sqrt{3}}{2} & 0 \\ 0 & 0 & 1 \end{bmatrix} \begin{bmatrix} \frac{\sqrt{3}}{2} & 0 & -\frac{1}{2} \\ 0 & 1 & 0 \\ \frac{1}{2} & 0 & \frac{\sqrt{3}}{2} \end{bmatrix}$$

$$\nabla v_2 = \begin{bmatrix} \frac{3\sqrt{3}}{8}a & \frac{3\sqrt{3}}{4}a & \frac{-3}{8}a \\ -\frac{\sqrt{3}}{4}a & -\frac{\sqrt{3}}{2}a & \frac{1}{4}a \\ \frac{-3}{8}a & \frac{-3}{4}a & \frac{\sqrt{3}}{8}a \end{bmatrix}$$

Performing Cauchy-Stoke's decomposition, we get,

$$\nabla v_2 = \begin{bmatrix} \frac{3\sqrt{3}}{8}a & \frac{3\sqrt{3}}{4}a & \frac{-3}{8}a \\ -\frac{\sqrt{3}}{4}a & -\frac{\sqrt{3}}{2}a & \frac{1}{4}a \\ \frac{-3}{8}a & \frac{-3}{4}a & \frac{\sqrt{3}}{8}a \end{bmatrix}$$

$$\nabla v_2 = \frac{1}{2}\left(\nabla v_2 + \nabla {v_2}^T\right) + \frac{1}{2}\left(\nabla v_2 - \nabla {v_2}^T\right)$$

$$\nabla v_2 = \begin{bmatrix} \frac{3\sqrt{3}}{8}a & \frac{\sqrt{3}}{4}a & \frac{-3}{8}a \\ \frac{\sqrt{3}}{4}a & \frac{-\sqrt{3}}{2}a & \frac{-1}{4}a \\ \frac{-3}{8}a & \frac{-1}{4}a & \frac{\sqrt{3}}{8}a \end{bmatrix} + \begin{bmatrix} 0 & \frac{\sqrt{3}}{2}a & 0 \\ \frac{-\sqrt{3}}{2}a & 0 & \frac{1}{2}a \\ 0 & \frac{-1}{2}a & 0 \end{bmatrix}$$

$$\nabla v_2 = A_1 + B_1 \tag{4.6}$$

It can be clearly seen that Cauchy-Stokes tensor decomposition before and after the coordinate's rotation given by equations (4.5) and (4.6) are different. So, the question arises, under which coordinates does the Cauchy-Stokes tensor decomposition give the right symmetric deformation and antisymmetric vorticity? We clearly see diagonal elements appear after the decomposition. So, components of velocity gradient tensor are not Galilean invariant in CS decomposition. Therefore, we assume that there is a unique coordinate system that can give a unique tensor decomposition for stretching (compression), shear, and rotation. We call this coordinate the "Principal Coordinates" and the tensor decomposition is "Principal Tensor Decomposition". Performing velocity gradient decomposition under this coordinate system is unique. Which means velocity gradient decomposition is independent of coordinate rotation or flipping or deformation of the coordinates.

4.3. Eigenvalues and eigenvectors of a velocity gradient tensor

Gradient tensor is a 3× 3 matrix that describes the motion of fluids in all directions. We can find the eigenvalues and eigen vectors of a velocity gradient tensor as we used to find them in a 3× 3 matrix in linear algebra.

Definition 4.1:

The eigen vector of a matrix A is given by $\lambda$ that satisfies the equation A$v$= $\lambda v$, where $v$ is the corresponding eigenvector.

Definition 4.2:

Let $\lambda$ be the eigenvalues of a matrix A, then the eigen equation related to matrix a is given by the equation $|\mathrm{A} - \lambda I| = 0$, where I is a unitary matrix with same dimensionality as A.

4.3.1. General method to solve eigenvalues and eigenvectors of a velocity gradient tensor.

The velocity gradient tensor of a 3-dimensional flow field is a 3x3 matrix which is given by,

$$\nabla\vec{v} = \begin{bmatrix} \frac{\partial u}{\partial x} & \frac{\partial u}{\partial y} & \frac{\partial u}{\partial z} \\ \frac{\partial v}{\partial x} & \frac{\partial v}{\partial y} & \frac{\partial v}{\partial z} \\ \frac{\partial w}{\partial x} & \frac{\partial w}{\partial y} & \frac{\partial w}{\partial z} \end{bmatrix}, \tag{4.7}$$

Let $\lambda$ be the eigenvalues of $\nabla\vec{v}$. Then, the eigenvalue equation is given by,

$$|\nabla\vec{v} - \lambda I| = 0$$

$$\begin{vmatrix} \frac{\partial u}{\partial x} - \lambda & \frac{\partial u}{\partial y} & \frac{\partial u}{\partial z} \\ \frac{\partial v}{\partial x} & \frac{\partial v}{\partial y} - \lambda & \frac{\partial v}{\partial z} \\ \frac{\partial w}{\partial x} & \frac{\partial w}{\partial y} & \frac{\partial w}{\partial z} - \lambda \end{vmatrix} = 0 \tag{4.8}$$

Performing the determinant of the matrix gives us:

$$\left(\frac{\partial u}{\partial x} - \lambda\right)\begin{vmatrix} \frac{\partial v}{\partial y} - \lambda & \frac{\partial v}{\partial z} \\ \frac{\partial w}{\partial y} & \frac{\partial w}{\partial z} - \lambda \end{vmatrix} - \frac{\partial u}{\partial y}\begin{vmatrix} \frac{\partial v}{\partial x} & \frac{\partial v}{\partial z} \\ \frac{\partial w}{\partial x} & \frac{\partial w}{\partial z} - \lambda \end{vmatrix} + \frac{\partial u}{\partial z}\begin{vmatrix} \frac{\partial v}{\partial x} & \frac{\partial v}{\partial x} - \lambda \\ \frac{\partial w}{\partial x} & \frac{\partial w}{\partial y} \end{vmatrix} = 0$$

Performing the determinant of $2\times 2$ submatrix gives us:

$$\left(\frac{\partial u}{\partial x} - \lambda\right)\left[\left(\frac{\partial v}{\partial y} - \lambda\right)\left(\frac{\partial w}{\partial z} - \lambda\right) - \frac{\partial w}{\partial y}\frac{\partial v}{\partial z}\right] - \frac{\partial u}{\partial y}\left[\frac{\partial v}{\partial x}\left(\frac{\partial w}{\partial z} - \lambda\right) - \frac{\partial w}{\partial x}\frac{\partial v}{\partial z}\right]$$

$$+\frac{\partial u}{\partial z}\left[\frac{\partial v}{\partial x}\frac{\partial w}{\partial y} - \frac{\partial w}{\partial x}\left(\frac{\partial v}{\partial y} - \lambda\right)\right] = 0$$

Simplifying,

$$\left(\frac{\partial u}{\partial x} - \lambda\right)\left[\lambda^2 - \left(\frac{\partial v}{\partial y} + \frac{\partial w}{\partial z}\right)\lambda + \frac{\partial v}{\partial y}\frac{\partial w}{\partial z} - \frac{\partial v}{\partial z}\frac{\partial w}{\partial y}\right] - \frac{\partial u}{\partial y}\left[-\frac{\partial v}{\partial x}\lambda + \frac{\partial v}{\partial x}\frac{\partial w}{\partial z} - \frac{\partial v}{\partial z}\frac{\partial w}{\partial x}\right] + \frac{\partial u}{\partial z}\left[\frac{\partial v}{\partial x}\frac{\partial w}{\partial y} - \frac{\partial v}{\partial y}\frac{\partial w}{\partial x} + \frac{\partial w}{\partial x}\lambda\right] = 0$$

This will give us a cubic equation. Let us write it in a general form.

$$\lambda^3 - \left(\frac{\partial u}{\partial x} + \frac{\partial v}{\partial y} + \frac{\partial w}{\partial z}\right)\lambda^2 + \left(\frac{\partial u}{\partial x}\frac{\partial v}{\partial y} + \frac{\partial u}{\partial x}\frac{\partial w}{\partial z} + \frac{\partial v}{\partial y}\frac{\partial w}{\partial z} - \frac{\partial v}{\partial z}\frac{\partial w}{\partial y} - \frac{\partial u}{\partial z}\frac{\partial w}{\partial x} - \frac{\partial v}{\partial x}\frac{\partial u}{\partial y}\right)\lambda$$

$$+ \left(\frac{\partial u}{\partial x}\frac{\partial v}{\partial z}\frac{\partial w}{\partial y} + \frac{\partial u}{\partial z}\frac{\partial v}{\partial y}\frac{\partial w}{\partial x} + \frac{\partial u}{\partial y}\frac{\partial v}{\partial x}\frac{\partial w}{\partial z} - \frac{\partial u}{\partial x}\frac{\partial v}{\partial y}\frac{\partial w}{\partial z} - \frac{\partial u}{\partial y}\frac{\partial v}{\partial z}\frac{\partial w}{\partial x} - \frac{\partial u}{\partial z}\frac{\partial v}{\partial x}\frac{\partial w}{\partial y}\right) = 0 \qquad (4.9)$$

The equation (4.9) is a cubic equation in $\lambda$ and, in general, it can be written as:

$$\lambda^3 + a\lambda^2 + b\lambda + c = 0 \ ,$$

Where,

$$a = -\left(\frac{\partial u}{\partial x} + \frac{\partial v}{\partial y} + \frac{\partial w}{\partial z}\right) \qquad (4.10)$$

$$b = \frac{\partial u}{\partial x}\frac{\partial v}{\partial y} + \frac{\partial u}{\partial x}\frac{\partial w}{\partial z} + \frac{\partial v}{\partial y}\frac{\partial w}{\partial z} - \frac{\partial v}{\partial z}\frac{\partial w}{\partial y} - \frac{\partial u}{\partial z}\frac{\partial w}{\partial x} - \frac{\partial v}{\partial x}\frac{\partial u}{\partial y} \qquad (4.11)$$

$$c = \frac{\partial u}{\partial x}\frac{\partial v}{\partial z}\frac{\partial w}{\partial y} + \frac{\partial u}{\partial z}\frac{\partial v}{\partial y}\frac{\partial w}{\partial x} + \frac{\partial u}{\partial y}\frac{\partial v}{\partial x}\frac{\partial w}{\partial z} - \frac{\partial u}{\partial x}\frac{\partial v}{\partial y}\frac{\partial w}{\partial z} - \frac{\partial u}{\partial y}\frac{\partial v}{\partial z}\frac{\partial w}{\partial x} - \frac{\partial u}{\partial z}\frac{\partial v}{\partial x}\frac{\partial w}{\partial y} \qquad (4.12)$$

This method of solving a cubic equation be found in Numerical Recipes in FORTRAN 77, Second Edition, Chapter 5, Quadratic and Cubic Equations, Page 179 [52].

This method can be described as follows:

If three coefficients *a*, *b*, *c* given by equations (4.10), (4.11) and (4.12) are real, then, we can write:

$$Q = \frac{a^2 - 3b}{9} \text{ and } R = \frac{2a^3 - 9ab + 27c}{54} \qquad (4.13)$$

1) If $R^2 < Q^3$, then the cubic equation has three real roots say $\lambda_1, \lambda_2 \ and \ \lambda_3$.
   Then these three roots are given by:

$$\lambda_1 = -2\sqrt{Q}\cos\left(\frac{\theta}{3}\right) - \frac{a}{3} \qquad (4.14)$$

$$\lambda_2 = -2\sqrt{Q}\cos\left(\frac{\theta + 2\pi)}{3}\right) - \frac{a}{3} \qquad (4.15)$$

$$\lambda_3 = -2\sqrt{Q}\cos\left(\frac{\theta - 2\pi)}{3}\right) - \frac{a}{3} \qquad (4.16)$$

   Where $\theta = \arccos(R/\sqrt{Q^3})$.

2) If $R^2 \geq Q^3$, then compute $A = -sign(R)\left[|R| + \sqrt{R^2 - Q^3}\right]^{1/3}$ where the square root is positive. Then compute

$$B = \begin{cases} \frac{Q}{A} & (A \neq 0) \\ 0 & (A = 0) \end{cases}$$

This will give us one real and two conjugate complex eigenvalues, which are given by:

$$\lambda_1 = (A + B) - \frac{a}{3} = \lambda_r \tag{4.17}$$

$$\lambda_2 = -\frac{1}{2}(A + B - \frac{a}{3} + i\,\frac{\sqrt{3}}{2}(A - B) = \lambda_{cr} + i\lambda_{ci} \tag{4.18}$$

$$\lambda_3 = -\frac{1}{2}(A + B - \frac{a}{3} - i\,\frac{\sqrt{3}}{2}(A - B) = \lambda_{cr} - i\lambda_{ci} \tag{4.19}$$

Since both A and B are real, $\lambda_1$ is real but $\lambda_2$ and $\lambda_3$ are the complex eigenvalues.

Next, we calculate corresponding normalized real eigenvector. Here, we discuss about the analytical method to find the normalized real eigenvector $\vec{r}$ corresponding to the real eigenvalue $\lambda_r$.

$$\text{Let A} = \begin{bmatrix} \frac{\partial u}{\partial x} & \frac{\partial u}{\partial y} & \frac{\partial u}{\partial z} \\ \frac{\partial v}{\partial x} & \frac{\partial v}{\partial y} & \frac{\partial v}{\partial z} \\ \frac{\partial w}{\partial x} & \frac{\partial w}{\partial y} & \frac{\partial w}{\partial z} \end{bmatrix},$$

And, $\vec{r}^* = \left[\mathrm{r}_x^*, \mathrm{r}_y^*, \mathrm{r}_z^*\right]^T$ which is a real eigenvector corresponding to $\lambda_r$.

Then, from the definition of eigenvalues and eigenvectors, we have:

$$\mathrm{A}\vec{r}^* = \lambda_r \vec{r}^*$$

This equation can also be expressed as,

$$(\mathrm{A} - \lambda_r I)\vec{r}^* = 0$$

$$\begin{bmatrix} \frac{\partial u}{\partial x} - \lambda_r & \frac{\partial u}{\partial y} & \frac{\partial u}{\partial z} \\ \frac{\partial v}{\partial x} & \frac{\partial v}{\partial y} - \lambda_r & \frac{\partial v}{\partial z} \\ \frac{\partial w}{\partial x} & \frac{\partial w}{\partial y} & \frac{\partial w}{\partial z} - \lambda_r \end{bmatrix} \begin{bmatrix} \mathrm{r}_x^* \\ \mathrm{r}_y^* \\ \mathrm{r}_z^* \end{bmatrix} = 0 \tag{4.20}$$

The three minors of determinant of this matrix can be written as

$$\Delta_x = \begin{vmatrix} \frac{\partial v}{\partial y} - \lambda_r & \frac{\partial v}{\partial z} \\ \frac{\partial w}{\partial y} & \frac{\partial w}{\partial z} - \lambda_r \end{vmatrix}, \Delta_y = \begin{vmatrix} \frac{\partial u}{\partial x} - \lambda_r & \frac{\partial u}{\partial z} \\ \frac{\partial w}{\partial x} & \frac{\partial w}{\partial z} - \lambda_r \end{vmatrix}, \Delta_z = \begin{vmatrix} \frac{\partial u}{\partial x} - \lambda_r & \frac{\partial u}{\partial y} \\ \frac{\partial v}{\partial x} & \frac{\partial v}{\partial y} - \lambda_r \end{vmatrix}$$

Then, the maximum absolute value of these minors is

$$\Delta_{max} = \max\left(|\Delta_x|, |\Delta_y|, |\Delta_z|\right)$$

Here, all the minors cannot be zero since otherwise, the real eigenvector will be non-unique or a zero a zero vector. So, $\Delta_{max} > 0$

Therefore, we might have three cases:

Case-1: Let $\Delta_{max} = |\Delta_x|$, then we can set: $r_x^* = 1$

So, the above matrix equation becomes:

$$\begin{bmatrix} \frac{\partial u}{\partial x} - \lambda_r & \frac{\partial u}{\partial y} & \frac{\partial u}{\partial z} \\ \frac{\partial v}{\partial x} & \frac{\partial v}{\partial y} - \lambda_r & \frac{\partial v}{\partial z} \\ \frac{\partial w}{\partial x} & \frac{\partial w}{\partial y} & \frac{\partial w}{\partial z} - \lambda_r \end{bmatrix} \begin{bmatrix} 1 \\ r_y^* \\ r_z^* \end{bmatrix} = 0$$

Then, we get:

$$\left(\frac{\partial u}{\partial x} - \lambda_r\right) + \frac{\partial u}{\partial y} r_y^* + \frac{\partial u}{\partial z} r_z^* = 0$$

$$\frac{\partial v}{\partial x} + \left(\frac{\partial v}{\partial y} - \lambda_r\right) r_y^* + \frac{\partial v}{\partial z} r_z^* = 0$$

$$\frac{\partial w}{\partial x} + \frac{\partial w}{\partial y} r_y^* + \left(\frac{\partial w}{\partial z} - \lambda_r\right) r_z^* = 0$$

Taking the last two equations, we get:

$$\frac{\partial v}{\partial x} + \left(\frac{\partial v}{\partial y} - \lambda_r\right) r_y^* + \frac{\partial v}{\partial z} r_z^* = 0$$

$$\frac{\partial w}{\partial x} + \frac{\partial w}{\partial y} r_y^* + \left(\frac{\partial w}{\partial z} - \lambda_r\right) r_z^* = 0$$

So,

$$\left(\frac{\partial v}{\partial y}-\lambda_r\right)\mathrm{r}_y^*+\frac{\partial v}{\partial z}\mathrm{r}_z^*=-\frac{\partial v}{\partial x}$$

$$\frac{\partial w}{\partial y}\,\mathrm{r}_y^*+\left(\frac{\partial w}{\partial z}-\lambda_r\right)\mathrm{r}_z^*=-\frac{\partial w}{\partial x}$$

Writing in matrix form:

$$\begin{bmatrix}\frac{\partial v}{\partial y}-\lambda_r & \frac{\partial v}{\partial z}\\ \frac{\partial w}{\partial y} & \frac{\partial w}{\partial z}-\lambda_r\end{bmatrix}\begin{bmatrix}\mathrm{r}_y^*\\ \mathrm{r}_z^*\end{bmatrix}=\begin{bmatrix}-\frac{\partial v}{\partial x}\\ -\frac{\partial w}{\partial x}\end{bmatrix}$$

$$\begin{bmatrix}\mathrm{r}_y^*\\ \mathrm{r}_z^*\end{bmatrix}=inverse\ of\begin{bmatrix}\frac{\partial v}{\partial y}-\lambda_r & \frac{\partial v}{\partial z}\\ \frac{\partial w}{\partial y} & \frac{\partial w}{\partial z}-\lambda_r\end{bmatrix}\times\begin{bmatrix}-\frac{\partial v}{\partial x}\\ -\frac{\partial w}{\partial x}\end{bmatrix}$$

$$\begin{bmatrix}\mathrm{r}_y^*\\ \mathrm{r}_z^*\end{bmatrix}=\frac{adjoint\ of\begin{bmatrix}\frac{\partial v}{\partial y}-\lambda_r & \frac{\partial v}{\partial z}\\ \frac{\partial w}{\partial y} & \frac{\partial w}{\partial z}-\lambda_r\end{bmatrix}}{\begin{vmatrix}\frac{\partial v}{\partial y}-\lambda_r & \frac{\partial v}{\partial z}\\ \frac{\partial w}{\partial y} & \frac{\partial w}{\partial z}-\lambda_r\end{vmatrix}}\times\begin{bmatrix}-\frac{\partial v}{\partial x}\\ -\frac{\partial w}{\partial x}\end{bmatrix}$$

$$\begin{bmatrix}\mathrm{r}_y^*\\ \mathrm{r}_z^*\end{bmatrix}=\frac{\begin{bmatrix}\frac{\partial w}{\partial z}-\lambda_r & -\frac{\partial w}{\partial y}\\ -\frac{\partial v}{\partial z} & \frac{\partial v}{\partial y}-\lambda_r\end{bmatrix}}{\begin{vmatrix}\frac{\partial v}{\partial y}-\lambda_r & \frac{\partial v}{\partial z}\\ \frac{\partial w}{\partial y} & \frac{\partial w}{\partial z}-\lambda_r\end{vmatrix}}\times\begin{bmatrix}-\frac{\partial v}{\partial x}\\ -\frac{\partial w}{\partial x}\end{bmatrix}$$

$$\begin{bmatrix}\mathrm{r}_y^*\\ \mathrm{r}_z^*\end{bmatrix}=\frac{\begin{bmatrix}\frac{\partial w}{\partial z}-\lambda_r & -\frac{\partial w}{\partial y}\\ -\frac{\partial v}{\partial z} & \frac{\partial v}{\partial y}-\lambda_r\end{bmatrix}\times\begin{bmatrix}-\frac{\partial v}{\partial x}\\ -\frac{\partial w}{\partial x}\end{bmatrix}}{\left(\frac{\partial v}{\partial y}-\lambda_r\right)\left(\frac{\partial w}{\partial z}-\lambda_r\right)-\frac{\partial v\partial w}{\partial z\partial y}}$$

Comparing the corresponding components, we get:

$$\mathrm{r}_y^*=\frac{-\left(\frac{\partial w}{\partial z}-\lambda_r\right)\frac{\partial v}{\partial x}+\frac{\partial v\partial w}{\partial z\partial x}}{\left(\frac{\partial v}{\partial y}-\lambda_r\right)\left(\frac{\partial w}{\partial z}-\lambda_r\right)-\frac{\partial v\partial w}{\partial z\partial y}}$$

$$\mathrm{r}_z^*=\frac{\frac{\partial w\partial v}{\partial y\partial x}-\left(\frac{\partial v}{\partial y}-\lambda_r\right)\frac{\partial w}{\partial x}}{\left(\frac{\partial v}{\partial y}-\lambda_r\right)\left(\frac{\partial w}{\partial z}-\lambda_r\right)-\frac{\partial v\partial w}{\partial z\partial y}}$$

Case-2: Let $\Delta_{max}=\left|\Delta_y\right|$, then we can take: $\mathrm{r}_y^*=1$,

$$r_x^* = \frac{-\left(\frac{\partial w}{\partial z} - \lambda_r\right)\frac{\partial u}{\partial y} + \frac{\partial u}{\partial z}\frac{\partial w}{\partial y}}{\left(\frac{\partial u}{\partial x} - \lambda_r\right)\left(\frac{\partial w}{\partial z} - \lambda_r\right) - \frac{\partial u}{\partial z}\frac{\partial w}{\partial x}}$$

$$r_y^* = 1$$

$$r_z^* = \frac{\frac{\partial w}{\partial x}\frac{\partial u}{\partial y} - \left(\frac{\partial u}{\partial x} - \lambda_r\right)\frac{\partial w}{\partial y}}{\left(\frac{\partial u}{\partial x} - \lambda_r\right)\left(\frac{\partial w}{\partial z} - \lambda_r\right) - \frac{\partial u}{\partial z}\frac{\partial w}{\partial x}}$$

Case-3: Let $\Delta_{max} = |\Delta_z|$, then we can take: $r_z^* = 1$,

$$r_x^* = \frac{-\left(\frac{\partial v}{\partial y} - \lambda_r\right)\frac{\partial u}{\partial z} + \frac{\partial u}{\partial y}\frac{\partial v}{\partial z}}{\left(\frac{\partial u}{\partial x} - \lambda_r\right)\left(\frac{\partial v}{\partial y} - \lambda_r\right) - \frac{\partial u}{\partial y}\frac{\partial v}{\partial x}}$$

$$r_y^* = \frac{\frac{\partial v}{\partial x}\frac{\partial u}{\partial z} - \left(\frac{\partial u}{\partial x} - \lambda_r\right)\frac{\partial v}{\partial z}}{\left(\frac{\partial u}{\partial x} - \lambda_r\right)\left(\frac{\partial v}{\partial y} - \lambda_r\right) - \frac{\partial u}{\partial y}\frac{\partial v}{\partial x}}$$

$$r_z^* = 1,$$

So, the normalized real eigenvector $\vec{r}$ can be written as:

$$\vec{r} = \vec{r}^*/|\vec{r}^*| \tag{4.21}$$

Where, $|\vec{r}^*|$ is an absolute value of $\vec{r}^*$.i.e., $|\vec{r}^*| = \sqrt{r_x^{*2} + r_y^{*2} + r_z^{*2}}$

4.3.2. Numerical algorithm for solving cubic equation:

1) Step 1:set velocity gradient tensor,

a(1,1) = du/dx(i, j, k)

a(1,2) = du/dy(i, j, k)

a(1,3) = du/dz(i, j, k)

a(2,1) = dv/dx(i, j, k)

a(2,2) = dv/dy(i, j, k)

a(2,3) = dv/dz(i, j, k)

a(3,1) = dw/dx(i, j, k)

a(3,2) = dw/dy(i, j, k)

a(3,3) = dw/dz(i, j, k)

2) Step 2: set a cubic equation,

$X^3 + (aa)\, x^2 + (bb)\, x + cc = 0$, where aa and bb are coefficients and cc is a constant.

3) Step 3: set coefficients of characteristic equation,

```
aa = -(a(1,1)+a(2,2)+a(3,3))
mm = matmul(a,a)
bb = -0.5*(mm(1,1)+mm(2,2)+mm(3,3)-(a(1,1)+a(2,2)+a(3,3))**2)
cc = -(a(1,1)*(a(2,2)*a(3,3)-a(2,3)*a(3,2))-a(1,2)*(a(2,1)*a(3,3)-a(2,3)*a(3,1))
    +a(1,3)*(a(2,1)*a(3,2)-a(2,2)*a(3,1)))
```

4) Sepe 4: find the discriminant of characteristic equation,

$delta = 18(aa)(bb)(cc)-4(aa)^3(cc)+(aa)^2\,(bb)^2-4(bb)^3-27(cc)^2$

5) Setp 5: for real aa, bb and cc, compute Q and R,

$Q = (aa^2-3bb)/9.0$

$R = (2(aa)^3-9(aa)(bb)+27cc)/54.0$

$Delta = R^2 - Q^3$

6) Setp 6: If Delta < 0, then compute,

$$\theta = \text{acos}(R/Q^{\frac{1}{3}})$$

The three real eigen values are given by,

$$\lambda_1 = -2Q^{\frac{1}{2}}\cos(\frac{\theta}{3}) - \frac{aa}{3}$$

$$\lambda_2 = -2Q^{\frac{1}{2}}\cos(\frac{\theta + 2\pi)}{3}) - \frac{aa}{3}$$

$$\lambda_3 = -2Q^{\frac{1}{2}}\cos(\frac{\theta - 2\pi)}{3}) - \frac{aa}{3}$$

7) Setp 5: if(delta > 0.0) then calculate one real root and two complex conjugate roots

```
A = -sign(1.0, R)*(abs(R)+sqrt(delta))**(1.0/3.0)
if(A == 0.0) then
  B = 0.0
```

else

B = Q/A

end if

$\lambda_1$ = cmplx(-0.5*(A+B)-aa/3.0, 0.5*sqrt(3.0)*(A-B))

$\lambda_2$ = cmplx(real(eig1c), -aimag(eig1c))

$\lambda_3$ = A+B-aa/3.0

8) Setp 5: find real right eigenvector

evec1 = (a(1,1)-eig3r)*(a(2,2)-eig3r) - a(2,1)*a(1,2)

evev2 = (a(2,2)-eig3r)*(a(3,3)-eig3r) - a(2,3)*a(3,2)

evec3 = (a(1,1)-eig3r)*(a(3,3)-eig3r) - a(1,3)*a(3,1)

if(delta1 == 0.0 .and. delta2 == 0.0 .and. delta3 == 0.0) then

write(*,*) 'ERROR: delta1 = delta2 = delta3 = 0.0'

end if

4.3.3. Velocity gradient tensor in new XYZ-frame

There are two possible cases for eigenvalues of a 3x3 matrix, which are

1) three real eigenvalues
2) one real and two conjugate complex eigenvalues, depending on the sign of Δ.

In a 3x3 real matrix, we must have at least one real eigenvalue and corresponding one real eigenvector. If all three eigenvalues of the matrix are three, then fluid particles in the flow field do not have rotation. However, it the matrix has one real and a pair of complex conjugate eigenvalues, then the matrix represents fluid rotation. The general form of three eigenvalues in the rotation points can be written:

$$\lambda_r,\ \lambda_{cr} + i\lambda_{ci}, and\ \ \lambda_{cr} - i\lambda_{ci}$$

From the eigen definition, we have:

$$\nabla\vec{v}\,\vec{r} = \lambda_r\,\vec{r}$$

Since we are primarily interested in fluid rotation, we only consider case-2 i.e., when the 3x3 matrix has one real and two conjugate complex eigenvalues.

Definition 4.3:

A matrix P is called an orthogonal matrix if its inverse equals to transpose. In another words, it is a real square matrix whose columns and rows are orthonormal vectors.

Mathematically, $PP^T = I$, where I is an identity matrix.

The velocity gradient tensor in a flow field is given by:

$$\nabla\vec{v} = \begin{bmatrix} \frac{\partial u}{\partial x} & \frac{\partial u}{\partial y} & \frac{\partial u}{\partial z} \\ \frac{\partial v}{\partial x} & \frac{\partial v}{\partial y} & \frac{\partial v}{\partial z} \\ \frac{\partial w}{\partial x} & \frac{\partial w}{\partial y} & \frac{\partial w}{\partial z} \end{bmatrix},$$

We can find an orthogonal rotation matrix Q which rotates the original coordinates xyz to new coordinates XYZ where the Z-axis of the new coordinate system coincide with the real eigenvector $\vec{r}$ of the velocity gradient tensor $\nabla\vec{V}$. In other words, the new velocity gradient tensor $\nabla\vec{V}$ in Rotated/new coordinates (X, Y, Z) has the Z-coordinate axis aligned with real eigenvector $\vec{r}$ of $\nabla\vec{V}$. Let U, V and W are velocity components along X,Y and Z directions in the new frame, then the velocity gradient tensor in the new coordinates is given by:

$$\nabla\vec{V} = \begin{bmatrix} \frac{\partial U}{\partial X} & \frac{\partial U}{\partial Y} & \frac{\partial U}{\partial Z} \\ \frac{\partial V}{\partial X} & \frac{\partial V}{\partial Y} & \frac{\partial V}{\partial Z} \\ \frac{\partial W}{\partial X} & \frac{\partial W}{\partial Y} & \frac{\partial W}{\partial Z} \end{bmatrix} \text{ and}$$

$$\nabla\vec{V} = Q\nabla\vec{v}Q^{-1} \tag{4.22}$$

where $Q$ is the orthogonal rotation matrix that rotates the frame from the original $xyz$-frame to the new $XYZ$-frame.

We first rotate our z-axis from the old frame by orthogonal rotation matrix $Q$ so that Z-axis in the new frame is parallel to the real eigenvector of $\nabla\vec{V}$. In this case, we have:

$$\begin{bmatrix} X \\ Y \\ Z \end{bmatrix} = Q \begin{bmatrix} x \\ y \\ z \end{bmatrix} \tag{4.23}$$

Where, $Q = Q_x(\alpha)Q_y(\beta)Q_z(\gamma), \quad QQ^T = I,$

$$Q_x(\alpha) = \begin{bmatrix} 1 & 0 & 0 \\ 0 & cos\alpha & -sin\alpha \\ 0 & sin\alpha & cos\alpha \end{bmatrix} \tag{4.24}$$

$$Q_y(\beta) = \begin{bmatrix} cos\beta & 0 & sin\beta \\ 0 & 1 & 0 \\ -sin\beta & 0 & cos\beta \end{bmatrix} \tag{4.25}$$

$$Q_z(\gamma) = \begin{bmatrix} cos\gamma & -sin\gamma & 0 \\ sin\gamma & cos\gamma & 0 \\ 0 & 0 & 1 \end{bmatrix} \tag{4.26}$$

This will give us the new matrix $\nabla\vec{V}$ in new frame (X, Y, Z), where Z-axis is aligned with real eigenvector $\vec{r}$ of $\nabla\vec{V}$. So, by the definition of eigenvalues and eigenvectors, we have,

$$\nabla\vec{V}\begin{bmatrix} 0 \\ 0 \\ 1 \end{bmatrix} = \lambda_r \begin{bmatrix} 0 \\ 0 \\ 1 \end{bmatrix},$$

$$\begin{bmatrix} \frac{\partial U}{\partial X} & \frac{\partial U}{\partial Y} & \frac{\partial U}{\partial Z} \\ \frac{\partial V}{\partial X} & \frac{\partial V}{\partial Y} & \frac{\partial V}{\partial Z} \\ \frac{\partial W}{\partial X} & \frac{\partial W}{\partial Y} & \frac{\partial W}{\partial Z} \end{bmatrix} \begin{bmatrix} 0 \\ 0 \\ 1 \end{bmatrix} = \lambda_r \begin{bmatrix} 0 \\ 0 \\ 1 \end{bmatrix}.$$

$$\begin{bmatrix} \frac{\partial U}{\partial Z} \\ \frac{\partial V}{\partial Z} \\ \frac{\partial W}{\partial Z} \end{bmatrix} = \begin{bmatrix} 0 \\ 0 \\ \lambda_r \end{bmatrix}.$$

So, we have,

$$\frac{\partial U}{\partial Z} = 0$$

$$\frac{\partial V}{\partial Z} = 0$$

$$\frac{\partial W}{\partial Z} = \lambda_r$$

So, the new $XYZ$-frame becomes:

$$\nabla\vec{V} = \begin{bmatrix} \frac{\partial U}{\partial X} & \frac{\partial U}{\partial Y} & 0 \\ \frac{\partial V}{\partial X} & \frac{\partial V}{\partial Y} & 0 \\ \frac{\partial W}{\partial X} & \frac{\partial W}{\partial Y} & \lambda_r \end{bmatrix} \tag{4.27}$$

This velocity gradient tensor in new rotated frame XYZ paves us a away to have thoughts about new unique Principal Coordinates and Principal Tensor.

4.4. The Novel Unique Principal Coordinates

We know the velocity gradient tensor is dependent on coordinates, and coordinates change. This will make velocity gradient tensor also change. So, there was a clear need to find the unique tensor that does change when the coordinates change. In another word, when a velocity gradient tensor was given, we had to find a unique coordinate system. So, we picked that unique coordinate as our Principal Coordinates which is uniquely determined by the velocity gradient tensor. In our case, the velocity gradient tensor had one real and a pair of conjugate complex eigenvalues, a Principal Coordinate was uniquely determined.

To find the Principal Coordinates of $\nabla\vec{v}$ at a local point in the flow field, we should first find the orthogonal rotation matrix $Q$ which rotates the coordinate axis so that Z-axis is aligned with real eigenvector $\vec{r}$. After that we need to rotate the coordinate axis by an orthogonal rotation matrix $P$ around $\vec{r}$ to get the principal coordinates. Here, Q is a three-dimensional rotation matrix that rotates the whole frame and P is a two-dimensional rotation matrix that rotates XY-plane around Z-axis. P and Q can be uniquely determined by $\nabla\vec{v}$. Mathematically,

$$\nabla\vec{V} = Q\nabla\vec{v}Q^{-1}$$

$$\nabla\vec{V}_\theta = P\nabla\vec{V}P^{-1}$$

where $P$ is the ratation matrix around the $Z$-axis, which is given by:

$$P = \begin{bmatrix} cos\theta & sin\theta & 0 \\ -sin\theta & cos\theta & 0 \\ 0 & 0 & 1 \end{bmatrix},$$

And its inverse is given by its transpose,

$$P^{-1} = \begin{bmatrix} cos\theta & -sin\theta & 0 \\ sin\theta & cos\theta & 0 \\ 0 & 0 & 1 \end{bmatrix}$$

This will give us the Principal Coordinates (X, Y, Z) in which the original velocity gradient tensor $\nabla\vec{v}$ becomes $\nabla\vec{V}_\theta$.

$$\nabla\vec{V}_\theta = P\nabla\vec{V}P^{-1} = P(Q\nabla\vec{v}Q^{-1})P^{-1} = \begin{bmatrix} \lambda_{cr} & -\frac{1}{2}R & 0 \\ \frac{1}{2}R + \epsilon & \lambda_{cr} & 0 \\ \frac{\partial W}{\partial X} & \frac{\partial W}{\partial Y} & \lambda_r \end{bmatrix} \quad (4.28)$$

where, $\lambda_r$ is the unique real eigenvalue, $\lambda_{cr}$ is the real part of the complex conjugate eigenvalues.

In the above tensor $\nabla\vec{V}_\theta$, the eigenvalues, $\lambda_r$, $\lambda_{cr} \pm i\lambda_{ci}$, and $\vec{\omega}$ are all Galilean invariant, i.e., invariant under coordinates change, and independent of coordinates flip or rotation. We only need orthogonal P and Q rotation to get $\frac{\partial W}{\partial X}$ and $\frac{\partial W}{\partial Y}$ in the Principal Coordinates which is the unique. So, we can obtain a unique Principal Coordinate and a unique 3x3 velocity gradient tensor (Principal Tensor) in the principal coordinates.

$$\nabla\vec{V}_\theta = \begin{bmatrix} \lambda_{cr} & -\frac{1}{2}R & 0 \\ \frac{1}{2}R + \epsilon & \lambda_{cr} & 0 \\ \xi & \eta & \lambda_r \end{bmatrix} \quad (4.29)$$

*Definition* 4.4: The Principal Coordinates at a point is a coordinate that satisfies:

1. Its *Z*-axis is parallel to the $\vec{r}$ (direction of Liutex)
2. The velocity gradient tensor under this coordinate is in the form of:

$$\nabla V = \begin{bmatrix} \lambda_{cr} & \frac{\partial U}{\partial Y} & 0 \\ \frac{\partial V}{\partial X} & \lambda_{cr} & 0 \\ \frac{\partial W}{\partial X} & \frac{\partial W}{\partial Y} & \lambda_r \end{bmatrix}, \tag{4.30}$$

where $\lambda_r$ and $\lambda_{cr}$ are the real eigenvalue and real part of the conjugate complex eigenvalue pair of the velocity gradient tensor, respectively, for rotation points.

3. $\frac{\partial U}{\partial Y} < 0$ and $\left|\frac{\partial U}{\partial Y}\right| < \left|\frac{\partial V}{\partial X}\right|$

*Theorem 4.1*:

Under the Principal Coordinates, $\frac{\partial U}{\partial Y} = -\frac{R}{2}$, where R is the magnitude of Liutex.

*Proof*:

For given velocity gradient tensor $\nabla v$, we have an orthogonal rotation matrix $Q_r$ which aligns Z-axis of new frame XYZ with Liutex direction $\vec{r}$ after the rotation.

$$\nabla V = Q_r \nabla v Q_r^T = \begin{bmatrix} \frac{\partial U}{\partial X} & \frac{\partial U}{\partial Y} & 0 \\ \frac{\partial V}{\partial X} & \frac{\partial V}{\partial Y} & 0 \\ \frac{\partial W}{\partial X} & \frac{\partial W}{\partial Y} & \frac{\partial W}{\partial Z} \end{bmatrix} \tag{4.31}$$

Then, a second rotation $P_r$ around Z-axes (P rotation) is applied.

$$P_r = \begin{bmatrix} cos\theta & sin\theta & 0 \\ -sin\theta & cos\theta & 0 \\ 0 & 0 & 1 \end{bmatrix} \tag{4.32}$$

And, the new velocity gradient tensor $\nabla V_\theta$ after rotation is:

$$\nabla V_\theta = P_r \nabla V P_r^T = \begin{bmatrix} \left.\frac{\partial U}{\partial X}\right|_\theta & \left.\frac{\partial U}{\partial Y}\right|_\theta & 0 \\ \left.\frac{\partial V}{\partial X}\right|_\theta & \left.\frac{\partial V}{\partial Y}\right|_\theta & 0 \\ \left.\frac{\partial W}{\partial X}\right|_\theta & \left.\frac{\partial W}{\partial Y}\right|_\theta & \left.\frac{\partial W}{\partial Z}\right|_\theta \end{bmatrix}$$

Where,

$$\left.\frac{\partial U}{\partial Y}\right|_{\theta} = \alpha \sin(2\theta + \varphi) - \beta \tag{4.33}$$

$$\left.\frac{\partial V}{\partial X}\right|_{\theta} = \alpha \sin(2\theta + \varphi) + \beta \tag{4.34}$$

$$\left.\frac{\partial U}{\partial X}\right|_{\theta} = -\alpha \cos(2\theta + \varphi) + \frac{1}{2}\left(\frac{\partial U}{\partial X} + \frac{\partial V}{\partial Y}\right) \tag{4.35}$$

$$\left.\frac{\partial V}{\partial Y}\right|_{\theta} = \alpha \cos(2\theta + \varphi) + \frac{1}{2}\left(\frac{\partial U}{\partial X} + \frac{\partial V}{\partial Y}\right) \tag{4.36}$$

$$\alpha = \frac{1}{2}\sqrt{\left(\frac{\partial v}{\partial y} - \frac{\partial u}{\partial x}\right)^2 + \left(\frac{\partial v}{\partial x} + \frac{\partial u}{\partial y}\right)^2} \tag{4.38}$$

$$\beta = \frac{1}{2}\left(\frac{\partial v}{\partial x} - \frac{\partial u}{\partial y}\right) \tag{4.39}$$

$$\varphi = \begin{cases} arctan\left(\frac{\frac{\partial v}{\partial x} + \frac{\partial u}{\partial y}}{\frac{\partial v}{\partial y} - \frac{\partial u}{\partial x}}\right), & \frac{\partial v}{\partial y} - \frac{\partial u}{\partial x} \neq 0 \\ \frac{\pi}{2}, & \frac{\partial v}{\partial y} - \frac{\partial u}{\partial x} = 0, \frac{\partial v}{\partial x} + \frac{\partial u}{\partial y} > 0 \\ -\frac{\pi}{2}, & \frac{\partial v}{\partial y} - \frac{\partial u}{\partial x} = 0, \frac{\partial v}{\partial x} + \frac{\partial u}{\partial y} < 0 \end{cases} \tag{4.40}$$

Then, the Liutex magnitude is defined as

$$R = \begin{cases} 2(|\beta| - \alpha), & \beta^2 > \alpha^2 \\ 0, & o.w. \end{cases} \tag{4.41}$$

Since for the points inside the vortex boundary, $\beta^2 > \alpha^2$, otherwise there is no vortex.

From part (2) in Def.4.4,

$$\left.\frac{\partial U}{\partial X}\right|_{\theta} = \left.\frac{\partial V}{\partial Y}\right|_{\theta} \tag{4.42}$$

Thus,

$$\cos(2\theta + \varphi) = 0 \tag{4.43}$$

Then,

$$\sin(2\theta + \varphi) = 1 \; or \; -1.$$

Case 1: $\beta > 0$ and $\sin(2\theta + \varphi) = 1$

$$\left.\frac{\partial U}{\partial Y}\right|_{\theta} = \alpha - \beta = -\frac{1}{2}R \tag{4.44}$$

Case 2: $\beta > 0$ and $\sin(2\theta + \varphi) = -1$

$$\left.\frac{\partial U}{\partial Y}\right|_{\theta} = -\alpha - \beta \tag{4.45}$$

$$\left.\frac{\partial V}{\partial X}\right|_{\theta} = -\alpha + \beta \tag{4.46}$$

However,

$$|-\alpha - \beta| > |-\alpha + \beta| \tag{4.47}$$

It violates the part (3) in Def. 2, and as a result $\sin(2\theta + \varphi) \neq -1$

Case 3: $\beta < 0$ and $\sin(2\theta + \varphi) = 1$

$$\left.\frac{\partial U}{\partial Y}\right|_{\theta} = \alpha - \beta \tag{4.48}$$

$$\left.\frac{\partial V}{\partial X}\right|_{\theta} = \alpha + \beta \tag{4.49}$$

$$\text{But, } |\alpha - \beta| > |\alpha + \beta| \tag{4.50}$$

The part (3) in Def.4.4 is not satisfied, so $\sin(2\theta + \varphi) \neq 1$

Case 4: $\beta < 0$ and $\sin(2\theta + \varphi) = -1$

$$\left.\frac{\partial U}{\partial Y}\right|_{\theta} = \alpha - \beta = -\frac{1}{2}R \tag{4.51}$$

Theorem 4.1 is verified.

*Theorem* 4.2: For an arbitrary velocity gradient tensor, there always exists unique Principal Coordinates.

Proof:

If directions of X, Y and Z axis are determined, the coordinate is well-defined. Firstly, the direction of Z-axis is unique, defined as $\vec{r}$. All the coordinates satisfying the Z-axis requirement can be achieved by rotating coordinate around $\vec{r}$.. Therefore, if the rotation angle is determined, so is the coordinate.

In the proof of theorem 4.1, if $\beta > 0$, then $\cos(2\theta + \varphi)$ and $\sin(2\theta + \varphi)$ must be 0 and 1, respectively.

Thus, $2\theta + \varphi = \frac{\pi}{2} \Rightarrow \theta = \frac{1}{2}(\frac{\pi}{2} - \varphi)$.

Similarly, if $\beta < 0$, then $\cos(2\theta + \varphi)$ and $\sin(2\theta + \varphi)$ must be 0 and -1.

So, $2\theta + \varphi = \frac{3\pi}{2} \Rightarrow \theta = \frac{1}{2}(\frac{3\pi}{2} - \varphi)$.

In conclusion, the Principal Coordinate is unique.

Next, we discuss about the Principal Tensor decomposition. But, before that I would like to recommend the paper explicit expressions for Rortex tensor and velocity gradient tensor decomposition [53].

4.5. Velocity gradient tensor decomposition in the principal coordinates

The velocity gradient tensor $\nabla V_\theta$ is unique for all rotation point. Additionally, we can further decompose $\nabla V_\theta$ in the Principal Coordinates:

$$\nabla V_\theta = \begin{bmatrix} \lambda_{cr} & -R & 0 \\ R+\varepsilon & \lambda_{cr} & 0 \\ \xi & \eta & \lambda_r \end{bmatrix}$$

$$= \begin{bmatrix} 0 & -R & 0 \\ R & 0 & 0 \\ 0 & 0 & 0 \end{bmatrix} + \begin{bmatrix} \lambda_{cr} & 0 & 0 \\ \varepsilon & \lambda_{cr} & 0 \\ \xi & \eta & \lambda_r \end{bmatrix}$$

$$= R + NR \tag{4.52}$$

Where R represents the rigid rotation part and NR is the non-rotational part since NR has three eigenvalues as the diagonal elements. NR also satisfies the condition of three zeros on the north east corner, which means three axes are not rotational.

The non-rotational part NR can be further decomposed as

$$\text{NR} = \begin{bmatrix} \lambda_{cr} & 0 & 0 \\ \varepsilon & \lambda_{cr} & 0 \\ \xi & \eta & \lambda_r \end{bmatrix} = \begin{bmatrix} \lambda_{cr} & 0 & 0 \\ 0 & \lambda_{cr} & 0 \\ 0 & 0 & \lambda_r \end{bmatrix} + \begin{bmatrix} 0 & 0 & 0 \\ \varepsilon & 0 & 0 \\ \xi & \eta & 0 \end{bmatrix} = \text{B+ C} \tag{4.53}$$

Where C represents stretching (compression), C is shear matrix. This decomposition can be done only in the principal coordinates and therefore is unique and is independent on selection of the original coordinates (x, y, z). This unique velocity gradient tensor decomposition is called Principal Tensor Decomposition and even the gradient components are Gallilean invariant . Unlike Cauchy-Stoke's decomposition, Principal Tensor decomposition is independent of coordinates change.

*Definition* 3: The Principal Decomposition is the decomposition under the Principal Coordinate i.e.

$$\nabla V = \begin{bmatrix} \lambda_{cr} & -\frac{R}{2} & 0 \\ \frac{R}{2}+\varepsilon & \lambda_{cr} & 0 \\ \xi & \eta & \lambda_r \end{bmatrix} = \begin{bmatrix} 0 & -\frac{R}{2} & 0 \\ \frac{R}{2} & 0 & 0 \\ 0 & 0 & 0 \end{bmatrix} + \begin{bmatrix} 0 & 0 & 0 \\ \varepsilon & 0 & 0 \\ \xi & \eta & 0 \end{bmatrix} + \begin{bmatrix} \lambda_{cr} & 0 & 0 \\ 0 & \lambda_{cr} & 0 \\ 0 & 0 & \lambda_r \end{bmatrix} = A + B + C \quad (4.54)$$

Where A represents the rotation part, B represents the shear part, and C represents the stretching part.

The Principal Decomposition correctly and uniquely decomposes the velocity gradient tensor into the rotation part, shear part, and stretching part. So, the shear and stretching contamination analysis can be done uniquely only in the Principal Coordinate, which will be discussed in the next chapter.

# CHAPTER 5

# CONTAMINATION ANALYSIS OF VORTEX IDENTIFICATION METHODS ON PRINCIPAL COORDINATES.

Fluid rotation is not a rigid rotation. It has a mixture if rigid rotation, stretching or compression, and shear or deformation. In this chapter, we given the formulae for some first- and second-generation vortex identification methods in Principal Coordinate. These formulae can measure the extent of contamination of fluid flow by shearing and stretching or compression. But, at first, an article on a selected review of vortex identification methods with applications by Zhang et. all is recommended [54].

## 5.1. Theoretical Contamination Analysis

Let the velocity gradient tensor in the Principal Coordinate is:

$$\nabla\vec{V} = \begin{bmatrix} \lambda_{cr} & -\frac{1}{2}R & 0 \\ \frac{1}{2}R + \varepsilon & \lambda_{cr} & 0 \\ \xi & \eta & \lambda_r \end{bmatrix} \tag{5.1}$$

The Principal Decomposition, which is the decomposition of velocity gradient tensor in Principal Coordinate, is given by:

$$\nabla\vec{V} = \begin{bmatrix} \lambda_{cr} & -\frac{1}{2}R & 0 \\ \frac{1}{2}R + \varepsilon & \lambda_{cr} & 0 \\ \xi & \eta & \lambda_r \end{bmatrix} = \begin{bmatrix} 0 & -\frac{R}{2} & 0 \\ \frac{R}{2} & 0 & 0 \\ 0 & 0 & 0 \end{bmatrix} + \begin{bmatrix} 0 & 0 & 0 \\ \varepsilon & 0 & 0 \\ \xi & \eta & 0 \end{bmatrix} + \begin{bmatrix} \lambda_{cr} & 0 & 0 \\ 0 & \lambda_{cr} & 0 \\ 0 & 0 & \lambda_r \end{bmatrix}$$

$$\nabla\vec{V} = A + B + C \tag{5.2}$$

Where A is the rotational part; B is the shear part and C is the stretching part.

On the basis of Principal Tensor Decomposition, for the first time in the literature, we are defining the several vortex identifications schemes in the Principal Coordinate, which will allow us to analyze the contamination effects on these traditional vortex identification methods. In another words, we are going to analyze how these traditional vortex identification methods are contaminated by shear and stretching.

5.1.1 Contamination of vorticity

Plugging in the gradient components from (5.1) into the vorticity equation of definition 3.1 gives us the vorticity vector as

$$\omega = (\eta, -\xi, R + \varepsilon)^T \tag{5.3}$$

and its magnitude is

$$\|\omega\| = \sqrt{\eta^2 + \xi^2 + (R + \varepsilon)^2} \tag{5.4}$$

From the equations (5.3) and (5.4), it can be concluded that a vorticity vector does not only represent rotation but also claims shearing and stretching components to be a part of the vortical structure, which is clearly contaminated by shears.

5.1.2 Contamination of Q method

The scalar magnitude of Q method can be calculated based on velocity gradient tensor in the Principal Coordinates.

$$\nabla\vec{V} = \begin{bmatrix} \lambda_{cr} & -\frac{1}{2}R & 0 \\ \frac{1}{2}R + \varepsilon & \lambda_{cr} & 0 \\ \xi & \eta & \lambda_r \end{bmatrix} = \begin{bmatrix} \lambda_{cr} & \frac{1}{2}\varepsilon & \frac{1}{2}\xi \\ \frac{1}{2}\varepsilon & \lambda_{cr} & \frac{1}{2}\eta \\ \frac{1}{2}\xi & \frac{1}{2}\eta & \lambda_r \end{bmatrix} + \begin{bmatrix} 0 & -\frac{1}{2}R - \frac{1}{2}\varepsilon & -\frac{1}{2}\xi \\ \frac{1}{2}R + \frac{1}{2}\varepsilon & 0 & -\frac{1}{2}\eta \\ \frac{1}{2}\xi & \frac{1}{2}\eta & 0 \end{bmatrix}$$

$$= A_Q + B_Q \tag{5.5}$$

$$Q = \frac{1}{2}\left(\|B_Q\|_F^2 - \|A_Q\|_F^2\right)$$

$$= \frac{1}{2}\left[2\left(\frac{R}{2} + \frac{\varepsilon}{2}\right) + 2\left(\frac{\xi}{2}\right)^2 + 2\left(\frac{\eta}{2}\right)^2\right] - \frac{1}{2}\left[2\,{\lambda_{cr}}^2 + {\lambda_r}^2 + 2\left(\frac{\varepsilon}{2}\right)^2 + 2\left(\frac{\xi}{2}\right)^2 + 2\left(\frac{\eta}{2}\right)^2\right]$$

$$= \left(\frac{R}{2}\right)^2 + \frac{1}{2}R \cdot \varepsilon - {\lambda_{cr}}^2 - \frac{1}{2}{\lambda_r}^2 \tag{5.6}$$

It can be clearly seen that from the expression of Q above there is not only R, which is the magnitude of rotation, but also $\varepsilon$, $\lambda_{cr}$ and $\lambda_r$ which are either the shear part or stretching part in the Q-criterion. Therefore, the value of Q is certainly contaminated by shear and stretching.

### 5.1.3 Contamination of $\lambda_{ci}$ Criterion

The characteristic equation of velocity gradient tensor given by (5.1) is

$$(\lambda - \lambda_r)\left[(\lambda - \lambda_{cr})^2 + \frac{R}{2\left(\frac{R}{2}+\varepsilon\right)}\right] = 0 \tag{5.7}$$

Thus, the eigenvalues are

$$\lambda_1 = \lambda_r, \lambda_2 = \lambda_{cr} + i\sqrt{R/2(R/2+\varepsilon)}, \lambda_3 = \lambda_{cr} - i\sqrt{R/2(R/2+\varepsilon)}$$

Since rotation is orthogonal, eigenvalues are the same as the original velocity gradient tensor,

$$\lambda_2 = \lambda_{cr} + i\sqrt{R/2(R/2+\varepsilon)} = \lambda_{cr} + i\lambda_{ci}$$

$$\lambda_3 = \lambda_{cr} - i\sqrt{R/2(R/2+\varepsilon)} == \lambda_{cr} - i\lambda_{ci}$$

Therefore, we have

$$\frac{R}{2}\left(\frac{R}{2}+\varepsilon\right) = \lambda_{ci}^2 \tag{5.8}$$

Thus,

$$\lambda_{ci} = \sqrt{\frac{R}{2}\left(\frac{R}{2}+\varepsilon\right)} \tag{5.9}$$

The expression of $\lambda_{ci}$ has $\varepsilon$, which is in the shear part of the Principal Decomposition. As a result, $\lambda_{ci}$ is contaminated by shear.

### 5.1.4 Contamination of $\Delta$ method

In section 4.2, it is known that three roots of the characteristic equation is

$$\lambda_1 = \lambda_r, \lambda_2 = \lambda_{cr} + i\sqrt{R/2(R/2+\varepsilon)}, \lambda_3 = \lambda_{cr} - i\sqrt{R/2(R/2+\varepsilon)}$$

Plug their values into (3.1),(3.2) and (3.3)

$$I_1 = -(\lambda_1 + \lambda_2 + \lambda_3) = -\lambda_r - 2\lambda_{cr} \tag{5.10}$$

$$I_2 = \lambda_1\lambda_2 + \lambda_2\lambda_3 + \lambda_3\lambda_1 = 2\lambda_r\lambda_{cr} + \lambda_{cr}^2 + \frac{R}{2}\left(\frac{R}{2} + \varepsilon\right) \tag{5.11}$$

$$I_3 = -\lambda_1\lambda_2\lambda_3 = -\lambda_r\left[\lambda_{cr}^2 + \frac{R}{2}\left(\frac{R}{2} + \varepsilon\right)\right] \tag{5.12}$$

$$\text{So, } \tilde{Q} = I_2 - \frac{1}{3}{I_1}^2 = -\frac{1}{3}(\lambda_{cr} - \lambda_r)^2 + \frac{R}{2}\left(\frac{R}{2} + \varepsilon\right) \tag{5.13}$$

$$\tilde{R} = I_3 + \frac{2}{27}{I_1}^3 - \frac{1}{3}I_1I_2 = \frac{2}{27}(\lambda_{cr} - \lambda_r)^3 + \frac{2}{3}(\lambda_{cr} - \lambda_r)\frac{R}{2}\left(\frac{R}{2} + \varepsilon\right) \tag{5.14}$$

Then, the expression of Δ can be written as

$$\Delta = \left(\frac{\tilde{Q}}{3}\right)^3 + \left(\frac{\tilde{R}}{2}\right)^2 = \frac{1}{243}\left[\begin{array}{c} 9\left(\frac{R}{2}\right)^3\left(\frac{R}{2} + \varepsilon\right)^3 - 6\left(\frac{R}{2}\right)^2\left(\frac{R}{2} + \varepsilon\right)^2(\lambda_{cr} - \lambda_r)^2 + \\ \frac{5R}{2}\left(\frac{R}{2} + \varepsilon\right)(\lambda_{cr} - \lambda_r)^4 \end{array}\right] \tag{5.15}$$

Obviously, $\varepsilon$, $\lambda_r$ and $\lambda_{cr}$ are included in the expression of $\Delta$, which indicates that $\Delta$ is contaminated by shear and stretching.

## 5.2. Vortex Example: Burger Vortex

A test case of a real vortex, namely Burger vortex, is examined to justify the comparison of the effects of shearing and stretching/compression on different criteria. The velocity gradient tensor has been obtained from the Burger vortex, which is an exact steady solution of the Navier-Stokes's equation and can be used to model fine scales of turbulence. The Burger vortex forms when an inward radial flow concentrates and spins around the symmetric axis, and the flow moves out in both directions along the z-axis.

The velocity components of Burger vortex in the cylindrical coordinate system are given by:

$$v_r = -\xi r \tag{5.16}$$

$$v_\theta = \frac{\Gamma}{2\Pi r}\left(1 - e^{\frac{-r^2\xi}{2\nu}}\right) \tag{5.17}$$

$$v_z = 2\xi z \tag{5.18}$$

where $\Gamma$ represents the circulation, $\xi$ the axisymmetric strain rate, $\nu$ the kinematic viscosity, and $r$ is the distance of the chosen point from the centerline in the Burger vortex.

For post-processing, the velocity components are converted into the Cartesians coordinate system given by:

$$u = -\xi x - \frac{\Gamma}{2\Pi r^2}\left(1 - e^{\frac{-r^2\xi}{2\nu}}\right)y \tag{5.19}$$

$$v = -\xi y + \frac{\Gamma}{2\Pi r^2}\left(1 - e^{\frac{-r^2\xi}{2\nu}}\right)x \tag{5.20}$$

$$w = 2\xi z \tag{5.21}$$

The existence of the vortex structure is highly contingent on the selection of parameters. For the proper vortex structure visualization, we take $\xi$ = 0.042, $\Gamma$ = 1.45 and $\nu = 0.01$. The calculation domain is taken with $50 \times 20 \times 20$ grid points with a step size of 0.5. The streamlines of Burger vortex exhibit a spiral pattern around the vortex rotation axis line, which has the maximum vortex strength. The streamlines representing such a flow are demonstrated in Fig. 1a and 1b, which show that flows enter from radial direction and stretches outward spinning around the axis. The vortex strength is strong in the core and becomes weak when moving away from the center. We can see this phenomenon in the following figures:

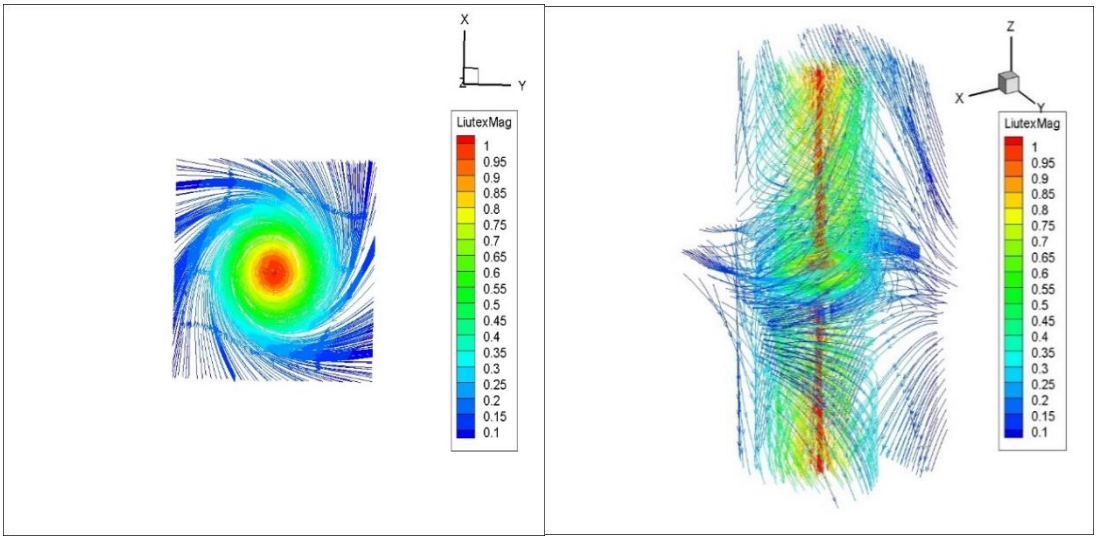


(a)Top View (b) Side View

Fig 5.1. (Color online) Streamlines of Burger vortex from top and side view with Liutex magnitude, which depicts the rotational strength of the fluid particles.

5.3. Numerical Contamination Analysis

The velocity gradient tensor in Principal Coordinate is:

$$\nabla V = \begin{bmatrix} \frac{\partial u}{\partial x} & \frac{\partial u}{\partial y} & \frac{\partial u}{\partial z} \\ \frac{\partial v}{\partial x} & \frac{\partial v}{\partial y} & \frac{\partial v}{\partial z} \\ \frac{\partial w}{\partial x} & \frac{\partial w}{\partial y} & \frac{\partial w}{\partial z} \end{bmatrix} = \begin{bmatrix} \lambda_{cr} & -\frac{1}{2}R & 0 \\ \frac{1}{2}R + \varepsilon & \lambda_{cr} & 0 \\ \xi & \eta & \lambda_r \end{bmatrix} \tag{5.22}$$

Where $u$, $v$ and $w$ are the three components of the velocity along $x$, $y$, and $z$ directions in Cartesian Coordinate.

Since our purpose is to demonstrate the shear and stretching contaminations of different criterion numerically, we add shear and stretching components separately and calculate how different criterion responds.

5.3.1 Adding Shear components on Principal Tensor.

The matrix corresponding to shear is of the form:

$$\nabla V_{shear} = \begin{bmatrix} 0 & 0 & 0 \\ \varepsilon_a & 0 & 0 \\ \xi_a & \eta_a & 0 \end{bmatrix} \tag{5.23}$$

The subscript "$a$" refers to "adding" of shearing components.

The new velocity gradient tensor in Principal Coordinates after adding shear is

$$\nabla V_1 = \begin{bmatrix} \lambda_{cr} & -\frac{1}{2}R & 0 \\ \frac{1}{2}R + \varepsilon + \varepsilon_a & \lambda_{cr} & 0 \\ \xi + \xi_a & \eta + \eta_a & \lambda_r \end{bmatrix} \tag{5.24}$$

Under Principal Coordinate, the local rotation axis is z-axis, so $\xi_a$ (value of $\frac{\partial w}{\partial x}$ component) and $\eta_a$ (value of $\frac{\partial w}{\partial y}$ component) are not in the rotation plane. Thus, these two issues will not influence the rotation strength. However, $\varepsilon_a$ is in the rotation plane, and it is possible to affect rotation strength. By Liutex definition, the magnitude of rotation strength is $\min_\theta \left\{ \left|\frac{\partial u}{\partial y}\right|_\theta, \left|\frac{\partial v}{\partial x}\right|_\theta \right\}$. $\left|\frac{\partial u}{\partial y}\right|_\theta$ and $\left|\frac{\partial v}{\partial x}\right|_\theta$ are the minimum absolute values of $\frac{\partial u}{\partial y}$ and $\frac{\partial v}{\partial x}$ respectively, when we rotate the coordinate $\theta$ angle anti-clockwise along z-axis.

Proposition 5.1: The rotation strength does not change if $\varepsilon_a \geq -\varepsilon$ and it changes if $\varepsilon_a < -\varepsilon$

Proof:

If $\varepsilon_a \geq -\varepsilon$, then, $\left|\frac{1}{2}R + \varepsilon + \varepsilon_a\right| \geq \left|-\frac{1}{2}R\right|$.

So, the Liutex magnitude is still $R$ which is defined as twice of the angular speed of the rigid rotation.

Remark: Physically, $\varepsilon_a < 0$ means adding a shear against the rotation direction and $\varepsilon_a < -\varepsilon$ indicates that shear is strong to the extent that it can affect rotation strength.

5.3.2 Adding Stretching components on Principal Tensor.

The matrix corresponding to stretching is of the form:

$$\nabla V_{stretching} = \begin{bmatrix} \alpha_a & 0 & 0 \\ 0 & \beta_a & 0 \\ 0 & 0 & \gamma_a \end{bmatrix} \tag{5.25}$$

The subscript "$a$" means "adding" the stretching components.

The new velocity gradient tensor after adding stretching is

$$\nabla V_2 = \begin{bmatrix} \lambda_{cr} + \alpha_a & -\frac{1}{2}R & 0 \\ \frac{1}{2}R + \varepsilon & \lambda_{cr} + \beta_a & 0 \\ \xi & \eta & \lambda_r + \gamma_a \end{bmatrix} \tag{5.26}$$

Proposition 5.2: The rotation strength does not change if $\alpha_a = \beta_a$.

Proof:

It is easy to know $\nabla V_2$ is the velocity gradient tensor under Principal Coordinate. Based on theorem 1, its rotation strength is still $R$. Therefore, to keep the rotation strength unchanged, the added $\nabla V_{stretching}$ should satisfy $\alpha_a = \beta_a$.

5.3.3 Stretching Contamination Analysis

The following procedure was implemented to depict how the vortex identification schemes react over the change in stretching effects. Firstly, we select a point in Burgers vortex, and its velocity gradient tensor is:

$$\nabla\vec{V}_B = \begin{bmatrix} -0.0419999994 & -0.0711665452 & 0.0000000000 \\ 0.0711665452 & -0.0419999994 & 0.0000000000 \\ 0.0000000000 & 0.0000000000 & 0.0839999988 \end{bmatrix} \tag{5.27}$$

Then for our convenience, the stretching matrix $\nabla V_{stretching}$ is added and the values of $Q, \Delta, \lambda_2, \lambda_{ci}$, and Liutex are recorded where $\nabla V_{stretching}$ is given by (note it satisfies the requirement of adding stretching):

$$\nabla V_{stretching} = \begin{bmatrix} 0.02 & 0 & 0 \\ 0 & 0.02 & 0 \\ 0 & 0 & -0.04 \end{bmatrix} \tag{5.28}$$

The sum of diagonals elements of $\nabla V_{stretching}$ is made zero, so it follows the continuity equation. The stretching effect given by $\nabla V_{stretching}$ is increased repeatedly, and the value of every scheme is recorded. The results are presented in the following graph, where the x-axis represents relative stretching rate, which is the ratio of stretching component and vorticity magnitude, and the y-axis gives the corresponding values of different vortex identification methods.

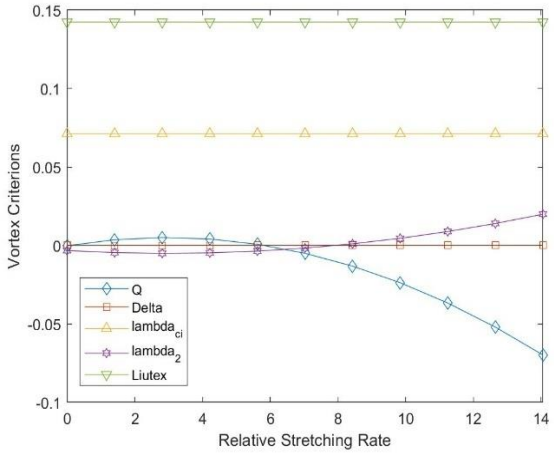


Fig. 5.2. Line graphs depicting the effect of stretching on different vortex identification methods.

The change in stretching components result in a change in $Q$, $\Delta$, $\lambda_2$, but $\lambda_{ci}$ and L are not changed, which means $\lambda_{ci}$ and L are not contaminated by stretching effect, as shown in Fig.5.2. It can also be observed that increasing the stretching effect would significantly decrease the positive value of $Q$ and ultimately becomes negative indicating non-vortical structure. However other criterions still show that there is a vortex structure. It can be concluded that $Q$ may conflict with other criterions. Theoretically, this makes sense, $\Delta$ could still be positive even if $Q$ is negative provided that the square of the third variant is large enough. The computational results shown in Fig. 5.2 are coincided with theoretical analysis.

### 5.3.4 Shear Contamination Analysis

A similar procedure to the stretching effect is implemented for the graphic representation of the shearing effect on the vortex identification schemes. Again, for our convenience, the shearing matrix $\nabla V_{shear}$ is defined as:

$$\nabla V_{shear} = \begin{bmatrix} 0 & 0 & 0 \\ 0.02 & 0 & 0 \\ 0.02 & 0.02 & 0 \end{bmatrix} \tag{5.29}$$

$\nabla V_{shear}$ is added to $\nabla \vec{V}_B$ for few times, and then the corresponding values of the different criterions are recorded. The results are presented in the following graph, where the x-axis represents relative shear rate, and the y-axis gives the corresponding values of different vortex identification methods.

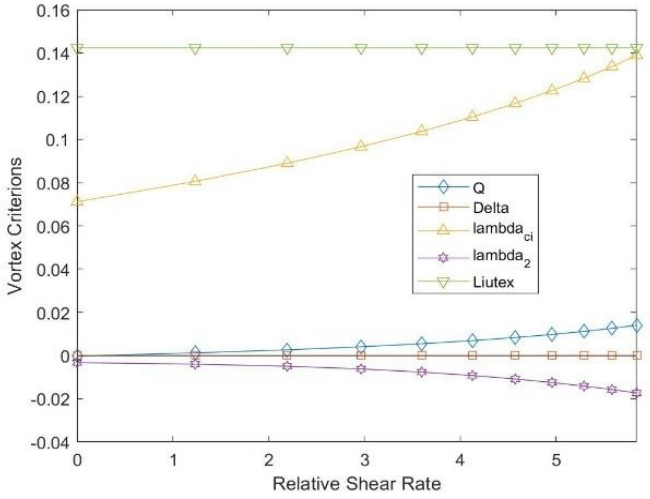


Fig. 5.3. Line graphs depicting the effect of shear on different vortex identification methods.

The relative shear rate is the ratio of the shearing component over vorticity magnitude. More precisely, it is the ratio of shear over vorticity at any point in our numerical domain. The reason we are dividing shear by vorticity is to refrain shear from getting too big. Fig. 5.3 indicates that $Q$, $\Delta$, $\lambda_2$, and $\lambda_{ci}$ are all greatly affected by the change in the shearing component, while L has remained unaffected by shear. It can be concluded from Fig. 5.2 and Fig. 5.3 that $Q$, $\Delta$, $\lambda_2$, and $\lambda_{ci}$ are all affected by either shear, stretching, or both at different levels whereas the Liutex method is affected by neither.

Since the values of $\Delta$ are very small, $\Delta$ looks to be consistently zero; however, if we use zoom in, it can be observed that the $\Delta$ values are increasing. The $\Delta$ - plots are given in Fig. 5.4 below:

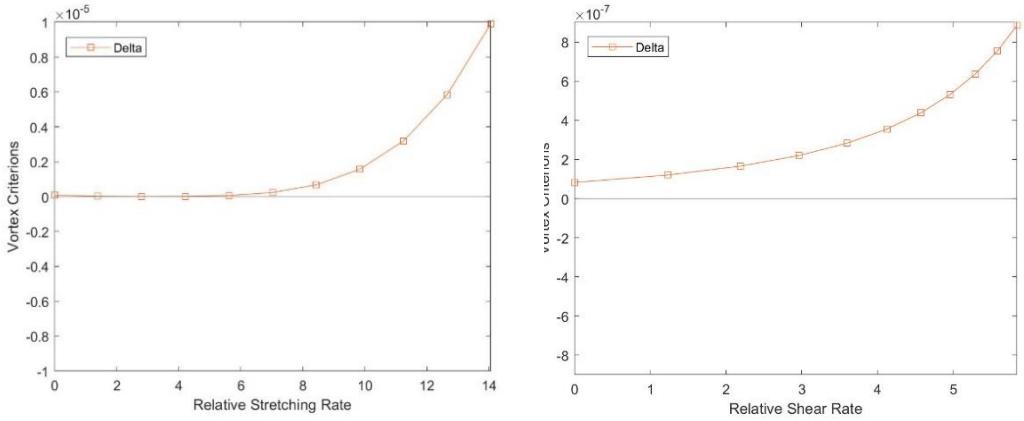


Fig. 5.4. Stretching and shearing effect on $\Delta$ method of vortex identification.

From above discussion and graphical representation, it can be concluded that:

1) All the second-generation methods are contaminated by shear, but Liutex is not.
2) $\lambda_{ci}$ and Liutex criterion are not contaminated by stretching.

# CHAPTER 6

# POD ANALYSIS VORTEX STRUCTURE IN LATE TRANSITION OF A FLAT PLATE BOUNDARY LAYER BY LIUTEX METHOD

## 6.1. Introduction

The proper orthogonal decomposition (POD) method is one of the most used data analysis and modeling technique in fluid mechanics. The POD methods enable us to reconstruct a flow with only a few most energetic modes. Sometimes, the fluid motion is not easily visible in raw data, in this case reconstructed POD modes can model the fluid motion. This method basically gives an orthogonal basis to represent a given set of data where we can find optimal lower-dimensional approximations for the given data set. The bases are also called POD modes. These POD modes best represent the data. The leading modes represent most of the kinetic energy of incompressible flow where as high-ordered POD modes represent a very few portions of total kinetic energy. In this chapter, POD is applied to study and analyze the vortex structure in late flow transition in the boundary layer of the flat plate obtained from DNS data provided by Texas Advanced Computing Center (TACC). Liutex vector is used as an input vector. So, leading modes have the highest rotational intensity while the trailing modes have lowest.

POD is used to find the most persistent spatial structures. The Modified Liutex-Omega vortex identification method is applied to DNS data to capture the vortex structure of flat plate boundary layer with iso-surfaces of $\Omega_L = 0.52$ with $\varepsilon = 0.001(b-a)_{max}$. Due to the limited computing memory capacity, snapshot POD is used. From the simulation of vortex structure in the flat plate boundary layer in a natural flow transition by DNS data, it is generally observed that the vortex structure starts with spanwise vortex, which is a vortex with its shape parallel to the y-axis, in the very early stage of transitional boundary layer. Then Λ-shaped vortex appears, and then hairpin vortices are formed one after another. These structures are periodic about y-axis and have the symmetry. Finally, in the late transition stage, these in flat plate flow transition in both experiments and DNS simulation for natural flow transition.

Most of the POD analysis have been done with velocity vector as an input. However, in this study, we use Liutex vector as an input as Liutex represents the local rigid rotation part of fluid motion without shear and stretching/compression contamination. The velocity modes are

related to the kinetic energy content whereas the Liutex mode represents the rotation intensity. Since Liutex vector represents local rigid rotation if fluids without any shear or stretching contamination, the Liutex vector is applied instead of velocity vector as an input for POD analysis.

## 6.2. Proper Orthogonal Decomposition (POD)

The POD is applied to late transition of boundary layer DNS data to find and analyze the elusive coherent structures that form random flow in late transition. This coherent structure can be constructed with first few modes. These POD modes also known as orthogonal basis which are ranked by fluctuating rotational intensity, where leading modes have the dominant rotational intensity and trailing modes have weak rotational intensity.

Definition 6.1:

POD modes are orthogonal basis for the given data set. In fluid mechanics, they are set of deterministic spatial functions received from decomposition of the random vector field representing the turbulent fluid motion. Each of these functions, also known as POD modes, can capture some portion of the total fluctuating kinetic energy of the flow. In general, leading modes captures the most kinetic energy and trailing modes captures the few.

Let $u(\mathrm{x},\mathrm{y},\mathrm{z},\mathrm{t})$ denote the vector field in the flow with fluctuating velocity. Then,

$$u(\mathrm{x},\mathrm{y},\mathrm{z},\mathrm{t}) = U(\mathrm{x},\mathrm{y},\mathrm{z}) - U'(\mathrm{x},\mathrm{y},\mathrm{z}), \tag{6.1}$$

Where, $U(\mathrm{x},\mathrm{y},\mathrm{z})$ is the velocity vector and $U'(\mathrm{x},\mathrm{y},\mathrm{z})$ is the temporal mean velocity vector (assumed to be stationary). Then, the POD decomposes the random vector field $u(\mathrm{x},\mathrm{y},\mathrm{z},\mathrm{t})$ into a sum of orthogonal basis functions/POD modes $\Phi_k(x,y,z)$ multiplied by random time coefficients $\mathrm{a}_k(t)$. i.e.,

$$u(\mathrm{x},\mathrm{y},\mathrm{z},\mathrm{t}) = \sum_{k=1}^{\infty} \mathrm{a}_k(t)\Phi_k(x,y,z)$$

Here, $\Phi_k$ is matrix of eigenvectors of covariance matrix $\frac{1}{m-1}U^T U$, where m is rows of $U$.
In matrix form, or it can be written as:

$$A = \Phi Q \tag{6.2}$$

Where the matrix $\Phi$ contains the spatial modes $\Phi_k(x, y, z)$ and $Q$ contains the temporal coefficients $a_k(t)$.

Definition 6.2:

Snapshot matrix is a matrix received from stacking vector of velocity values at several time steps. If our data has m velocity values, then our data (velocity vector) has the dimension $m \times 1$. If we combine the date set for n time steps, then we get a snapshot matrix with dimension $m \times n$.

POD has many a formulations and variants over the years. In this dissertation, we have use singular value decomposition for POD, which is equivalent to equation 6.1 or matrix form equation 6.2.

### 6.1.1 Singular value decomposition(SVD)

Singular value decomposition(SVD) is a method that factorizes a real $m \times n$ matrix A in to three matrices U, S, and V which is given as:

$$A = USV^T \tag{6.3}$$

Where, U is an $m \times n$ orthogonal matrix, S is a $m \times n$ singular matrix and V is a $m \times n$ orthogonal matrix. The diagonal elements of S are singular values arranged in decreasing order.

### 6.1.2 SVD algorithm

Step 1: Compile the data set at several snapshot (or time steps) from DNS data to get a snapshot matrix A. Each snapshot of our data set contains Liutex vectors at several spatial points. Each snapshot is of the form $x_j = p(x, y, z, t)$.

Suppose each snapshot has m spatial points. Let us combine n snapshots into a snapshot matrix A:

$$A = \begin{bmatrix} | & | & | & | \\ x_1 & x_2 & \dots & x_n \\ | & | & | & | \end{bmatrix}_{m \times n} \tag{6.4}$$

Here, $m \gg n$. In our case at each specific snapshot $x_j$, we have 6.2 million Liutex vectors and about 100 time-steps. So, the dimension of snapshot matrix in our case is about $6{,}220{,}800 \times 100$.

Step 2: Compute the SVD of matrix $A$.

$$A = USV^T, \tag{6.5}$$

Where, $U$ is an $m \times m$ and $V$ is $n \times n$ orthogonal matrices. The left matrix $U$ has spatial structure whereas the right matrix $V$ has temporal structure. $S$ is $m \times n$, which has the same dimension as $A$, singular matrix with singular values on the diagonal in decreasing order. i.e., $\sigma_1 \geq \sigma_2 \geq \cdots \geq \sigma_n$, $\sigma_i$ is singular values of $A$ and represent the rotational intensity of the flow.

The matrices $U, S$ and $V$ can be expressed as:

$$U = \begin{bmatrix} | & | & | & | \\ u_1 & u_2 & \cdots & u_m \\ | & | & | & | \end{bmatrix},\ S = \begin{bmatrix} \sigma_1 & 0 & \cdots & 0 \\ 0 & \sigma_2 & \cdots & 0 \\ \vdots & \vdots & \cdots & \vdots \\ \vdots & \vdots & \ddots & \vdots \\ 0 & 0 & 0 & \sigma_n \\ \vdots & \vdots & \vdots & \vdots \\ 0 & 0 & 0 & 0 \end{bmatrix},\ V = \begin{bmatrix} | & | & | & | \\ v_1 & v_2 & \cdots & v_n \\ | & | & | & | \end{bmatrix}. \tag{6.6}$$

So, the SVD decomposition of $A$ becomes:

$$A_{m\times n} = \begin{bmatrix} | & | & | & | \\ u_1 & u_2 & \cdots & u_m \\ | & | & | & | \end{bmatrix}_{m\times m} \begin{bmatrix} \sigma_1 & 0 & \cdots & 0 \\ 0 & \sigma_2 & \cdots & 0 \\ \vdots & \vdots & \cdots & \vdots \\ \vdots & \vdots & \ddots & \vdots \\ 0 & 0 & 0 & \sigma_n \\ \vdots & \vdots & \vdots & \vdots \\ 0 & 0 & 0 & 0 \end{bmatrix}_{m\times n} \begin{bmatrix} | & | & | & | \\ v_1 & v_2 & \cdots & v_n \\ | & | & | & | \end{bmatrix}_{n\times n} \tag{6.7}$$

6.1.3 Procedure to solve $U, S$ and $V$

Step 1: First, we find right orthogonal matrix $V$ and Singular matrix $S$. $V$ is the matrix of eigenvector of the covariance matrix $C$ i.e.,

$$C = A^T A,$$

Substituting the values of $A$ from SVD decomposition, we get:

$$C = (USV^T)^T USV^T$$

$$C = VSU^T USV^T$$

Since $U$ is an orthogonal matrix, $U^T U = I$. Then we have,

$$C = VS(I)SV^T$$

$$C = VS^2V^T$$

Multiplying both side by $V$,

$$CV = VS^2(V^T V)$$

Since $V$ is also orthogonal, $V^T V = I$, then we have:

$$CV = VS^2(I)$$

$$CV = VS^2 \tag{6.8}$$

Which is an eigen decomposition of the matrix $C$ with eigenvector matrix $V$ and eigenvalue matrix $S^2$.

$S^2$ has squared singular values ($\sigma^2$) along the diagonal. i.e., if $\lambda_i$ denote the eigenvalues of the covariance matrix $A^T A$, them $\lambda_i = {\sigma_i}^2$. So,

$$\sigma_i = \sqrt{\lambda_i} \tag{6.9}$$

The covariance matrix $C$ is symmetric and positive-semidefinite, so its eigenvalues $\lambda_i$ are real and nonnegative with $\lambda_1 \geq \lambda_2 \geq \cdots \geq \lambda_n \geq 0$. So, $\sigma_i$ are real and nonnegative with $\sigma_1 \geq \sigma_2 \geq \cdots \geq \sigma_n \geq 0$. When we know the eigenvectors and eigenvalues $\lambda_i$ of covariance matrix $C$, then we can get the right orthogonal matrix $V$ and singular matrix $S$.

$$V = \begin{bmatrix} | & & | & | & | \\ v_1 & v_2 & \cdots & v_n \\ | & & | & | & | \end{bmatrix} \tag{6.10}$$

$$S = \begin{bmatrix} \sigma_1 & 0 & \cdots & 0 \\ 0 & \sigma_2 & \cdots & 0 \\ \vdots & \vdots & \cdots & \vdots \\ \vdots & \vdots & \ddots & \vdots \\ 0 & 0 & 0 & \sigma_n \\ \vdots & \vdots & \vdots & \vdots \\ 0 & 0 & 0 & 0 \end{bmatrix} = \begin{bmatrix} \sqrt{\lambda_1} & 0 & \cdots & 0 \\ 0 & \sqrt{\lambda_2} & \cdots & 0 \\ \vdots & \vdots & \cdots & \vdots \\ \vdots & \vdots & \ddots & \vdots \\ 0 & 0 & 0 & \sqrt{\lambda_3} \\ \vdots & \vdots & \vdots & \vdots \\ 0 & 0 & 0 & 0 \end{bmatrix} \tag{6.11}$$

Step 2: Solve for the left orthogonal matrix $U$ by plugging $S$ and $V$ into SVD equation (6.5). From SVD equation (6.5),

$A = USV^T$.

Multiplying both sides by $V$,

$AV = US$

Again, multiplying both sides by $S^{-1}$,

$$AVS^{-1} = U \tag{6.12}$$

Despite being able to decompose the huge snapshot matrix $A$ and represent it with singular matrix $S$, we are still far away from being done as S still is as large as $A$ dimensionally. So, in the next section, we are going to discuss about the reduction of dimension and the reduction criteria. This is very important because it speeds up the computation algorithmically and saves the computation cost and time.

6.1.4 Criteria for dimensionality reduction

The dimension of left orthogonal matrix $U$ is $m \times m$ which is very large as we picked a lot of points in the flow field . In our case, we the dimension of $U$ is approximately 6.2 M × 6.2 M, which is a huge matrix to manage. This leads us to a situation that we still need to spend a lot of time in computation. So, we try to reduce the dimension of $U$. The singular matrix has the most features of original data and it has $n$ singular values along the diagonal and rest of the elements are zeros. So, we can reduce the size of singular matrix $S$ is from $m \times n$ to $n \times n$.

$$S = \begin{bmatrix} \sigma_1 & 0 & \cdots & 0 \\ 0 & \sigma_2 & \cdots & 0 \\ \vdots & \vdots & \ddots & \vdots \\ 0 & 0 & 0 & \sigma_n \end{bmatrix}. \tag{6.13}$$

Which is a reduced form of S with significantly lower dimension but with the same rank. This reduction will also decrease the size of left orthogonal matrix from $m \times m$ to $m \times n$.

$$U = \begin{bmatrix} | & | & | & | \\ u_1 & u_2 & \cdots & u_n \\ | & | & | & | \end{bmatrix}_{m\times n} \tag{6.14}$$

Now, the SVD decomposition of $A$ can be written as:

$$A_{m\times n} = \begin{bmatrix} | & | & | & | \\ u_1 & u_2 & \cdots & u_n \\ | & | & | & | \end{bmatrix}_{m\times n} \begin{bmatrix} \sigma_1 & 0 & \cdots & 0 \\ 0 & \sigma_2 & \cdots & 0 \\ \vdots & \vdots & \ddots & \vdots \\ 0 & 0 & 0 & \sigma_n \end{bmatrix}_{n\times n} \begin{bmatrix} | & | & | & | \\ v_1 & v_2 & \cdots & v_n \\ | & | & | & | \end{bmatrix}_{n\times n} \tag{6.15}$$

We can further reduce the dimension of left orthogonal matrix $U$ from $m \times n$ to $m \times r$, where $r \leq n$, by truncating the last $m - r$ columns of $U$. Now, to satisfy the multiplication criteria of matrices, we need to truncate the last $n - r$ rows and columns of singular matrix $S$. This will make the dimension of $S$ be $r \times r$. For the same reason we truncate the last $n - r$ rows of right orthogonal matrix $V$. This will make the dimension of matrix $V$ be $r \times n$.

Now, the SVD decomposition of the snapshot matrix $A$ in much lowered dimension can be written as:

$$A_{m\times n} = \begin{bmatrix} | & | & | & | \\ u_1 & u_2 & \cdots & u_m \\ | & | & | & | \end{bmatrix}_{m\times r} \begin{bmatrix} \sigma_1 & 0 & \cdots & 0 \\ 0 & \sigma_2 & \cdots & 0 \\ \vdots & \vdots & \ddots & \vdots \\ 0 & 0 & 0 & \sigma_r \end{bmatrix}_{r\times r} \begin{bmatrix} | & | & | & | \\ v_1 & v_2 & \cdots & v_n \\ | & | & | & | \end{bmatrix}_{r\times n} \tag{6.16}$$

Definition 6.3:

The snapshot matrix after the SVD decomposition is called reconstruction matrix. The new matrix $A$ given by above equation (6.16) is the approximated reconstruction of original snapshot matrix $A$ and it has significantly lower dimension, but it has most of the kinetic energy of the original matrix $A$. This is one of the most useful advantages of POD as it can model the fluid motion by few modes with same level of kinetic energy and with much lower dimension.

Next, we talk about how to choose the proper value of $r$. In another words, how to find the first $r$ POD basis functions. In fact, with the given tolerance condition, it can be calculated from the cumulative relative kinetic energy of snapshot matrix $A$ by the following formula:

$$\epsilon(r) = \frac{\sum_{i=1}^{r} \sigma_i^2}{\sum_{i=1}^{n} \sigma_i^2} \times 100\%, \tag{6.17}$$

$r$ is the possible minimum integer such that,

$$100 - \epsilon(r) \leq tol\ \% \tag{6.18}$$

where $tol$ % is a tolerance with $0 < tol\% < 1\%$. In our research, $tol = 1\%$

6.1.5. Snapshot matrix as a linear combination of POD modes

The reduced SVD decomposition of the snapshot matrix $A$ given by the equation (6.16) can be written in the summation of basis functions as:

$$A = \sum_{k=1}^{r} \sigma_k u_k v_k^T = \sigma_1 u_1 v_1^T + \sigma_2 u_2 v_2^T + \cdots + \sigma_r u_r v_r^T. \tag{6.19}$$

where the vector $v_i$ represents the spatial POD modes. The whole snapshot matrix $A$ that represent the fluid flow can be extracted into $r$ spatial POD modes where each mode symbolizes coherent structures. The main aim of dimensional reduction is to keep the modes with higher energy content as a basis. The first mode has the dominant kinetic energy while the last mode has the least kinetic energy. As the mode number increases, the amount of kinetic energy in each mode keeps decreasing.

6.2 POD analysis for boundary late transition by Modified Liutex Omega method

Modified Liutex-Omega method is used to present the iso-surface of POD modes to avoid the contamination by Shear and stretching or compression effect. First, a snapshot matrix $A$ is taken from DNS data of flat plate boundary layer with 100 snapshots in time between $t = 20.505T$ to $t = 21.00T$ , where T is period of Tollmein Schlichting wave, to study orthogonal basis functions (POD modes) of the coherent vortex structures , especially in the late transition of the boundary layer. Then, we have chosen the proper subzone in the late boundary layer transition defined by the parameters given in the Table 6.1 to study the POD decompositions of flow structure.

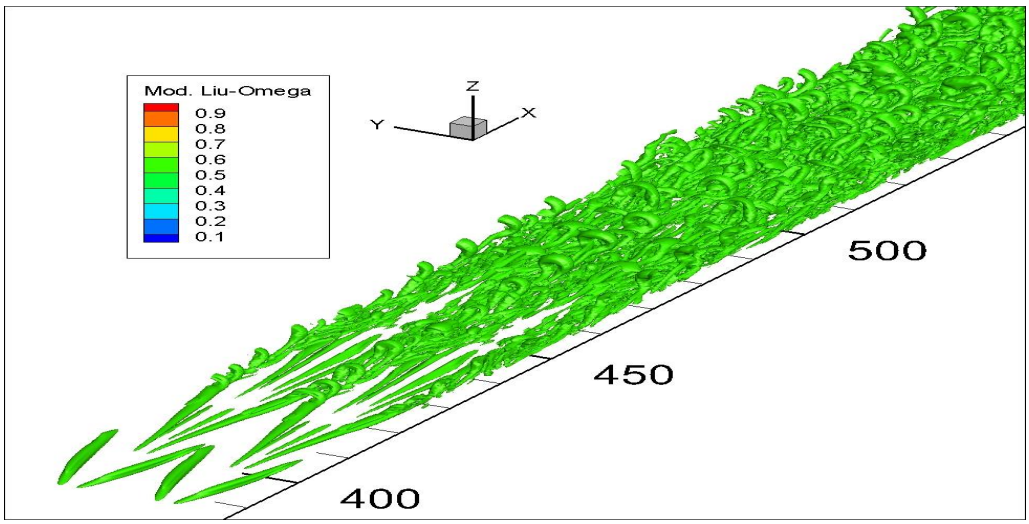


Fig 6.1. Vortex structure of transitional boundary layer by modified Liutex-Omega method.

The starting and ending points of index I , j, k along x, y and z directions are given the following table.

| Grid direction | Starting Index | Ending Index |
|---|---|---|
| i | 500 | 580 |
| j | 1 | 128 |
| k | 1 | 200 |

Table 6.1. Parameters of subzone

We compiled the data between the timesteps $t = 20.5\,T$ to $t = 21.0T$ into a snapshot matrix A,

$$\mathrm{A} = \begin{pmatrix} L_{x}{}^{(j)}_{500,1,1} \\ \vdots \\ L_{x}{}^{(j)}_{580,128,200} \\ L_{y}{}^{(j)}_{500,1,1} \\ \vdots \\ L_{y}{}^{(j)}_{580,128,200} \\ L_{z}{}^{(j)}_{500,1,1} \\ \vdots \\ L_{z}{}^{(j)}_{580,128,200} \end{pmatrix} \text{ for } j = 1, \dots, 100,$$

where $L_x{}^{(j)}, L_y{}^{(j)}$ and $L_z{}^{(j)}$ are Liutex vectors in x, y, z directions in the flow fields at several time steps $t = (20.50 + 0.005j)T$ where $j$ is from 1 to 100.

We have calculated the singular values through SVD decomposition method, and the singular values are ordered according to the portion of total rotational intensity they possess. The results of singular values are shown in Figures 6.2. It shows that the singular values converge to zero in this case. Which means the leading modes have the highest amplitude compared with trailing modes and ultimately, trailing modes have almost no rotational intensity. The appropriate number of modes $r$ is chosen in such a way that they contain about 99% of the total rotational intensity altogether. We can get the value of r by dimensional reduction equation (6.17) and equation (6.18). In figure 6.3, when cumulative rotational intensity reaches 99% of the total energy, that is where we get our required number of modes. In our case, the appropriate number of modes to reconstruct the vortex structure with 99% of the total rotational intensity is 34, so we choose r equals to 34.

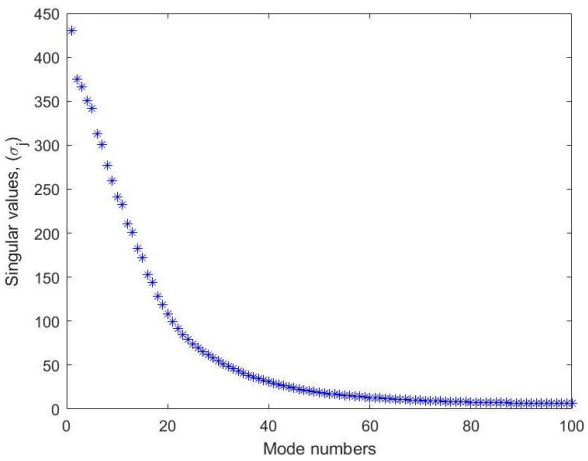


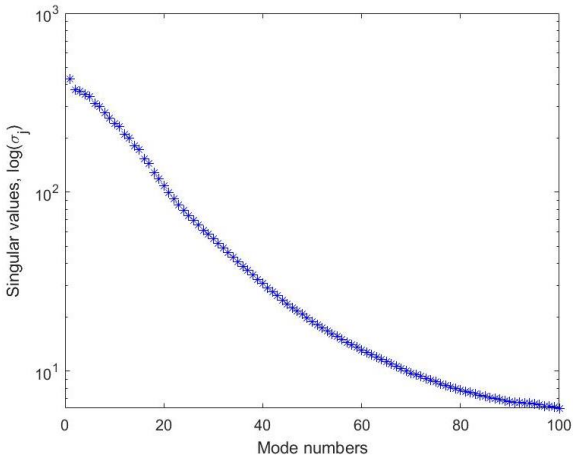


Fig 6.2. a) Singular values $\sigma_i$ of the matrix A (b) log scale plot of $\sigma_i$ of the matrix A

The figure 6.3. is drawn according to the dimension reduction criteria equation (6.17) and (6.18). Figure 6.3.a) show the rotational intensity possessed by various modes. From the same figure, we can see that mode 1 has more than 12% of the total rotational intensity of the fluid motion whereas mode 2 and 3 have approximately 10 % and 8% contribution. When the mode numbers keep going up, the amount of the rotational intensity possessed by these modes goes down and ultimately, they converge to zero.

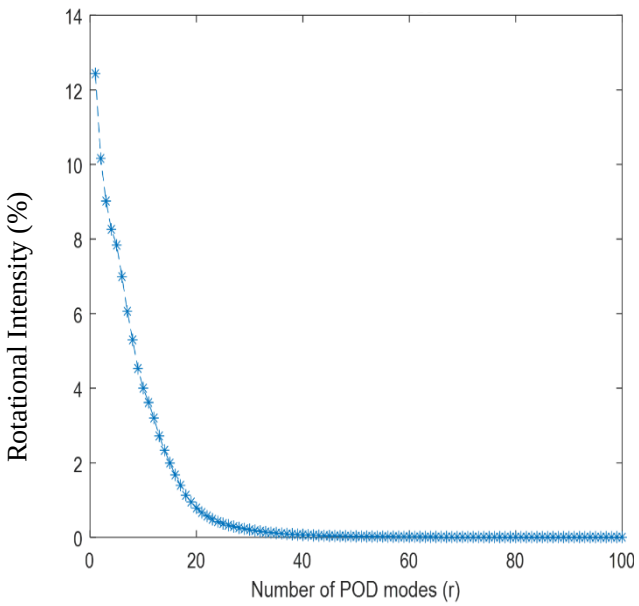


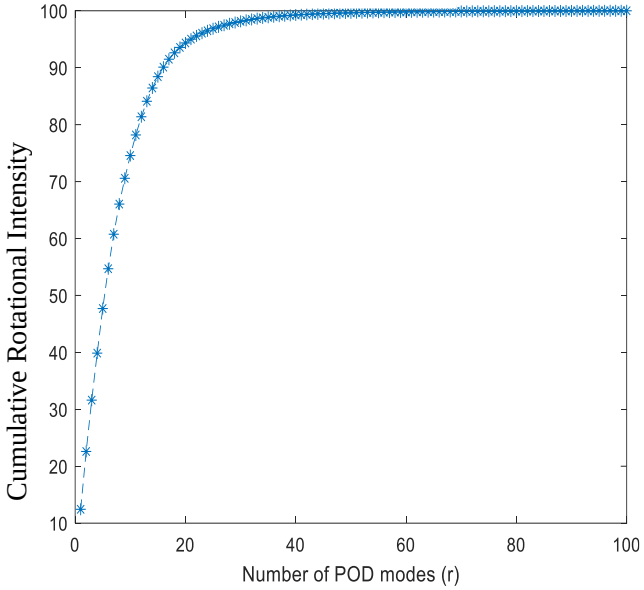


Fig 6.3.a) Rotational Intensity at various POD modes b) Cumulative Rotational Strength of POD modes.

The followings figures represent the structure of first ten POD modes. As the mode numbers goes up, they contain negligible (very few) amount of rotational intensity. In physical appearance of vortex structure also, they look quite similar. So, we have not included the remaining modal vortex structures.

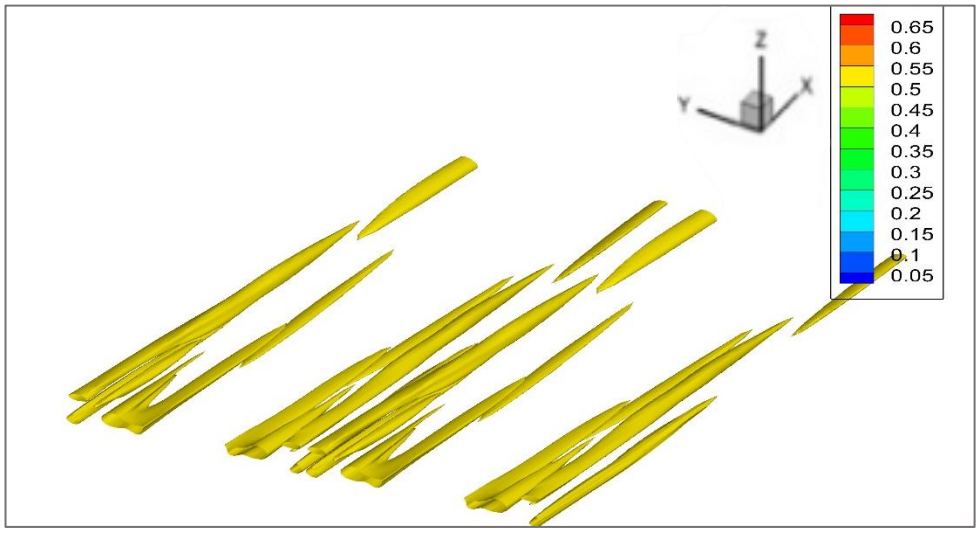


a) Mode 1

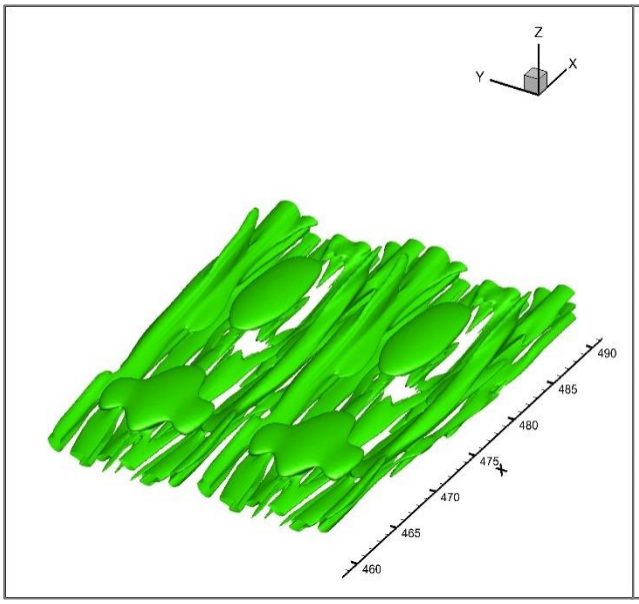


b) Mode 2

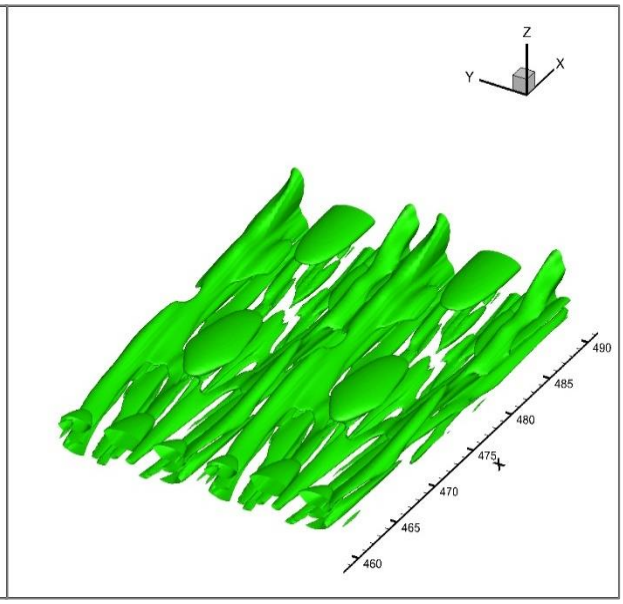


c) Mode 3

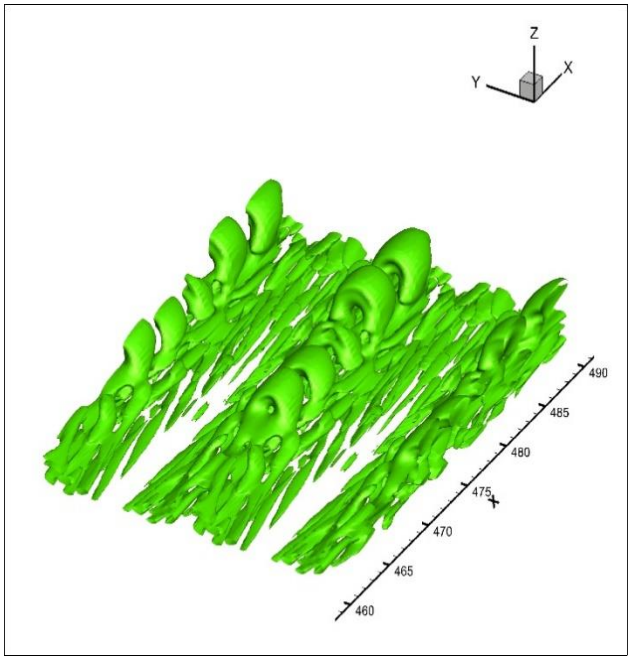


d) Mode 4

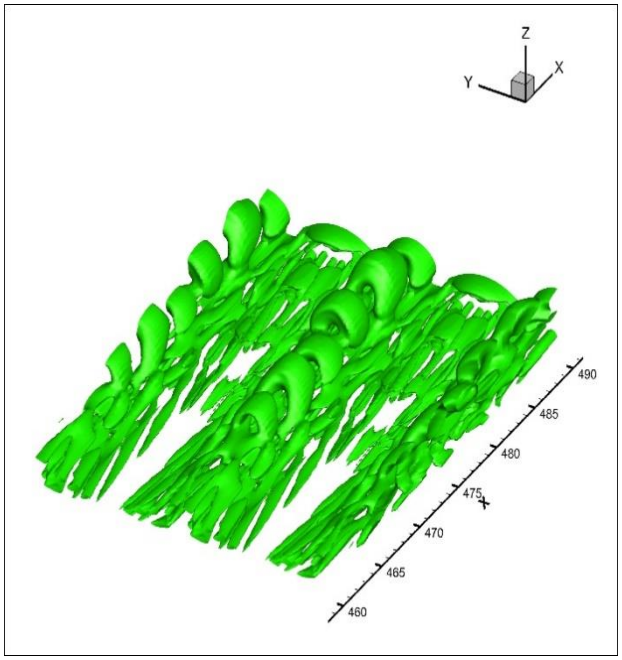


e) Mode 5

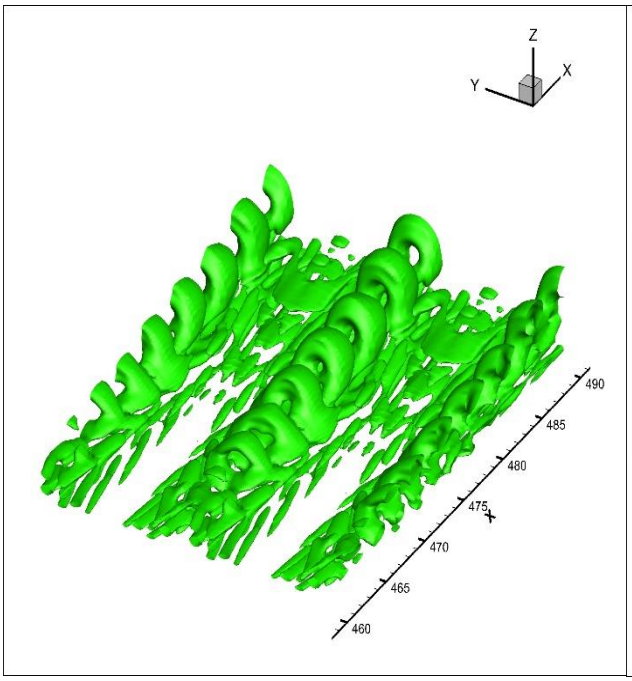


f) Mode 6

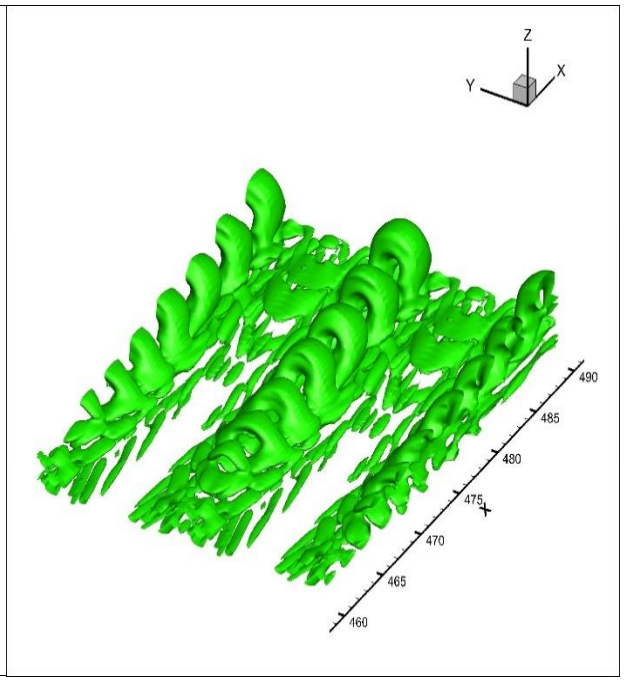


g) Mode 7

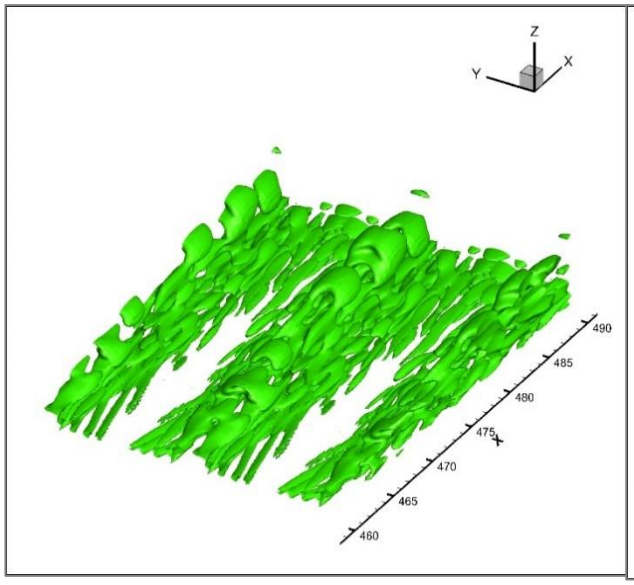


h) Mode 8

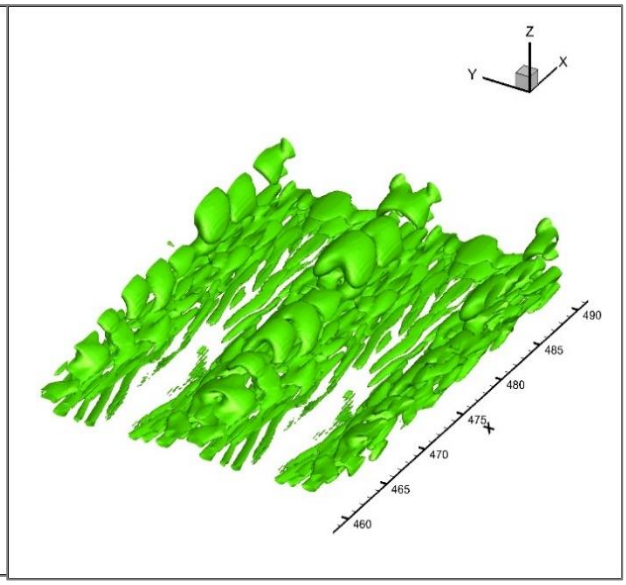


i) Mode 9

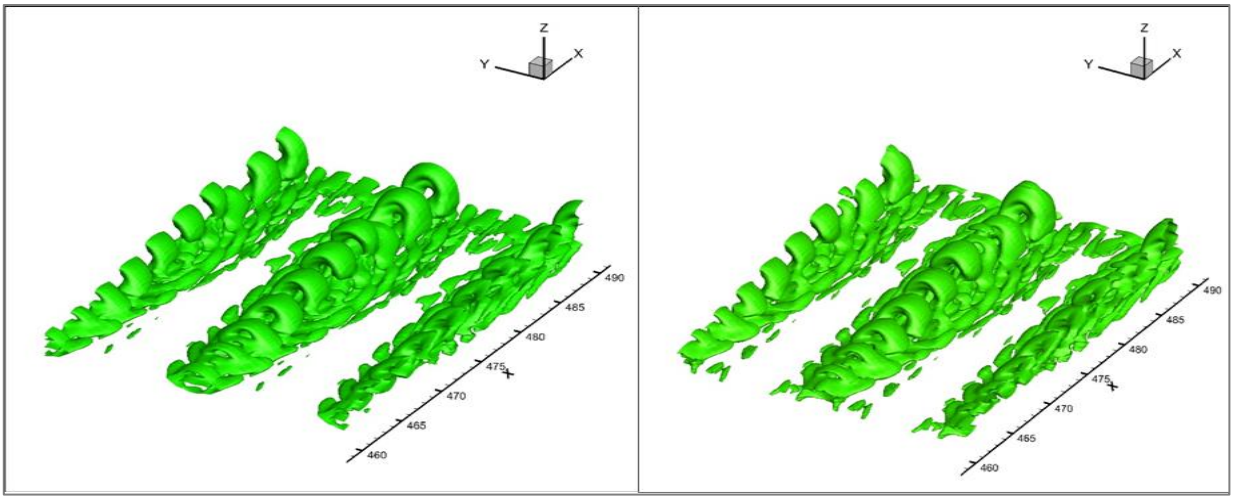


i) Mode 10 k) Mode 11

Figure 6.4. Vortex structures of first 10 modes with iso-surfaces of $\widetilde{\Omega}_L = 0.52$.

Mode 1 has stream wise velocity. Mode 2, 3 and 4 also have the stream wise vortex structure but a little bit less than mode 1. When the modes number goes up, spanwise characteristic dominates the vortex structure. In another word, spanwise vortex structure is dominant in leading modes whereas streamwise characteristic is dominant in trailing modes. To justify this nature of POD modes, we have taken the intersection of XY-slice with the vortex structure which is shown is figure 6.5.

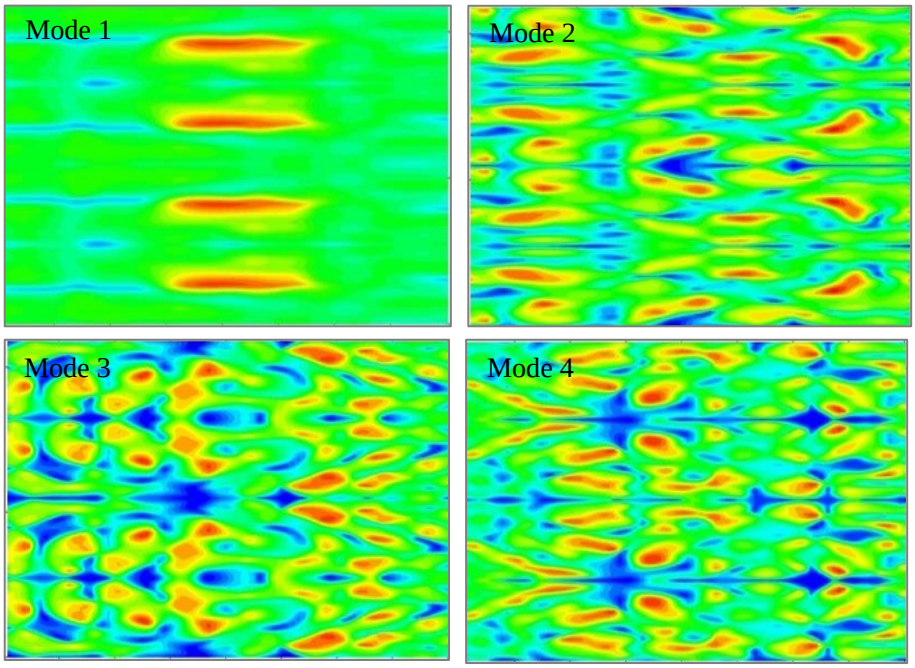


Figure 6.5. a)-d). Interior structure of some POD modes by XY- cross section.

The interior vortex structure given by intersection of XY-plane with iso-surface plotting of different POD modes is presented in the above figure 6.5. a) - f). As we can see in the figure , the first POD mode, also known as mean flow, has dominant streamwise vortex structure. From the study of interior structure, streamwise structure can be seen in mode 3 also. However, intensity of the vortex structures is smaller than the first mode. As mode number goes up, the spanwise characteristics become dominant in the vortex structure. In the figure 6.5, all the trailing modes are spreading in y-direction as higher modes show fluctuation distributions of vortex structures which are resulted by the creation of spanwise characteristics. Moreover, we can see strength of leading vortex structure are larger than that of the trailing modes. The mean flow has the largest scale flow structures since the modes are ordered by amplitudes.

Since the leading modes with streamwise structures possess significantly higher rotational strength than the other trailing modes, the original vortex structures can be reconstructed by few leading modes. So, we can model the original flow by reconstruction data of first few POD modes as they contain larger portion of the total rotational intensity. This will reduce the size of the original data, keeping most of the features of data (fluctuating vortex strength) intact. This can be seen in the figure 6.6, where original fluid flow is modeled by first 5 POD modes.

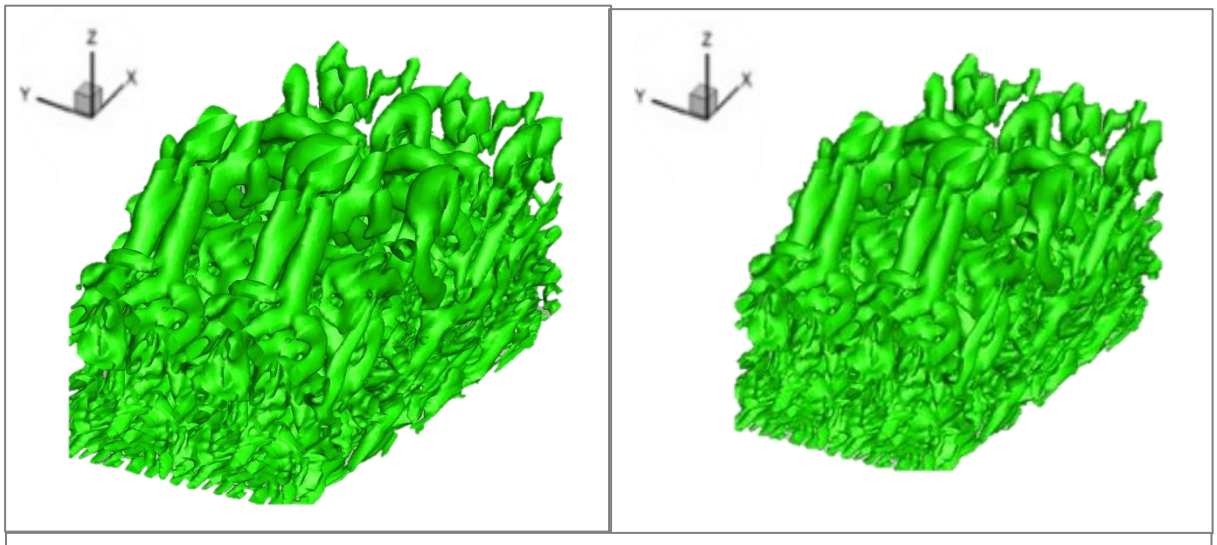


a) Original flow b) Reconstructed flow

Figure 6.6. Vortex structures of original flow and reconstructed flow by first 5 modes with of $\widetilde{\Omega}_L = 0.52$

Definition 6.4:

The coefficients that we get when the eigenvectors $v_i$ are scaled by the singular values of original matrix is known as POD time coefficients. The POD time coefficients function as a weight factor for each mode.

The time coefficients are representative of flow dynamics. They can be obtained from the matrix of temporal structure $Q = SV^T$, which is obtained from equations (6.10) and (6.11). Each column of matrix $V$ represents the time evolution of the respective mode. The first column gives the time coefficient of the mean flow (1st mode). Similarly, the second column of eigenvector matrix $V$ gives the time coefficient of the 2nd mode and so on. Then, they are scaled by the corresponding singular values $\sigma_i$.

The following graphs show the POD time coefficients of first few modes. Remaining time coefficients show the similar structure, so they are not included.

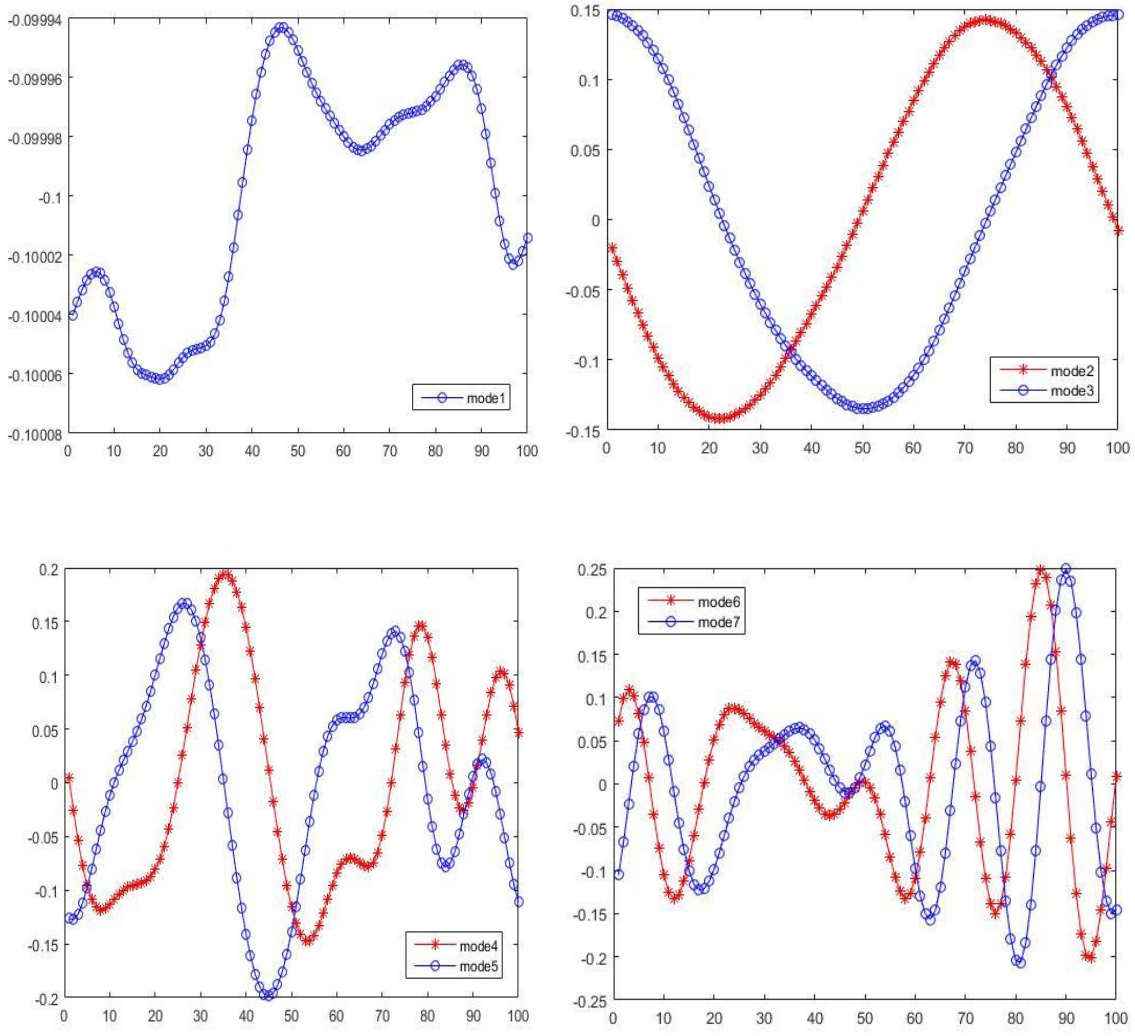

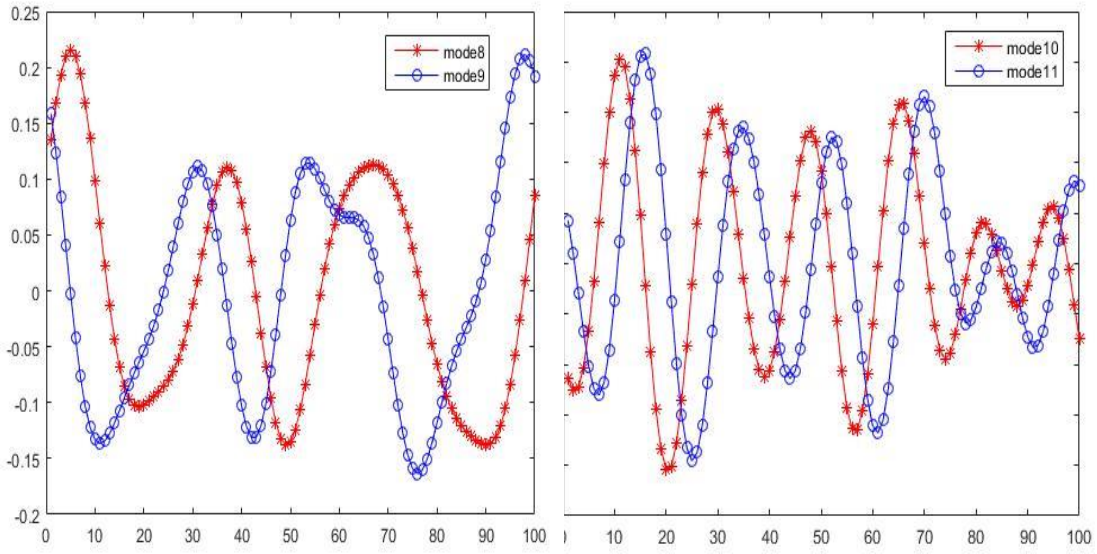

Figure 6.7. POD time coefficients of mode 1 to mode 11 where x-axis represents time steps and y axis represents time coefficients.

These graphs demonstrate the dynamics (fluctuations) of fluid motion . The mean flow has the least fluctuation whole the higher modes have larger fluctuations. It can be seen some similar fluctuations of some trailing modes.

6.3. POD analysis on formation of hairpin vortex.

The figure 6.1 shows that in the boundary layer transition, first we have spanwise vortex structure, then lambda vortices, and hairpin vortices. These vortex structures are symmetric about y-axis initially but, in late transition, they randomize and develop into a complex structure. In this dissertation we study the reason for generation of hairpin vortices by POD method.

According to the DNS studies of flow field transition [56,57], lambda-vortex self-deforms into hairpin vortex. But, Liu et. all [2,3], proposes that the hairpin vortex is formed by the high shear layer (K-H type) instability near the tip of the Λ-structure.

Definition 6.5:

When there are velocity differences between two layers of fluid, then the instability kicks in and the fluid flow transition into turbulent flow. This process is called K-H instability.

The following figure shows the formation of turbulent could structure by K-H instability.

Figure 6.8 Formation of wave clouds by K-H instability.

Picture source: https://commons.wikimedia.org/wiki/File:Wavecloudsduval.jpg

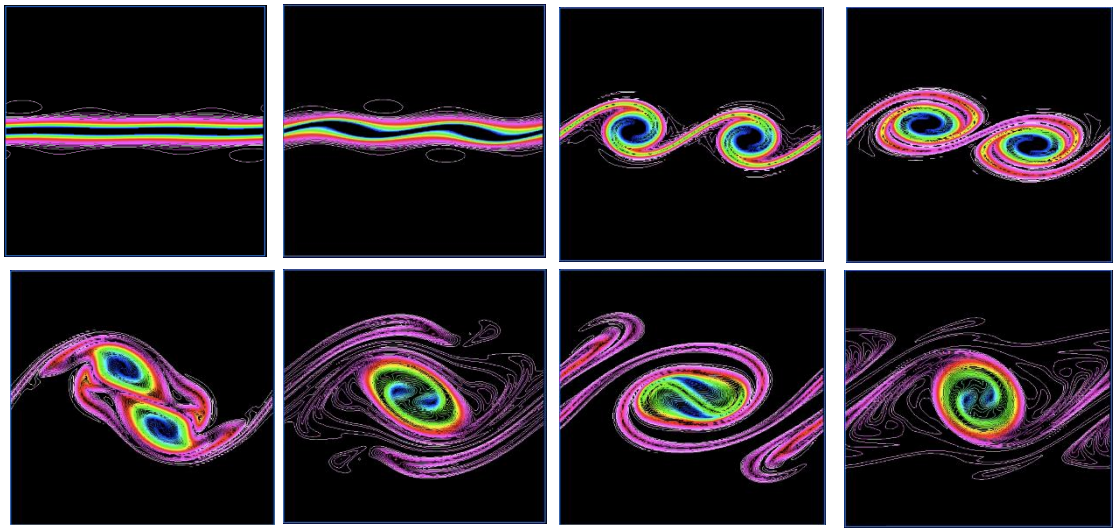

Fig. 6.9 Numerical simulation of K-H instability.

The K-H instability occurs when there is a shear velocity at the interface between two fluid layers. Figure 6.9 shows that a shear velocity is transformed into a pair rotational fluid motions and then transforms into a single vortex with two vortex cores. Therefore, pairing of vortex core is an outcome of K-H instability.

Next, from the above POD analysis of vortex structure in the boundary layer transition, we support the hypothesis presented by Liu et. all [2,3] that the hairpin vortex is generated by the high shear layer (K-H type) instability near the tip of the Λ-structure.

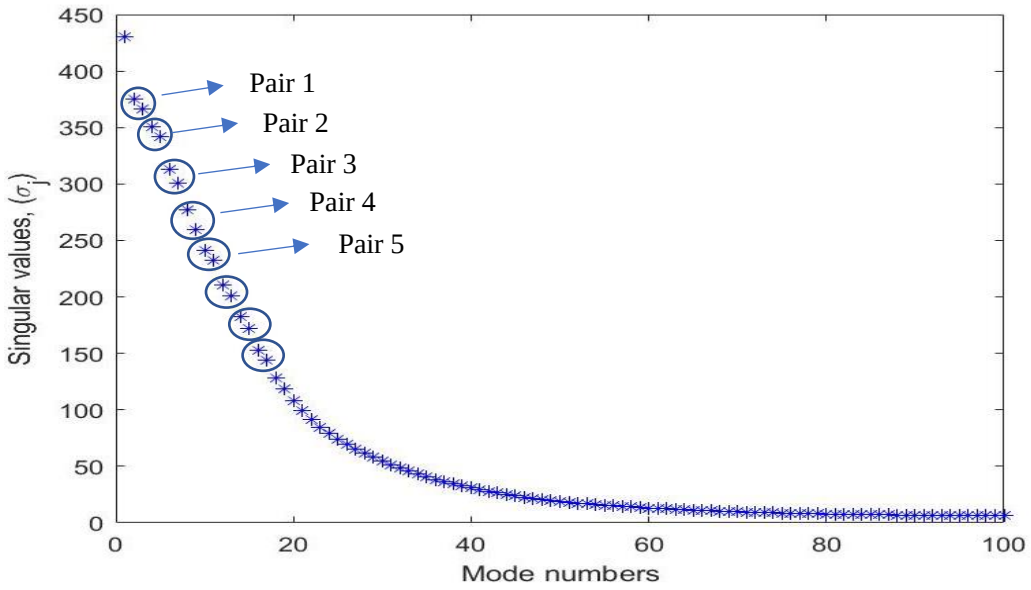


Fig. 6.10. Eigen values of modes expressed in pairs.

The exact values of eigenvalues of first eleven modes are given below.

| Modal pair | Mode number | Eigenvalues |
|---|---|---|
| Mean flow | 1 | 430.508579629457 |
| Pair 1 | 2 | 375.147973014816 |
| | 3 | 366.607543731766 |
| Pair 2 | 4 | 349.810202416080 |
| | 5 | 341.714032099057 |
| Pair 3 | 6 | 312.778080874447 |
| | 7 | 300.554436867078 |
| Pair 4 | 8 | 270.931632321952 |
| | 9 | 259.767231054683 |
| Pair 5 | 10 | 241.140266256180 |
| | 11 | 226.109992049960 |

Table 6.1. Paired eigenvalues of first eleven modes

Since singular values of each leading modes are in pairs, we can relate this to pairing of vortex core centers and say that K-H instability plays an important role in the formation of turbulence flow.

6.4. POD analysis on loosing symmetry of vortex structure.

The entire vortex structure in the early boundary layer is symmetric but it starts to lose the symmetry in the mid transition boundary layer. We have investigated the zone where symmetry is being lost and have investigated from where it starts to lose symmetry. The following figure shows that the top part of vortex structure is symmetric near X= 470 but at the same time step and position, bottom is already antisymmetric.

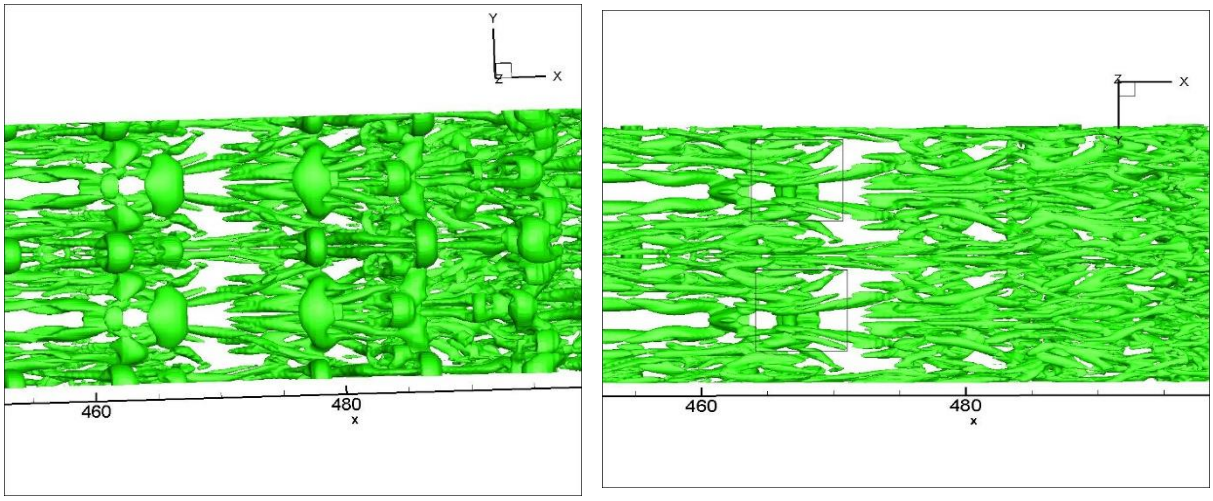


Fig. 6.11. Top and bottom view of vortex structure at the same position.

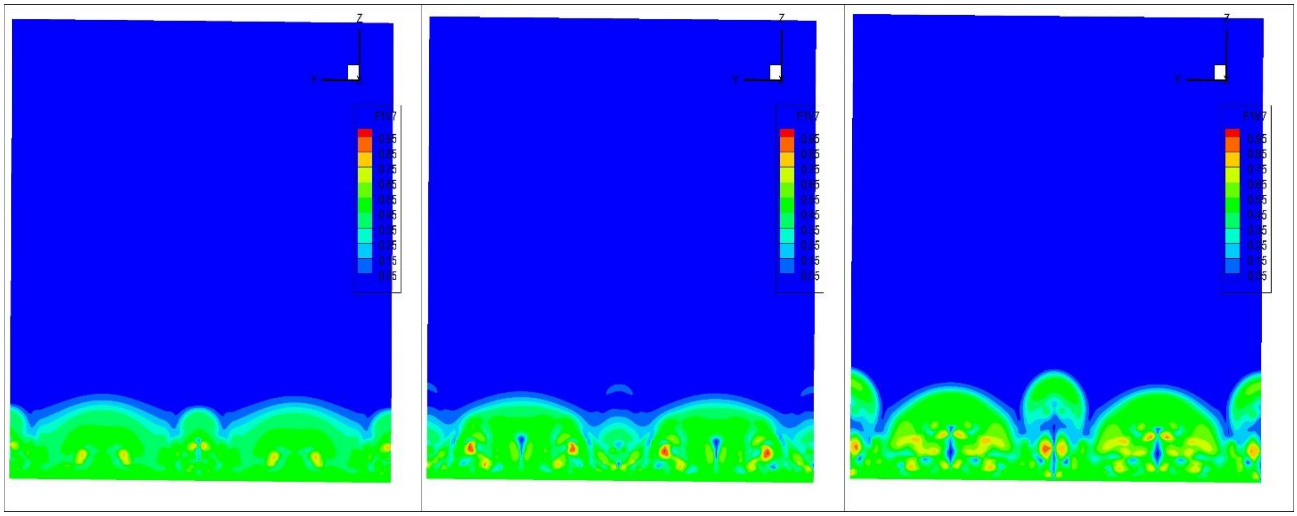

a) b) c)

Fig. 6.12. YZ-slice of flow structure at X=470, X=475 and X=480.

From fig.6.11, at X=47, the vortex structure at top, middle and bottom are all symmetric. In fig 6.11 b) the middle part is antisymmetric while top and bottom are still symmetric. But in fig 6.11 c), we can see that all top, middle, and bottom of vortex structure are antisymmetric. The z grid level for bottom, middle and top are k = 0-1, k = 1-4 and k = 4+.

Definition 6.6.

The function $f(x, y, z)$ is symmetric about plane $y = 0$ axis along the spanwise direction in the domain $-\pi \leq y \leq \pi$ if $f(x, -y, z) = f(x, y, z)$ for $\forall x, y, z \, \epsilon \, Z^+$.

Definition 6.7.

Let $L_{i,j,k}$ be the Liutex magnitude where $i, j, k$ are grid points along x, y and z directions, respectively. Let the domain of grids be $i \in [i_1, i_2]$, $j \in [2,128]$ and and $k \in [1,200]$. The YZ plane at y = 0 ($i.e. j = 64$)is the axis of symmetry. $L_{j,k}$ and $L_{128-j,k}$ are the Liutex magnitudes for $j = 2,3, \ldots,64$ in the YZ-plane on the left and right of the axis of symmetry, respectively.

(i) Two points, x(: ,j, k ) and x(: , 128-j, k ) , at any $i \in [i_1, i_2]$ are symmetric about the plane $y = 0$ at $z = k$ for $k = 1,2, \ldots,200$ if

$$\left|L_{j,k} - L_{130-j,k}\right| < 0.001,$$

Otherwise, these two points are not symmetric about the plane y = 0.

(ii) Let $m(d_i)$ and $n(d_i)$ are the number of pairs of points that are symmetric and antisymmetric, respectively. The antisymmetric index is defined by

$$\alpha_i = \left(\frac{n(d_i)}{m(d_i) + n(d_i)}\right)$$

(iii) For $i \in [i_1, i_2]$, the contour of Liutex magnitude in the YZ-plane is symmetric about the plane $y = 0$ if $\alpha_i < 0.01$.

Otherwise, the contour of Liutex magnitude in the YZ-plane is antisymmetric about $y = 0$. i.e., the vortex structure is symmetric about $y = 0$ if

$$\alpha_i < 1, \ \forall i \in [i_1, i_2].$$

Otherwise, the vortex structure is antisymmetric about $y = 0$.

From the above definition, if $\alpha_i \geq 1$, then the vortex structure is antisymmetric. The higher the value of $\alpha_i$, the more antisymmetric the vortex structure is. If $\alpha_i < 1$, then symmetric vortex exists.

The following figure is YZ-slice contour of reconstruction of vortex structure by first five modes at timestep t= 20.00T, where T is T-S wavelength.

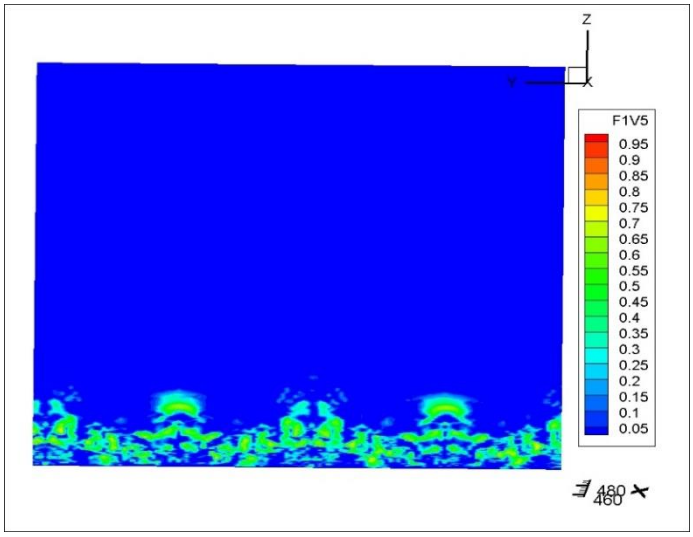


Fig. 6.13 YZ-slice of reconstructed flow by first five POD modes at X=470.

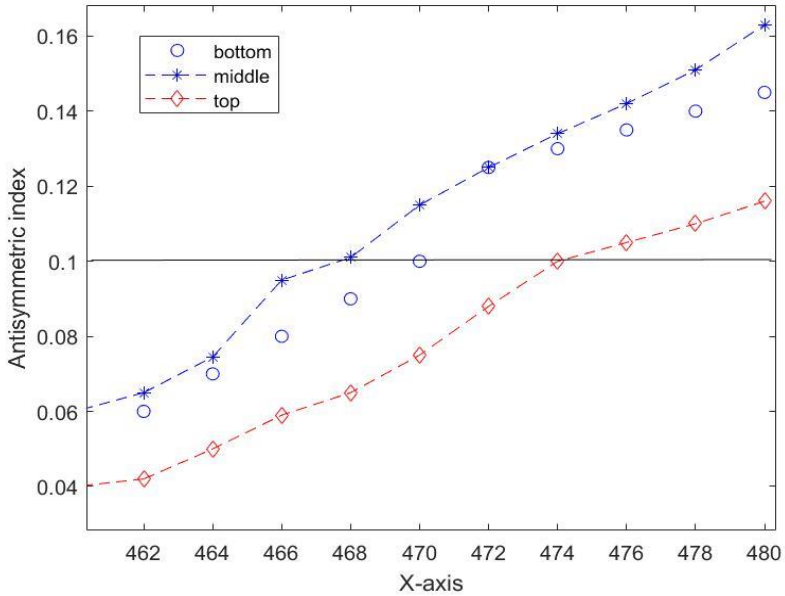


Fig. 6.14. The antisymmetric index of top, bottom, and mid part of reconstructed vortex structure by first five POD modes.

This figure shows that in reconstructed data, the bottom part has crossed the antisymmetric index threshold (i.e., 0.01) at around X=468 and then middle and top part cross that limit at X=470 and X=475 respectively, indicating that the vortex antisymmetric structure starts from middle, then spreads to bottom then to the top.

## 6.4. Conclusion

From the POD analysis on boundary layer transition, we can conclude the followings:

1) POD can be used to reduce the dimension of the large data, keeping most of the features intact. This will reduce the cost and time of computation.
2) First Mode is Knows as mean flow. First three modes have streamwise flow but when we take the higher mode, spanwise characteristic of the flow becomes dominant.
3) Mode 1 has most of the rotational intensity of the flow. As we go higher, rotational strength of every mode keeps dropping gradually.
4) Eigen values of POD modes exist in pairs. Also, modal shape and fluctuating nature of each mode exist in pairs. This supports the hypothesis that turbulence is generated by K-H instability.
5) The antisymmetric of the vortex starts from the middle, then the antisymmetric structure of bottom part starts and spreads to top level.

# CHAPTER 7

# CONCLUSION AND DISCUSSION

First generation vortex identification methods are based on the definition of vorticity vector. But the vorticity vector itself cannot represent the vortex as it counts on shearing as a vortex structure. In the flat plate boundary layer, there is a huge amount of shear near the wall. Since vorticity treats shear as vortex, it shows large vortex strength near the wall, but the truth is other way around. In fact, we have minimal vortex strength near the wall. Also, it is found that vorticity direction and actual vortex direction do not align in the same direction. Moreover, vorticity core center and vortex core center might not match. So, despite being convenient to use and having the direction of rotation, the first-generation vortex method is not deemed to be the appropriate method to model and visualize the vortex structure.

Second-generation vortex methods such as Q, $\Delta$, $\lambda_2$ , $and\ \lambda_{ci}$ are based on eigenvalues of velocity gradient tensor. All these methods are scalar quantities. So, they cannot be used to depict the direction of the fluid rotation. If a method does not show the direction in which the fluid particles are rotating, then we could say that this method is not good enough. So, these method cannot define the vortex core center as vortex core centers also have rotation direction. Moreover, these methods need iso-surface plotting to demonstrate the vortex structure. But iso-surface is manmade concept, and it is arbitrary. Different iso-surface threshold gives the different vortex structures. So, for the same data, we might end up getting various iso-surface vortex structure. This will just confuse the people more. To visualize the vortex structure properly we need to know the iso-surface threshold prior to simulating a vortex structure. So, this method does not help much, especially to the new ones who studying the fluid dynamics. Being threshold confined methods, these methods can capture only one strength throughout the vortex region, which means these methods are unable to capture both weak and strong vortex structure simultaneously. Also, just like vorticity-based methods, all the second-generation vortex identification methods are severely affected by shear contamination at various levels. Q, $\Delta$, and $\lambda_2$ criteria are contaminated by stretching effect too. Moreover, these methods are highly contingent upon selection of coordinates. Which means for different coordinates, these methods give different values, defining the different vortex structure. So, they are not Gallilean invariant. In addition, none of these methods were able to answer the following six core issues of vortex definition and identification:

7) What is the absolute strength of vortex?
8) What is the relative strength of vortex?
9) What is the rotation axis of vortex?
10) What is the vortex core center?
11) What is the size of vortex core?
12) Where is the vortex boundary?

As first and second-generation method had so many problems on them. Professor Dr. Chaoqun Liu addressed these problems and proposed Liutex method. Since then, methods like Liutex core lines, Liutex tube, Liutex-Omega, Modified Liutex-Omega have been proposed and these Liutex based methods are known as third-generation vortex identification method. Liutex method is eigenvector-based method unlike first and second-generation vortex identification method. It is a measure of rigid rotation of fluid rotation, and it can give the direction of local fluid rotation. It is not affected by shearing and stretching or compression. Moreover, Liutex method has vector, scalar, and tensor form.

Liutex core lines gives the vortex structure where vortex strength is maximum in the plane perpendicular to direction of the fluid flow. Liutex core line is unique and is free from iso-surface. Therefore, there is no need for threshold adjustments. Also, Liutex core lines can show the vortex strength at different region of vortex areas unlike iso-surface plotting. The important achievement of Liutex based method is that they are Gallilean invariant, which means they do not change according to coordinate selection. So, third-generation methods like Liutex, Modified Liutex-Omega, and Liutex core lines methods can be considered as best methods available as they resolve so many problems mentioned earlier. These methods also address the six core issues on vortex definition and identification.

1) The absolute strength of vortex is Liutex magnitude.
2) The relative strength is Modified Liutex method.
3) The local rotation axis is Liutex direction.
4) Liutex core lines give the vortex core center.
5) The vortex core size is given by Liutex tube which is 95% of the local maximum value.
6) The vortex boundary is the region where Liutex magnitude is positive. i.e., $R > 0$.

The proper orthogonal (POD) method reconstructs the given data with significantly much lower dimension but keeps the features of the data intact. In fluid motion, first few modes can keep up to 99% of the total kinetic energy. The following conclusion can be made from POD analysis of vortex structure from the late flow boundary layer transition.

1) Singular values are ordered in descending order. Leading modes have larger singular values while trailing modes have smaller singular values. Singular values represent the fluctuating kinetic energy. So, first mode has the largest percent of total kinetic energy. In our research, first POD mode has approximately about 12% of the total kinetic energy.
2) Kinetic energy of the trailing POD modes keeps decreasing and ultimately converge to zero. So, we can neglect the higher modes.
3) Leading modes have streamwise vortex characteristic while trailing modes have spanwise vortex characteristic.
4) First four or five modes contain about 99 % of the total kinetic energy. So, we can model the fluid motion by first four or five modes. This will keep the features of fluid motion same but, significantly reduce the dimension. So, we can save computation cost and time.
5) The time coefficients demonstrate the dynamics (fluctuations) of fluid motion . The mean flow has the least fluctuation whole the trailing modes have larger fluctuations.

The proper orthogonal decomposition (POD) method used in this dissertation decomposes the given data into different deterministic spatial modes and random time coefficients. The Snapshot POD method proposed by Sirovich decomposes the original data into deterministic temporal modes and random spatial coefficients. To apply snapshot POD method, first we need to transpose our original snapshot matrix and follow the same algorithm. In this method, covariance matrix is built by averaging in space instead of time. I really recommend this method if somebody is interested in modal decomposition of big data.

Future work:

A lot of scientists and researchers are using Liutex vortex identification methods in their research. Dr. Liu and his team are working on Liutex kinematics and Liutex dynamics at CNSM, University of Texas at Arlington. After graduation, I would like to continue to collaborate with Dr. Liu and his team.

References:

[1] Wu, X. and Moin, P., Direct numerical simulation of turbulence in a nominally zero-pressure gradient flat-plate boundary layer, *JFM,* vol 630, pp5-41, 2009

[2] Yan, Y., Chen, C., Huankun, F., and Liu, C., "DNS study on Λ -vortex and vortex ring formation in the flow transition at Mach number 0.5," *J. Turbulence,* Vol. 15, No.1, 2014, pp.1-21.

[3] Liu, C., Yan, Y., and Lu, P., "Physics of turbulence generation and sustenance in a boundary layer," *Computers & Fluids*, Vol. 102, 2014, pp. 353-384.

[4] Helmholtz H., On the integrals of the hydrodynamic equations corresponding to vortex motions, Journal für die reine und angewandte Mathematik, 55 (1858) 22-25. (in German).

[5] Saffman, P., Vortices dynamics. Cambridge, UK: Cambridge University Press, 1992.

[6] Zhou, Y., and Antonia, R. A., A study of turbulent vortices in the near wake of a cylinder. Journal of Fluid Mechanics, 253, 643-661 (1993).

[7] Epps, B., Review of vortex identification methods. AIAA 2017-0989 (2017).

[8] Yu, Y. & Shrestha, P., Alvarez, O., Nottage, C. & Liu, C. (2020). Correlation analysis among vorticity, Q method and Liutex. *Journal of Hydrodynamics. 32*. https://doi.org/*10.1007/s42241-020-0069-2.*

[9] Lugt, H. J., The dilemma of defining a vortex. In recent developments in theoretical and experimental fluid mechanics. Berlin Heidelberg, Germany: Springer-Verlag, 1979.

[10] Robinson, S. K., A review of vortex structures and associated coherent motions in turbulent boundary layers. In structure of turbulence and drag reduction. Berlin Heidelberg, Germany: Springer-Verlag, 1990.

[11] Perry , A.M. and Chong, M. S., A description of eddying motions and flow patterns using critical-point concepts, *Annu. Rev. Fluid Mech 19,* 125-155(1987)

[12] Chong, M. S., and Perry, A. E., A general classification of three-dimensional flow fields. *Physics of Fluids A, 2(5),* 765-777 (1990).

[13] Jeong, J., and Hussain, F., On the identification of a vortex. Journal of Fluid Mechanics, 285, 69-94 (1995).

[14] Hunt, J. C. R., Wray, A. A., and Moin, P., Eddies, stream, and convergence zones in turbulent flows. Center for Turbulent Research Report CTR-S88, 193-208 (1988).

[15] Zhou, J., Adrian, R., Balachandar, S., and Kendall, T. M., Mechanisms for generating coherent packets of hairpin vortices in channel flow. Journal of Fluid Mechanics, 387, 353-396 (1999).

[16] Liu, C., Gao, Y., Dong X., Wang, Y., Liu, J., Zhang, Y., Cai, X., and Gui, N., "Third generation of vortex identification methods: Omega and Liutex/Rortex based systems", *Journal of Hydrodynamics*, 31(2): 205-223 (2019).

[17] Liu, C., Wang, Y., Yang, Y., and Duan, Z., "New Omega Vortex Identification Method," Science China Physics, Mechanics & Astronomy, Vol. 59, No. 8, 2016, pp.1-9.

[18] Liu, C., Gao, Y., Tian, S., and Dong, X., "Rortex- A new vortex vector definition and vorticity tensor and vector decompositions." *Physics of Fluids* 30, 035103 (2018).

[19] Gao, Y. and Liu, C., "Rortex and comparison with eigenvalue-based identification criteria", *Physics of Fluid* 30, 085107 (2018).

[20] Yu, Y., Shrestha, P., Nottage, C., and Liu. C., Principal Coordinates, and Principal Velocity Gradient Tensor Decomposition. *J Hydrodyn* (2020). https://doi.org/10.1007/s42241-020-0035-z

[21] X. Dong, Y. Gao, C. Liu, New normalized Rortex/vortex identification method, Physics of Fluids, 2019, 31(1): 011701.

[22] J. Liu, C. Liu, Modified normalized Rortex/vortex identification method, Physics of Fluids, 2019, 31(6): 061704.

[23] Gao, Y., Liu, J., Yu, Y., and Liu, C., "A Liutex based definition and identification of vortex core center lines", *J. Hydrodynamics,31(3),* (2019).

[24] Gao, Y., and Liu, C., "Rortex based velocity gradient tensor decomposition", *Physics of Fluids* 31, 011704 (2019).

[25] Haller, G., "An objective definition of the vortex", *J. Fluid Mech.*, 525, 1-26 (2005).

[26] Wang, Y., Gao, Y., and Liu, C., "Galilean invariance of Rortex*", Physics of Fluids* 30, 111701 (2018).

[27] Lumley, J. L., "The structure of inhomogeneous turbulent flows," Atmospheric Turbulence and Radio Wave Propagation, 1967, pp.166-178.

[28] Sirovich, L., “Turbulence and the dynamics of coherent structures. Part I: Coherent structures,” *Quarterly of applied mathematics*, Vol. 45, No. 3, 1987, pp. 561-571.

[29] Hellström, L., Ganapathisubramani, B., and Smits, A. J., “Coherent structures in transitional pipe flow,” *Phys. Rev. Fluids*, Vol. 1, 2016, Article ID 024403.

[30] Gunes, H., “Proper orthogonal decomposition reconstruction of a transitional boundary layer with and without control,” *Physics of Fluids*, Vol. 16, 2004, Article ID 2763.

[31] Yang, Y., Tian, S., and Liu, C., “POD Analyses on Vortex Structure in Late-stage Transition,” AIAA paper 2018-0821, January 2018.

[32] Charkrit, S., Dong, X., and Liu, C., “POD analysis of losing symmetry in late flow transition,” AIAA paper 2019-1870, January 2019.

[33] Dong, X., Cai, X., Dong, Y., Liu, C., POD analysis on vortical structures in MVG wake by Liutex core line identification, Journal of Hydrodynamics, (2020)

[34] Gunes, H., “Proper orthogonal decomposition reconstruction of a transitional boundary layer with and without control,” *Physics of Fluids*, Vol. 16, 2004, Article ID 2763.

[35] Yang, Y., Tian, S., and Liu, C., “POD Analyses on Vortex Structure in Late-stage Transition,” AIAA paper 2018-0821, January 2018.

[36] Charkrit, S., Dong, X., and Liu, C., “POD analysis of losing symmetry in late flow transition,” AIAA paper 2019-1870, January 2019.

[37] Cavalieri, A., Schlatter P., Vinuesa, R. and Henningson, D. and Abreu, L., “SPOD and resolvent analysis of near-wall coherent structures in turbulent pipe flows,” *Journal of Fluid Mechanics*, 2020

[38] Robinson S. K. Coherent motions in the turbulent boundary layer [J]. *Annual Review of Fluid Mechanics*, 1991, 23: 601-639.

[39] Wang Y., Yang Y., Yang G. et al. DNS study on vortex and vorticity in late boundary layer transition [J]. *Communications in Computational Physics*, 2017, 22(2): 441-459.

[40] J. Liu, Y. Deng, Y. Gao, S. Charkrit, C. Liu, Mathematical foundation of turbulence generation from symmetric to asymmetric Liutex, Journal of Hydrodynamics, 2019, 31(3): 632-636.

[41] Chakraborty, P., Balachandar, S., and Adrian, R., "On the relationships between local vortex identification schemes". *Journal of Fluid Mechanics, 535*, 189-214. doi:10.1017/S0022112005004726 (2005).

[42] J. Liu, Y. Wang, Y. Gao, C. Liu, Galilean invariance of Omega vortex identification method, Journal of Hydrodynamics, 2019, 31(2): 249-255.

[43] Y. Zhang, X. Wang, Y. Zhang, C. Liu, Comparisons, and analyses of vortex identification between Omega method and Q criterion, 2019, 31(2): 224-230.

[44] Dong, Xiang-rui & Wang, Yiqian & Chen, Xiao-ping & Dong, Yinlin & Zhang, Yuning & Liu, Chaoqun. (2018). Determination of epsilon for Omega vortex identification method. Journal of Hydrodynamics. 30. 1-9.10.1007/s42241-018-0066-x.

[45] Wang, Yq., Gao, Ys., Liu, Jm. *et al.* Explicit formula for the Liutex vector and physical meaning of vorticity based on the Liutex-Shear decomposition. *J Hydrodyn* 31, 464–474 (2019). https://doi.org/10.1007/s42241-019-0032-2

[46] Y. Wang, Y. Gao, H. Xu, X. Dong, J. Liu, W. Xu, M. Chen, C. Liu, Liutex theoretical system and six core elements of vortex identification, Journal of Hydrodynamics, 2020, 32: 197-221.

[47] W. Xu, Y. Gao, Y. Deng J. Liu, C. Liu, An explicit expression for the calculation of the Rortex vector, Physics of Fluids, 2019, 31(9): 095102.

[48] J. Liu, Y. Gao, C. Liu, An objective version of the Rortex vector for vortex identification, Physics of Fluids, 2019, 31(6): 065112.

[49] Y. Wang, C. Liu, Liutex cores in transitional boundary layer with spanwise-wall oscillation, Journal of Hydrodynamics, 2019, 31(6): 1178-1189.

[50] H. Xu, X. Cai, C. Liu, Liutex (vortex) core definition and automatic identification for turbulence vortex structures, Journal of Hydrodynamics, 2019, 31(5): 857-863

[51] Galilean G. Dialogue concerning the two chief world systems [M]. Florence, 1632.

[52] W.H. Press, S.A. Teukolsky, W.T. Vetterling, and B.P. Flannery, *Numerical Recipes in FORTRAN 77: The Art of Scientific Computing*, 2nd ed. (Cambridge University Press, Cambridge, 1996).

[53] Y. Gao, Y. Yu, J. Liu, C. Liu, Explicit expressions for Rortex tensor and velocity gradient tensor decomposition, Physics of Fluids, 2019, 31(8): 081704.

[54] Y. Zhang, X. Qiu, F. Chen, K. Liu, X. Dong, C. Liu, A selected review of vortex identification methods with applications, Journal of Hydrodynamics, 2018, 30(5): 767-779.

[55] Shrestha, P., Nottage, C., Yu, Y. *et al.* Stretching and shearing contamination analysis for Liutex and other vortex identification methods. *Adv. Aerodyn.* **3,** 8 (2021). https://doi.org/10.1186/s42774-020-00060-9

[56] Hama, F.R., and Nutant, J., "Detailed flow-field observations in the transition process in a thick boundary layer," Proceedings of the 1963 Heat Transfer and Fluid Mechanics Institute, Stanford University Press, Palo Alto, CA, 1963, pp. 77–93.

[57] Moin, P., Leonard, A., and Kim, J., "Evolution of curved vortex filament into a vortex ring," Phys. Fluids, Vol. 29, No. 4, 1986, pp. 955–963.

# BIOGRAPHICAL INFORMATION

Pushpa Shrestha was born in Bhumlu-1, Ritthe, Kavre, Nepal in January 1990. He completed his high school from Shree Seti Devi Higher Secondary School, Bhumlu-1, Ritthe, Kavre, Nepal. He then moved to Lalitpur for his higher studies. He received his bachelor's degree in mathematics from Patan Multiple Campus, Lalitpur, Nepal, in 2010. He did his bachelor's degree in education from Mahendra-Ratna Campus, Kathmandu, Nepal, in 2012. He received his master's degree in mathematics from Amrit Science Campus, Kathmandu, Nepal, in 2015. Then, he then moved to USA for his Ph.D. in applied mathematics. He joined University of Texas at Arlington in fall 2017 for his Ph.D. in applied and computational mathematics.

Pushpa's research interest includes computational fluid dynamics, numerical analysis, scientific computation, data science and statistical analysis.